The Abdus Salam
International Centre for Theoretical Physics

United Nations
Educational, Scientific and
Cultural Organization

IAEA
International Atomic Energy Agency

1939-6

Joint ICTP-IAEA Workshop on Nuclear Structure and Decay Data: Theory and Evaluation

28 April - 9 May, 2008

Theory: Structure of odd-odd nuclei in the interacting boson fermion-fermion model.

Slobodan BRANT

Dept. of Physics, Faculty of Science
University of Zagreb
Croatia

3.

Structure of odd-odd nuclei in the interacting boson fermion-fermion model

The IBFFM is able to give an accurate description of the structure of odd-odd nuclei. Odd-odd nuclei constitute a very stringent test of the model:

- A detailed knowledge of even-even cores and odd-mass neighbours is required

- Odd-odd nuclei do not provide the same sort of smoothly varying systematics as do other types of nuclei

IBFFM vs other models ?

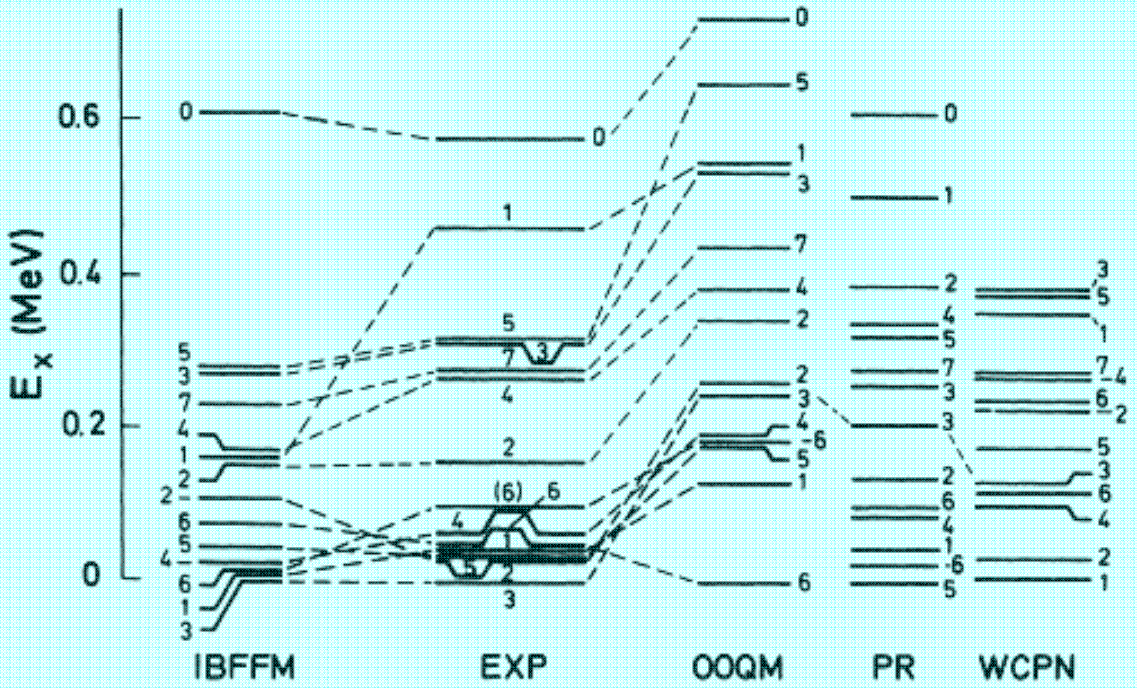

FIG. 7. IBFFM negative-parity energy spectrum of ^{140}La compared with the experimentally known energy spectrum and with the three previous calculations performed using the odd-odd quasiparticle model (OOQM) (Ref. 10), the parabolic rule (PR) (Ref. 2), and the weak-coupling shell model in the proton-neutron formalism (WCPN) (Ref. 11).

IBFFM is successful in describing and predicting

- Level energies
- Electromagnetic properties
- Transfer properties
- Isomers

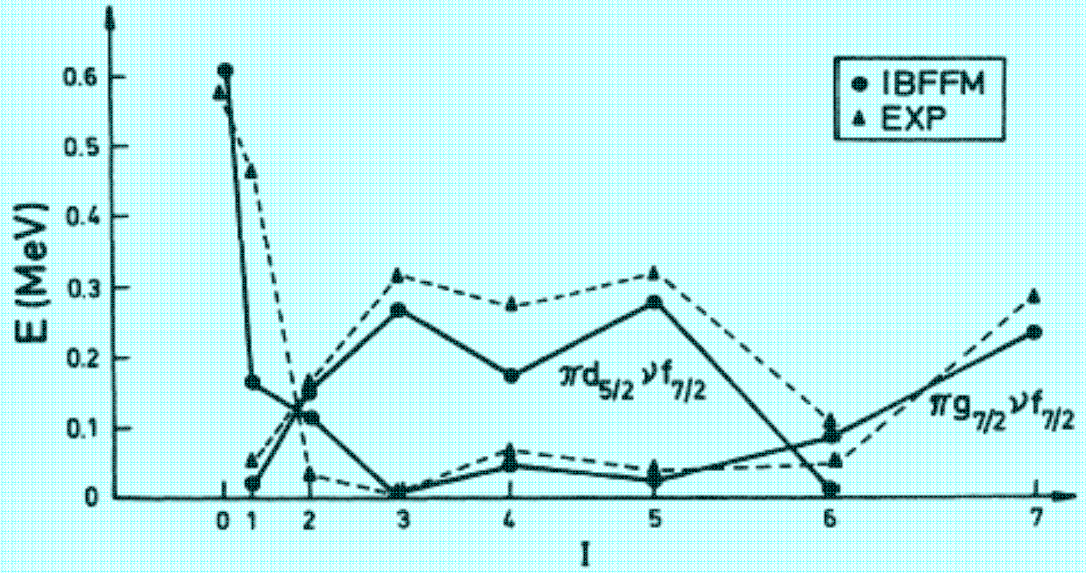

FIG. 8. Classification of the IBFFM levels into multiplets on the basis of largest components in the wave functions. The experimental levels of ^{140}La are compared with the theoretical spectra on the basis of level energies, electromagnetic deexcitation, and transfer properties. IBFFM and experimental levels are presented by solid circles and triangles, respectively.

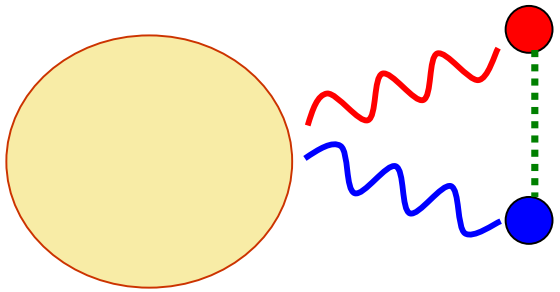

proton

neutron

boson –fermion interactions from odd – A neighbours

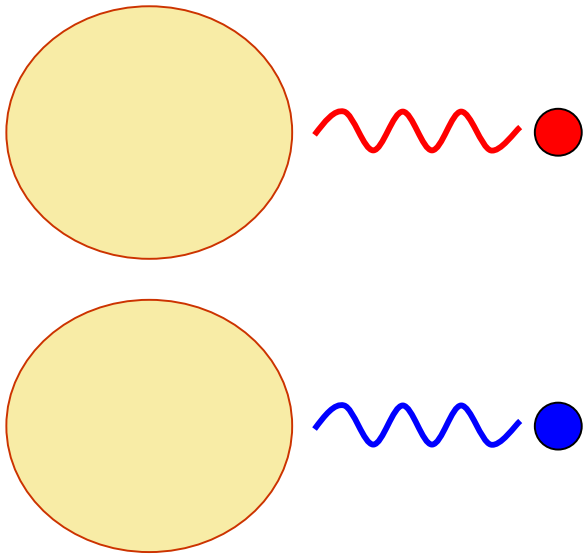

Odd – Odd nucleus

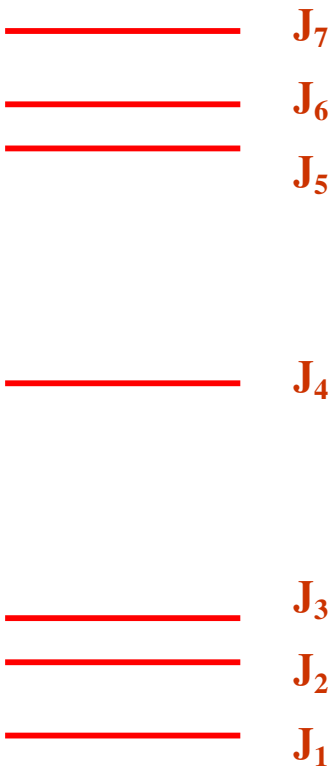

Important data

excitation energies

γ branchings

B(E2)

B(M1)

Q

μ

B(M1) for spherical soft transitional

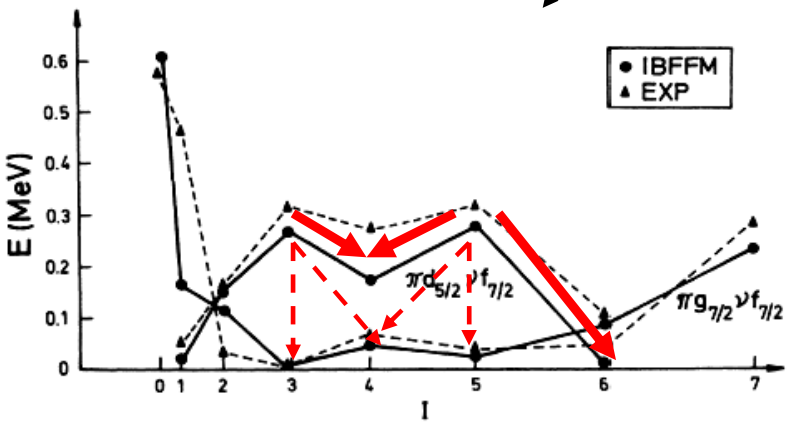

The IBFFM Hamiltonian for an odd-odd nucleus is:

$$H = H_B + H_{\nu F} + H_{\pi F} + V_{\nu BF} + V_{\pi BF} + V_{\pi\nu}$$

H_B is the boson Hamiltonian of IBM-1 describing a system of N interacting bosons (correlated S and D pairs) that approximate the valence nucleon pairs:

$$\begin{aligned} H_B &= \varepsilon\, \hat{N} + \frac{1}{2}\, v_0\, \left([d^\dagger \times d^\dagger]_{(0)} \times [\tilde{s} \times \tilde{s}]_{(0)} + h.c.\right)_{(0)} \\ &+ \frac{1}{\sqrt{2}}\, v_2\, \left([d^\dagger \times d^\dagger]_{(2)} \times [\tilde{d} \times \tilde{s}]_{(2)} + h.c.\right)_{(0)} \\ &+ \sum_{L=0,2,4} \frac{1}{2}\, C_L\, \sqrt{2L+1}\, \left([d^\dagger \times d^\dagger]_{(L)} \times [\tilde{d} \times \tilde{d}]_{(L)}\right)_{(0)} \end{aligned}$$

$$n_s = N - n_d$$

$H_{\pi F}$ and $H_{\nu F}$ are the fermion Hamiltonians containing quasiparticle energies of protons and neutrons, respectively. The quasiparticle energies and occupation probabilities contained in the fermion Hamiltonian, and other terms, are obtained in a BCS calculation with some standard set of single fermion energies. For protons ($\alpha = \pi$) and for neutrons ($\alpha = \nu$).

$$H_{\alpha F} = \sum_i \varepsilon_{\alpha_i} \, a^\dagger_{\alpha_i} \tilde{a}_{\alpha_i}$$

$V_{\nu BF}$ and $V_{\pi BF}$ are the IBFM-1 boson-fermion interactions containing the dynamical, exchange and monopole interactions. For protons ($\alpha = \pi$) and for neutrons ($\alpha = \nu$).

$$V_{\alpha BF} = V_{\alpha DYN} + V_{\alpha EXC} + V_{\alpha MON}$$

$$V_{\alpha DYN} = \Gamma_0 \sum_{\alpha j_1 \alpha j_2} \sqrt{5} \, (u_{\alpha j_1} u_{\alpha j_2} - v_{\alpha j_1} v_{\alpha j_2}) \, \langle \alpha j_1 \parallel Y_2 \parallel \alpha j_2 \rangle \, \left([a^\dagger_{\alpha j_1} \times \tilde{a}_{\alpha j_2}]^{(2)} \times Q_B^{(2)} \right)^{(0)}$$

$Q_B^{(2)}$ is the standard boson quadrupole operator

$$Q_B^{(2)} = [s^\dagger \times \tilde{d} + d^\dagger \times \tilde{s}]^{(2)} + \chi [d^\dagger \times \tilde{d}]^{(2)}$$

$$V_{\alpha EXC} = \Lambda_0 \sum_{\alpha j_1 \alpha j_2 \alpha j_3} (-2) \sqrt{\frac{5}{2\ \alpha j_3 + 1}} \left(u_{\alpha j_1} v_{\alpha j_3} + v_{\alpha j_1} u_{\alpha j_3}\right)\ \left(u_{\alpha j_2} v_{\alpha j_3} + v_{\alpha j_2} u_{\alpha j_3}\right)$$
$$\langle \alpha j_3 \parallel Y_2 \parallel \alpha j_1 \rangle \langle \alpha j_3 \parallel Y_2 \parallel \alpha j_2 \rangle\ : \left([a^\dagger_{\alpha j_1} \times \tilde{d}\ ]_{\alpha j_3} \times [\tilde{a}_{\alpha j_2} \times d^\dagger\ ]_{\alpha j_3} \right)^{(0)} :$$

$$V_{\alpha MON} = A_0 \sum_{\alpha j} \sqrt{5}\ (2\alpha j + 1)\ \left([a^\dagger_{\alpha j} \times \tilde{a}_{\alpha j}]^{(0)} \times [d^\dagger \times \tilde{d}]^{(0)} \right)^{(0)}$$

$V_{\pi\nu}$ is the residual proton-neutron interaction taken in the form of spin-spin, surface-delta, spin-spin-delta, tensor or multipole-multipole interaction.

$$H_{\sigma\sigma} = -\sqrt{3}\, V_{\sigma\sigma}\, [\vec{\sigma}_\pi \cdot \vec{\sigma}_\nu]$$

$$H_{\delta} = 4\pi\, V_{\delta}\, \delta(\vec{r}_\pi - \vec{r}_\nu)\, \delta(r_\pi - R_0)\, \delta(r_\nu - R_0)$$

$$H_{\sigma\sigma\delta} = 4\pi\, V_{\sigma\sigma\delta}\, [\vec{\sigma}_\pi \cdot \vec{\sigma}_\nu]\, \delta(\vec{r}_\pi - \vec{r}_\nu)\, \delta(r_\pi - R_0)\, \delta(r_\nu - R_0)$$

$$H_{T} = V_T \left(3\, \frac{[\vec{\sigma}_\pi \cdot \vec{r}_{\pi\nu}]\, [\vec{\sigma}_\nu \cdot \vec{r}_{\pi\nu}]}{r_{\pi\nu}^2} - [\vec{\sigma}_\pi \cdot \vec{\sigma}_\nu] \right)$$

$$H_{MM} = 4\pi\, \frac{\delta(r_\pi - r_\nu)}{r_\pi r_\nu} \sum_{\kappa\mu} V_\kappa\, Y^*_{\kappa\mu}(\pi)\, Y_{\kappa\mu}(\nu)$$

$$\vec{r}_{\pi\nu} = \vec{r}_\pi - \vec{r}_\nu \qquad R_0 = 1.2\, A^{\frac{1}{3}} \quad fm$$

The electromagnetic operators have the form (for protons ($\alpha = \pi$) and for neutrons ($\alpha = \nu$)):

$$M(E2) \quad = \quad M_B(E2) + M_\pi(E2) + M_\nu(E2)$$

$$M_B(E2) \quad = \quad \frac{3}{4\pi}\ R_0^2\ e^{VIB}\ \left([s^\dagger \times \tilde{d} + d^\dagger \times \tilde{s}]^{(2)} + \chi [d^\dagger \times \tilde{d}]^{(2)} \right)$$

$$R_0^2 = 0.0144\ A^{\frac{2}{3}} \qquad barn$$

$$M_\alpha(E2) \quad = \quad \frac{3}{5}\ R_0^2\ e_\alpha\ Y_2(\alpha)$$

$$\vec{M}(M1) \quad = \quad \vec{M}_B(M1) + \vec{M}_\pi(M1) + \vec{M}_\nu(M1)$$

$$\vec{M}_B(M1) \quad = \quad \sqrt{\frac{3}{4\pi}}\ \sqrt{10}\ g_R\ [d^\dagger \times \tilde{d}]^{(1)}$$

$$\vec{M}_\alpha(M1) \quad = \quad \sqrt{\frac{3}{4\pi}}\ [\ g_l(\alpha)\ \vec{l}(\alpha)\ +\ g_s(\alpha)\ \vec{s}(\alpha)\ +\ g_T(\alpha)\ (Y_2(\alpha)\ \times\ \vec{s}(\alpha)\ )_1\ ]$$

Spherical nuclei

Parabolic rule for proton-neutron multiplets in the particle-vibration model

Exchange of the quadrupole phonon

The particle-quadrupole vibration interaction is

$$H_2 = \sqrt{20\pi}\, a_2 |Y_2(b_2^\dagger + b_2)|_0$$

$$a_2 = \tfrac{1}{3}(4\pi)^{\frac{1}{2}} \frac{1}{ZR_0^2} \langle k \rangle [B(\mathrm{E2}; 2_1^+ \rightarrow 0_1^+)_{\mathrm{vib}}]^{\frac{1}{2}}$$

For the quasiparticle, we also include the usual blocking factors U and V in the interaction strength a_2. The symbol $b_2^\dagger$ denotes the creation operator of the quadrupole phonon.

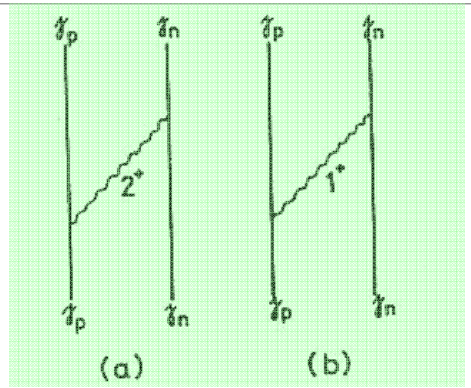

Second-order diagrams for exchange of the quadrupole (fig. a) and spin-vibrational phonons (fig. b).

The contribution to the splitting of the multiplet $|(j_p, j_n)I = |j_p - j_n|, \ldots, j_p + j_n\rangle$ coming from the exchange of quadrupole phonons (fig. a) is

$$\delta E_2 = -\alpha_2 \mathscr{V} \cdot \frac{[I(I+1) - j_n(j_n+1) - j_p(j_p+1)]^2 + [I(I+1) - j_n(j_n+1) - j_p(j_p+1)]}{2j_n(2j_n+2)2j_p(2j_p+2)}$$

$$+ \frac{\alpha_2 \mathscr{V}}{12},$$

$$\alpha_2 = 15a_2^2/\hbar\omega_2$$

Here $\hbar\omega_2$ is the energy of the quadrupole phonon. We assume the coupling strength a_2 to be equal both for protons and for neutrons.

We rewrite the I-dependent terms

$$\delta E_2(I) = A[I(I+1)]^2 + BI(I+1)$$

where A and B stand for the factors which multiply $[I(I+1)]^2$ and $I(I+1)$ respectively.

The quantity $\mathscr{V}$ is the occupation number defined as $\mathscr{V} = 1$ if $|j_p\rangle$ and $|j_n\rangle$ are both particle-like or both hole-like: $\mathscr{V} = -1$ if $|j_n\rangle$ is particle-like and $|j_n\rangle$ is hole-like, or vice versa.

Inclusion of the spin-vibrational 1^+ phonon

The particle-spin-vibration interaction reads

$$H_1 = \sqrt{3}a_1[\sigma_1 \times (b_1^\dagger + b_1)]_0$$

Here a_1 is the coupling strength defined as $a_1 = \kappa_1(\hbar\omega_1/2c_1)^{\frac{1}{2}}$, σ_1 is the spin operator and $b_1^\dagger$ the creation operator of the $\lambda = 1^+$ spin vibration

We derive the expression for the contribution to the energy shift of the $|(j_p j_n)I\rangle$ states due to the exchange of the 1^+ phonon

$$\delta E_1(I) = B_1 I(I+1) + \alpha_1 \frac{j_n(j_n+1)+j_p(j_p+1)}{(2j_n+2)(2j_p+2)}$$

$$B_1 = -\alpha_1 \frac{\xi}{(2j_p+2)(2j_n+2)} \qquad \alpha_1 = 4\frac{a_1^2}{\hbar\omega_1}$$

$$\xi = \begin{cases} 1 & \text{if } \mathcal{N} = -1, \quad \dfrac{(2j_p+2)(2j_n+2)}{2j_p 2j_n} \quad \text{if } \mathcal{N} = 1, \\ -\dfrac{2j_p+2}{2j_p} & \text{if } \mathcal{N} = 0^-, \quad -\dfrac{2j_n+2}{2j_n} \quad \text{if } \mathcal{N} = 0^+. \end{cases}$$

$\mathcal{N}$ is the Nordheim number defined as

$$\mathcal{N} = j_p - l_p + j_n - l_n$$

For $\mathcal{N} = 0$, we use the labels $-$ and $+$. The symbols $\mathcal{N} = 0^-$ and $\mathcal{N} = 0^+$ denote the situations $j_n - l_n = -\frac{1}{2}$, $j_p - l_p = \frac{1}{2}$ and $j_n - l_n = \frac{1}{2}$, $j_p - l_p = -\frac{1}{2}$, respectively.

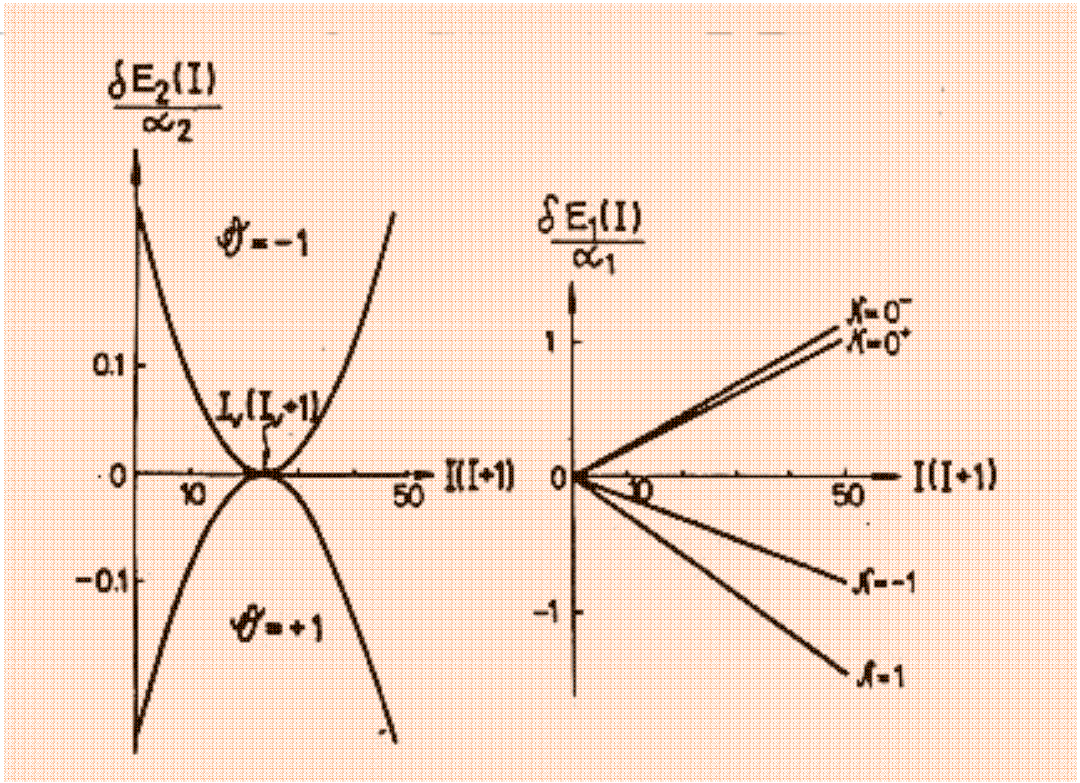

Illustration of energy contributions coming from the exchange of the quadrupole phonon (a) and the spin-vibrational phonon (b) for the multiplet ($j_p = \frac{5}{2}, j_n = \frac{3}{2}$), for four possible combinations of the pair ($\mathcal{Y}$, $\mathcal{N}$).

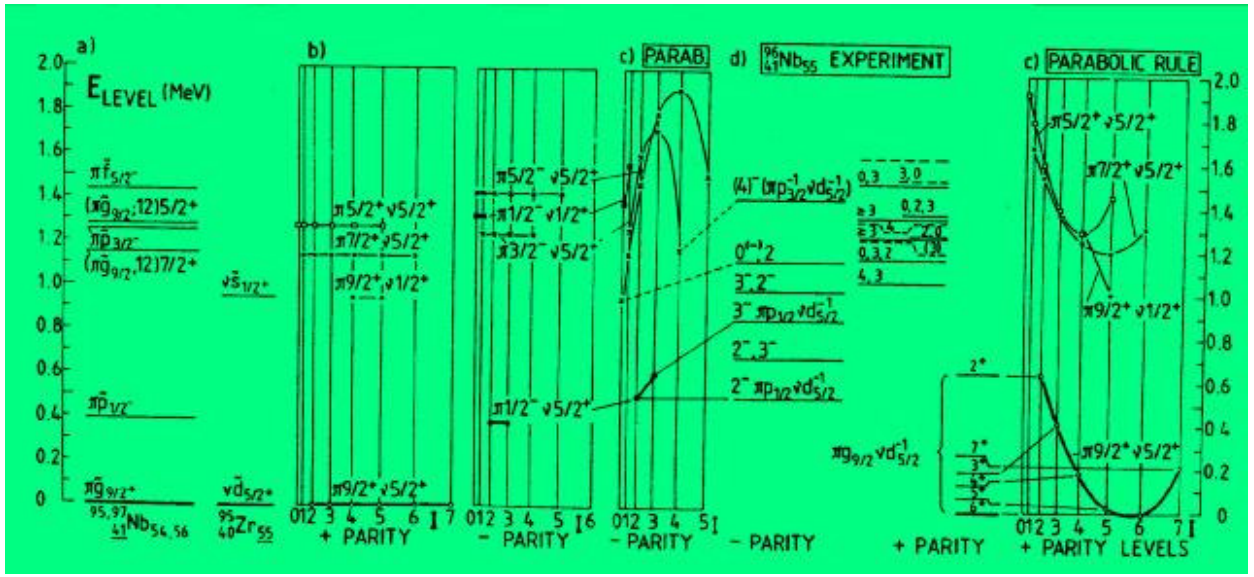
a)
b)
c) PARAB.
d) $^{96}_{41}Nb_{55}$ EXPERIMENT
c) PARABOLIC RULE
E_{LEVEL} (MeV)
+ PARITY
- PARITY
- PARITY
- PARITY
+ PARITY
+ PARITY LEVELS
$^{95,97}_{41}Nb_{54,56}$
$^{95}_{40}Zr_{55}$

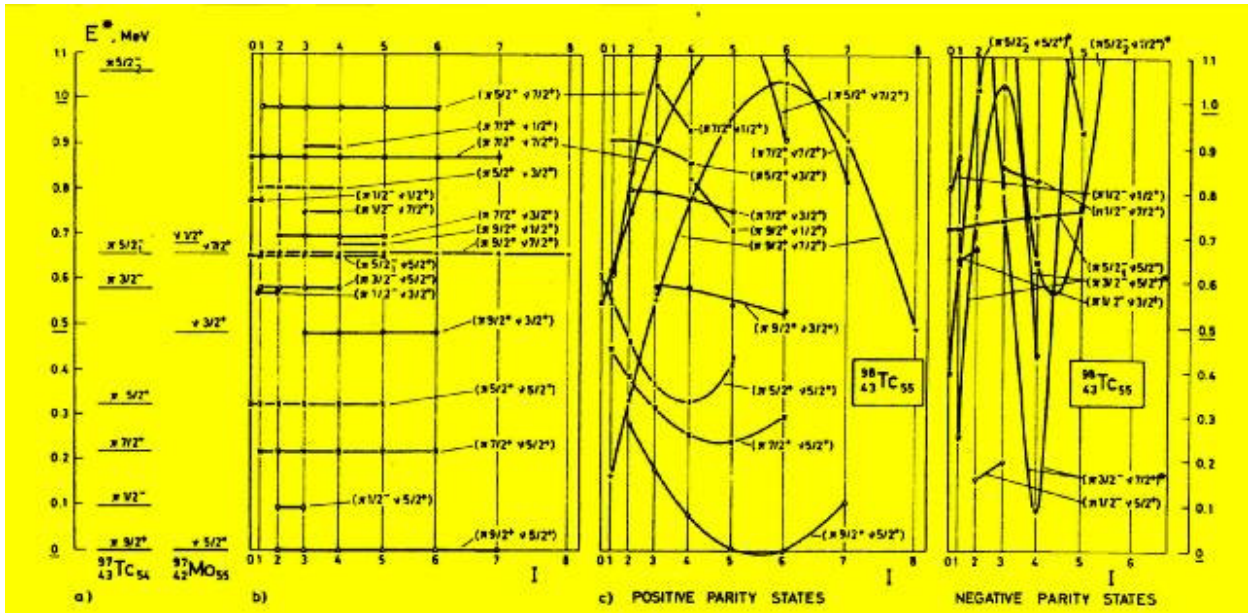
E^*, MeV
a)
b)
c) POSITIVE PARITY STATES
NEGATIVE PARITY STATES
$^{97}_{43}Tc_{54}$
$^{97}_{42}Mo_{55}$
$^{98}_{43}Tc_{55}$

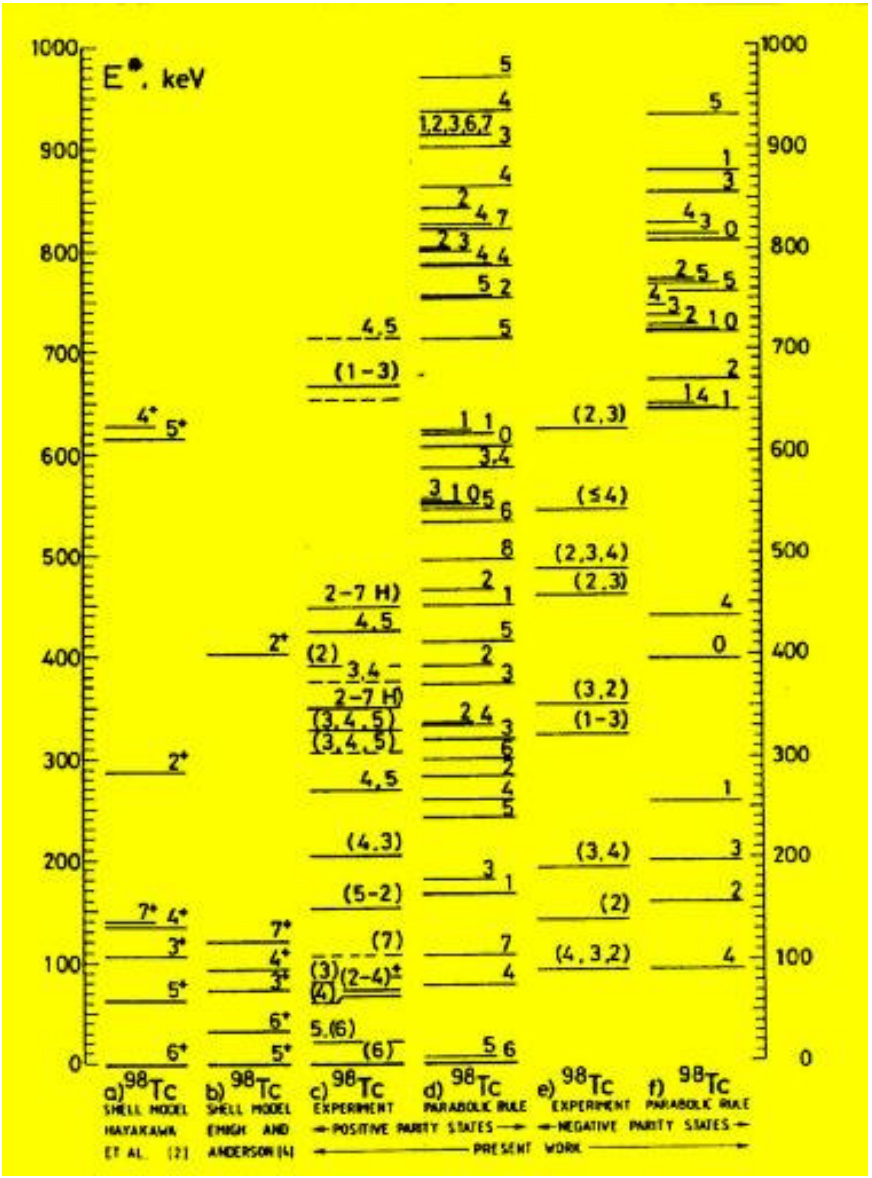
E*, keV
a) 98Tc SHELL MODEL HAYAKAWA ET AL. [2]
b) 98Tc SHELL MODEL EMIGH AND ANDERSON [4]
c) 98Tc EXPERIMENT
d) 98Tc PARABOLIC RULE
e) 98Tc EXPERIMENT
f) 98Tc PARABOLIC RULE
POSITIVE PARITY STATES
NEGATIVE PARITY STATES
PRESENT WORK

For spherical nuclei, with only the dynamical interaction and $\chi = 0$

$$\Gamma_0 = a \sqrt{\frac{4\ \pi}{5\ N}}$$

^{96}Y

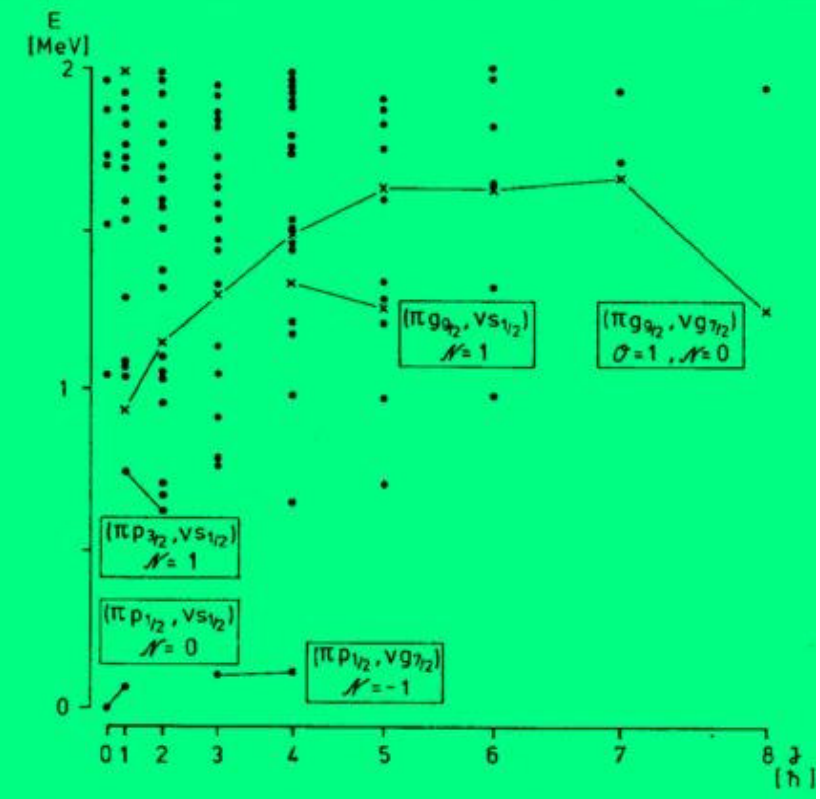

Fig. 4. Negative- and positive-parity levels of ^{96}Y calculated in IBFFM. Negative parity levels are denoted by full circles and positive-parity by crosses. The states classified into the same multiplet on the basis of largest components in the wave functions, are connected by full line

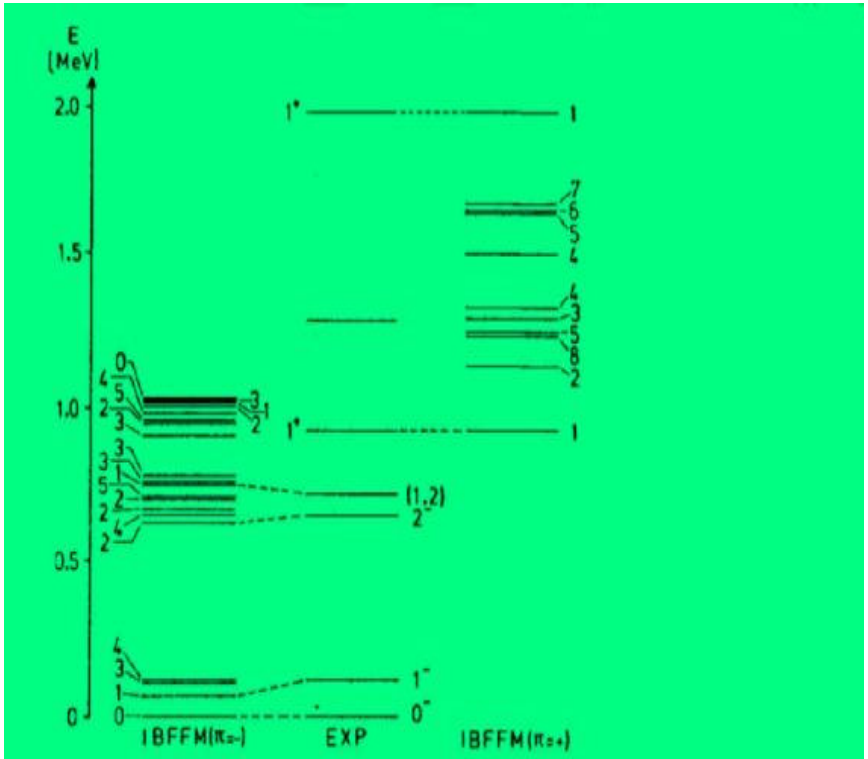

Fig. 5. IBFFM positive- and negative-parity energy spectrum of ^{96}Y in comparison to the available experimental data. The excitation energy of the 8^+ level is not known, but it should amount to $\geqq 1$ MeV, see text

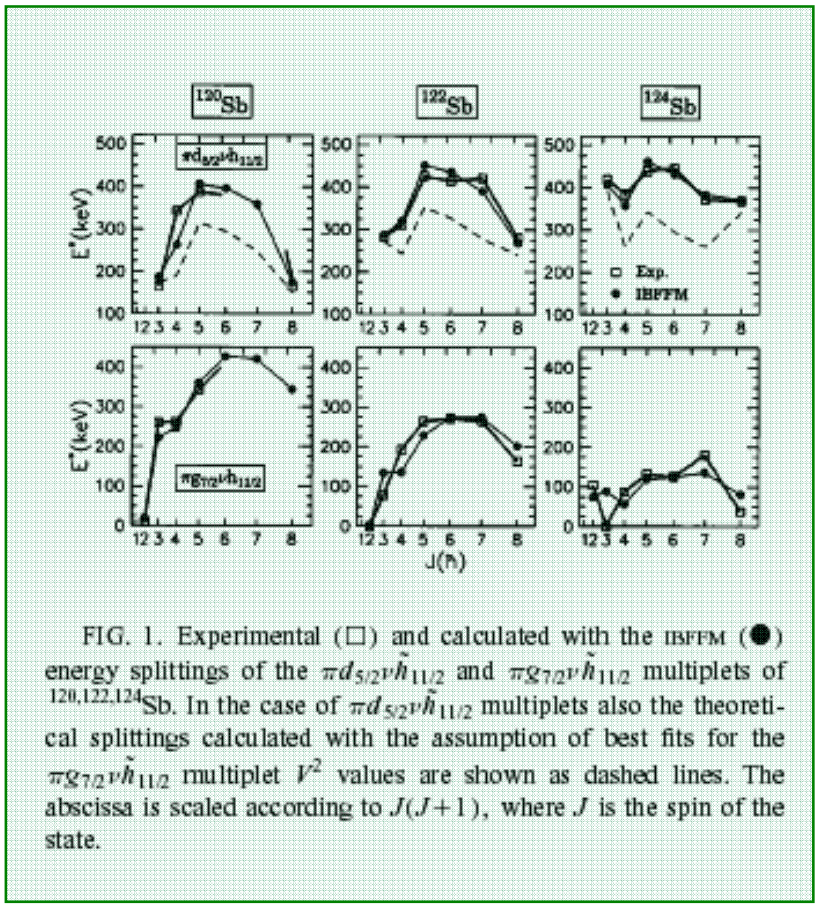

FIG. 1. Experimental (□) and calculated with the IBFFM (●) energy splittings of the $\pi d_{5/2}\nu\tilde{h}_{11/2}$ and $\pi g_{7/2}\nu\tilde{h}_{11/2}$ multiplets of ^{120,122,124}Sb. In the case of $\pi d_{5/2}\nu\tilde{h}_{11/2}$ multiplets also the theoretical splittings calculated with the assumption of best fits for the $\pi g_{7/2}\nu\tilde{h}_{11/2}$ multiplet V^2 values are shown as dashed lines. The abscissa is scaled according to $J(J+1)$, where J is the spin of the state.

In the whole sequence of nuclei it have been used the same:

Cores

Dynamical, exchange and monopole interactions for protons

Dynamical, exchange and monopole interactions for neutrons

Occupation probabilities for protons

Residual proton-neutron delta interaction

Occupation probabilities for neutrons depend on the isotope

Parabolic like structures are present in spherical nuclei even in cases when other interactions (not the dynamical) dominate.

Sb isotopes

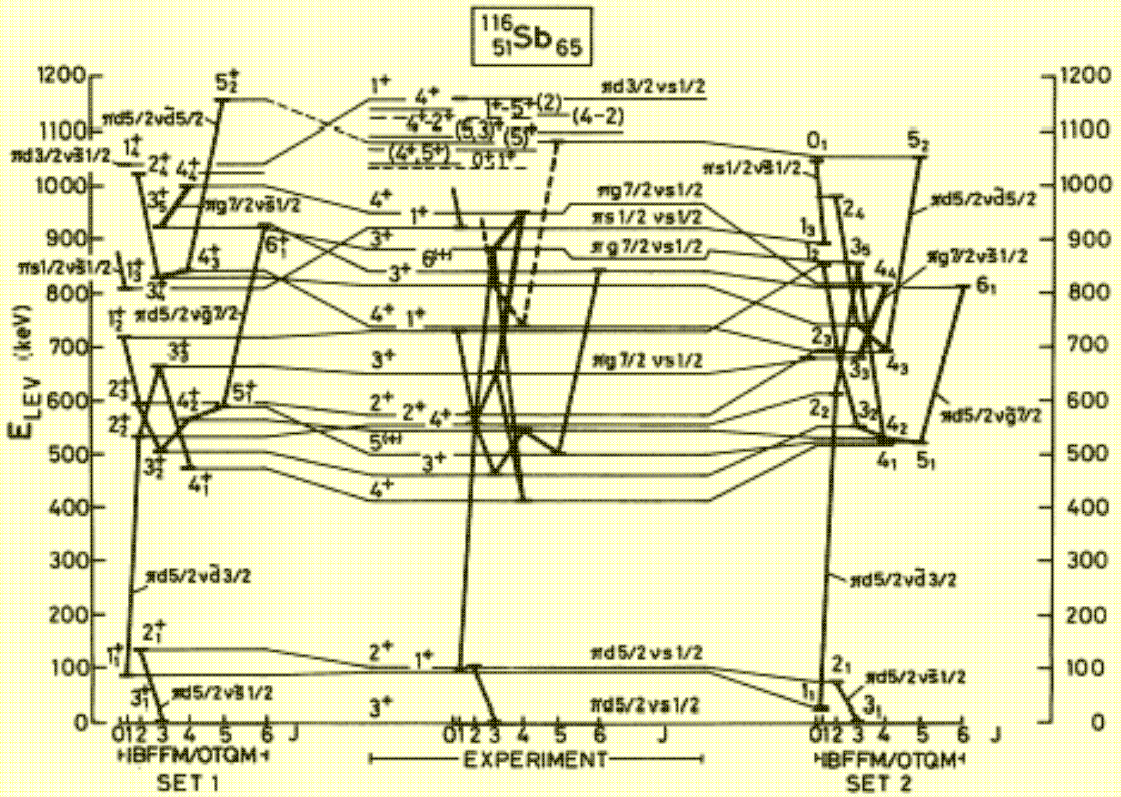

FIG. 6. IBFFM energy spectrum of ^{116}Sb in comparison with experimental data. The solid lines connect the members of the given multiplet. The leading proton-neutron configurations for several multiplets were identified on the basis of the (^3He,d) proton transfer results [4].

TABLE III. Comparison of measured and calculated in IBFFM spectroscopic factors for the ^{121}Sb$(p,d)^{120}$Sb one-neutron transfer reaction. The first two columns contain the energy, spin, and parity of the final states involved in the reaction taken from Ref. [8].

Energy (keV)	J^π	ℓ_n	$S_{(p,d)}$ [a]	S_{IBFFM} [b]
0	1^+	2	0.11	0.15
78	3^+	0	0.19	0.12
149	3^+	0	0.05	0.03
166	3^-	5	0.63	0.44
193	2^+	0	0.11	0.08
		2	0.07	0.05
233	2^+	0	0.06	0.03
		2	0.12	0.05
334	$4^{(+)}$	2	0.10	0.19
343	$4^{(-)}$	5	0.54	0.39
387	$(3-5)$	5	0.44	0.61
390	$(2,3)^+$	2	0.06	0.07
438	(2)	0	0.01	0.02
		2	0.02	0.13

[a] Reference [9].
[b] $S/(2j_{\mathrm{target}}+1)$.

TABLE IV. Comparison of measured and calculated in IBFFM spectroscopic factors for the one-neutron transfer reactions leading to ^{122}Sb. The first two columns contain the energy, spin, and parity of the final states involved in the reaction taken from Ref. [13].

Energy (keV)	J^π	ℓ_n	$S_{(p,d)}$ [a]	ℓ_n	$S_{(d,t)}$ [b]	S_{IBFFM} [d]	ℓ_n	$S_{(d,p)}$ [c]	S_{IBFFM}
0	2^-	5	0.20		0.46	0.46			
61	3^+	0	0.23	(0)	0.45	0.13	(2)	0.05	0.00
78	3^-	5	0.46			0.52			
121	1^+						(2)	0.30	0.47
137	5^+	2	0.38	(2)	0.37	0.20			
164	8^-	5	0.50			0.53			
167	2^+	2	0.10			0.14	(2)	0.09	0.09
193	4^-	5	0.41			0.58			
210	4^+	0	0.30	(0)	0.34	0.11			
255	3^+						0	0.34	0.44
264	5^-					0.66			
265	7^-	5	0.62			0.57			
272	6^-					0.68			
283	3^-						(5)	2.40	0.40
311	4^-						(5)	0.80	0.43
323	2^+						0	0.30	0.40
334	3^+	2	0.07		0.09	0.22	2	0.16	0.01
394	4^+						2	0.45	0.46
397	2^+	2	0.03		0.10		2	0.45	0.38
414	6^-								0.55
$\approx$ 420	7^-	5	0.03			0.16	(5)	1.70	0.43
425	5^-								0.49
481	4^+	2	0.19	(2)	0.30	0.22			
484	3^+						2	0.51	0.60

[a] Reference [9].
[b] Reference [7].
[c] Reference [13].
[d] $S/(2j_{\mathrm{target}}+1)$.

TABLE VI. Magnetic dipole (μ in μ_N) and electric quadrupole (Q in e b) moments of some $^{120-124}$Sb states.

Nucleus	E^*	J^π	μ_{expt} [a]	μ_{IBFFM}	Q_{expt} [a]	Q_{IBFFM}
^{120}Sb	0 keV	1^+	$\pm$2.34(22)	+2.25		–0.10
	78 keV	3^+	+2.584(6)	+2.67	$\pm$0.41(4)	–0.47
		8^-	$\pm$2.34(4)	+2.45		–0.51
^{122}Sb	0 keV	2^-	–1.905(20)	–2.33	+0.85(11)	–0.08
	61 keV	3^+	+2.983(12)	+3.07	$\pm$0.41(4)	–0.48
	137 keV	5^+	+3.05(10)	+3.07		–0.62
^{124}Sb	0 keV	3^-	$\pm$1.20(2)	–1.23	+1.87(38)	+0.35
	41 keV	3^+	+2.970(33)	+3.01		–0.46
	125 keV	6^-	+0.384(12)	+0.36		+0.16

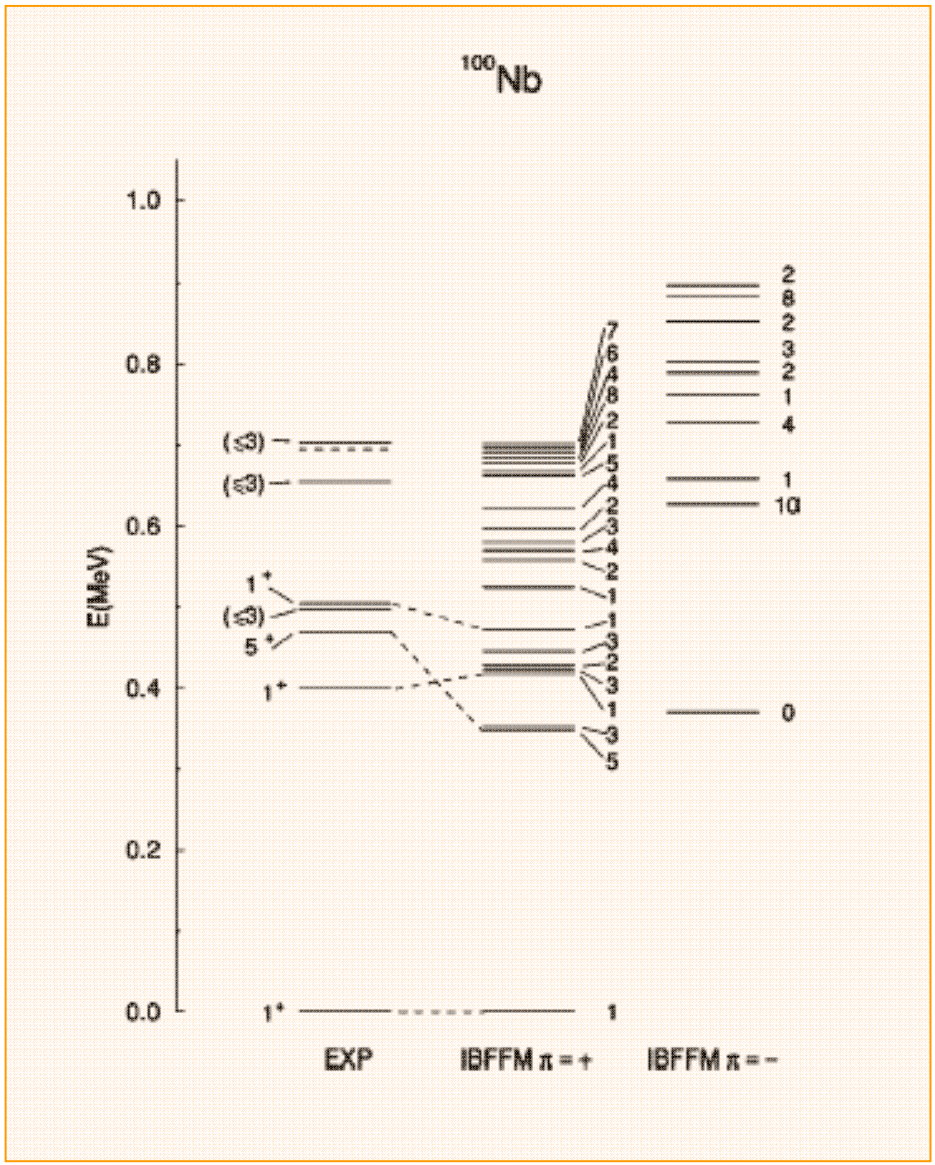

1^+ π g9/2 ν g7/2

5^+ π g9/2 ν s1/2

8^+ π g9/2 ν g7/2

10^- π g9/2 ν h11/2

5^+ 1.5 s isomer

10^- possibly 100 – 150 keV higher

10^- or 8^+ candidates for the 12 µs isomer

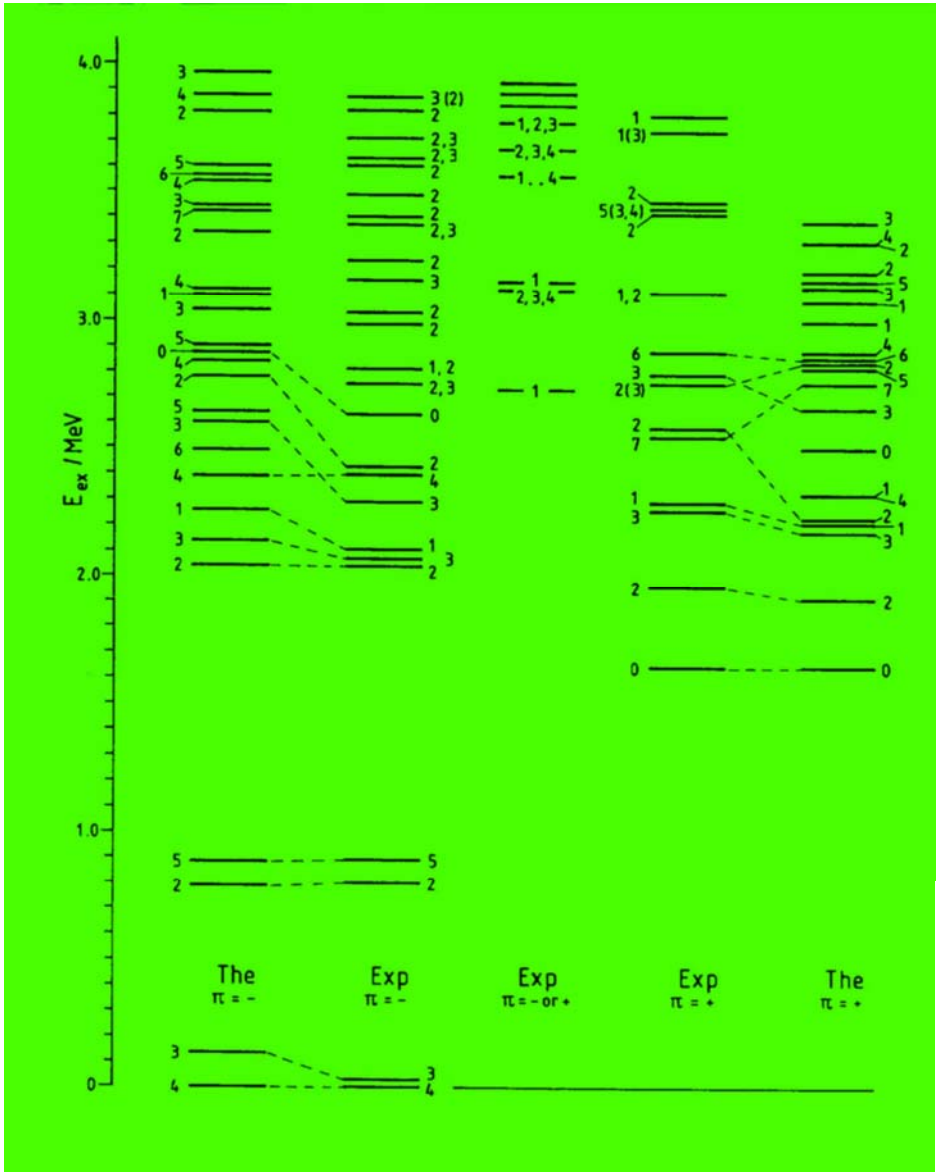

^{40}K

State (keV)	$T_{1/2}$	
	Exp	The
3_1^- (30)	4.24(8) ns	5.2 ns
2_1^- (800)	0.28(4) ps	0.23 ps
5_1^- (891)	0.87(14) ps	0.6 ps
2_2^- (2047)	0.34(4) ps	0.3 ps
3_2^- (2070)	0.47(10) ps	0.1 ps
1_1^- (2104)	0.52(10) ps	0.14 ps
4_2^- (2397)	0.035(14) ps	0.03 ps
0_1^- (2626)	0.21(4) ps	0.2 ps
1_1^+ (2290)	0.083(14) ps	0.25 ps
3_2^+ (2787)	<0.04 ps	0.07 ps
6_1^+ (2879)	0.27(10) ps	0.6 ps

^{40}K

Transition[a]		E_{tr}/keV	Gamma-branching	
			Exp[b]	The[c]
2_1^- (800)	$\rightarrow 4_1^-$ (0)	800	0.15	0.17
	$\rightarrow 3_1^-$ (30)	770	100	100
5_1^- (891)	$\rightarrow 4_1^-$ (0)	891	99	99
	$\rightarrow 3_1^-$ (30)	862	1	0.1
2_2^- (2047)	$\rightarrow 4_1^-$ (0)	2047	29	128
	$\rightarrow 3_1^-$ (30)	2018	29	100
	$\rightarrow 2_1^-$ (800)	1247	41	41
3_2^- (2070)	$\rightarrow 4_1^-$ (0)	2070	36	56
	$\rightarrow 3_1^-$ (30)	2040	49	49
	$\rightarrow 2_1^-$ (800)	1270	9	6
	$\rightarrow 5_1^-$ (891)	1178	7	3
1_1^- (2104)	$\rightarrow 3_1^-$ (30)	2074	70	70
	$\rightarrow 2_1^-$ (800)	1304	29	96
	$\rightarrow 2_2^-$ (2047)	57	—	0.1
	$\rightarrow 3_2^-$ (2070)	34	—	0.0
4_2^- (2397)	$\rightarrow 4_1^-$ (0)	2397	26	7
	$\rightarrow 3_1^-$ (30)	2367	67	67
	$\rightarrow 2_1^-$ (800)	1597	—	0.4
	$\rightarrow 5_1^-$ (891)	1506	—	0.1
	$\rightarrow 2_2^-$ (2047)	350	—	0.0
	$\rightarrow 3_2^-$ (2070)	327	7	1
	$\rightarrow 3_3^-$ (2291)	106	—	0.01
0_1^- (2626)	$\rightarrow 2_1^-$ (800)	1826	30	41
	$\rightarrow 2_2^-$ (2047)	579	—	0.001
	$\rightarrow 1_1^-$ (2104)	522	70	70
	$\rightarrow 2_3^-$ (2419)	207	—	0.0
1_1^+ (2290)	$\rightarrow 0_1^+$ (1644)	646	56	56
	$\rightarrow 2_1^+$ (1959)	331	9	10
	$\rightarrow 3_1^+$ (2260)	30	—	0.0
3_2^+ (2787)	$\rightarrow 2_1^+$ (1959)	828	17.4	17.4
	$\rightarrow 3_1^+$ (2260)	527	—	0.5
	$\rightarrow 1_1^+$ (2290)	497	—	0.0
	$\rightarrow 2_2^+$ (2576)	211	—	0.0
	$\rightarrow 2_3^+$ (2757)	30	—	0.0

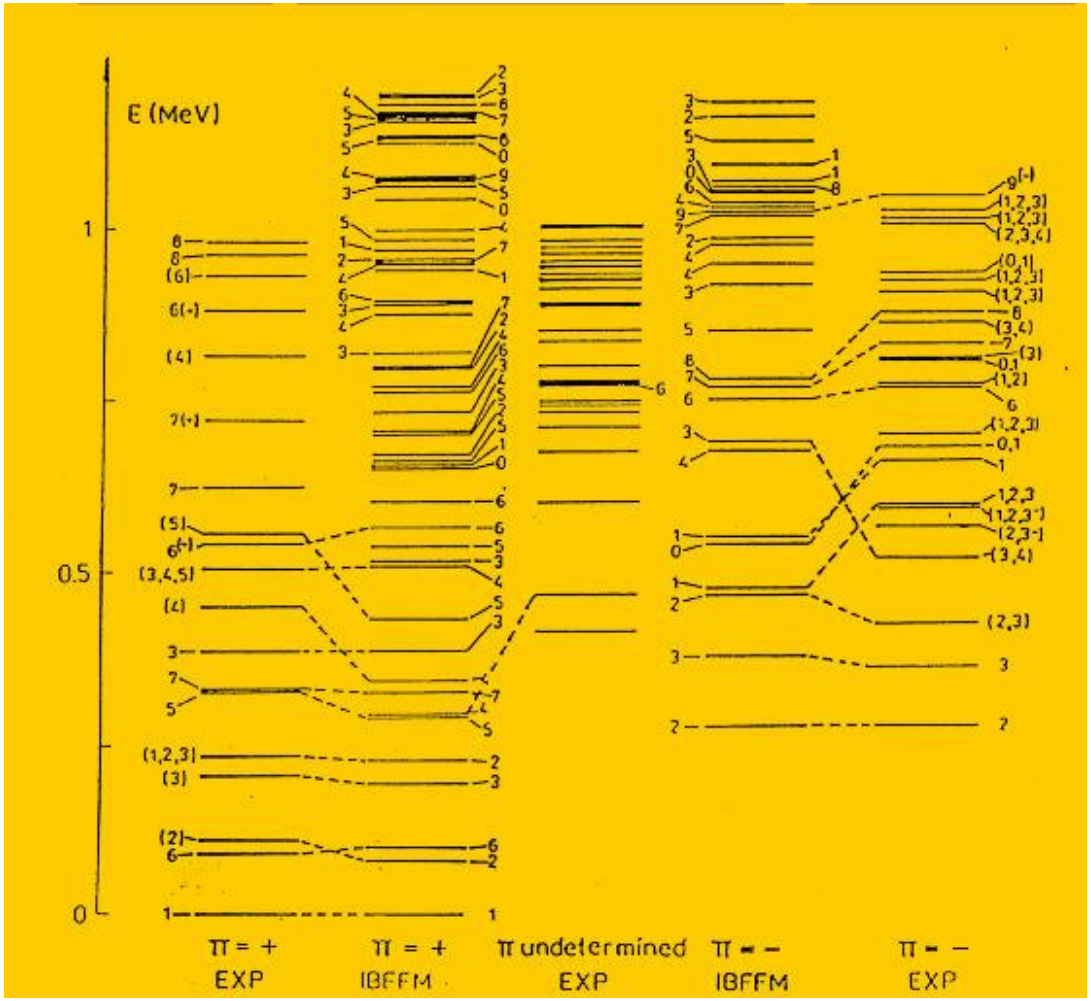

The structure of ^{106}Ag is very complex. The ground states of odd-mass Ag nuclei are $7/2^+$ states based on the proton g9/2 configuration. The IBFFM is successful in the description even of such nuclei.

Deformed nuclei

protons **neutrons**

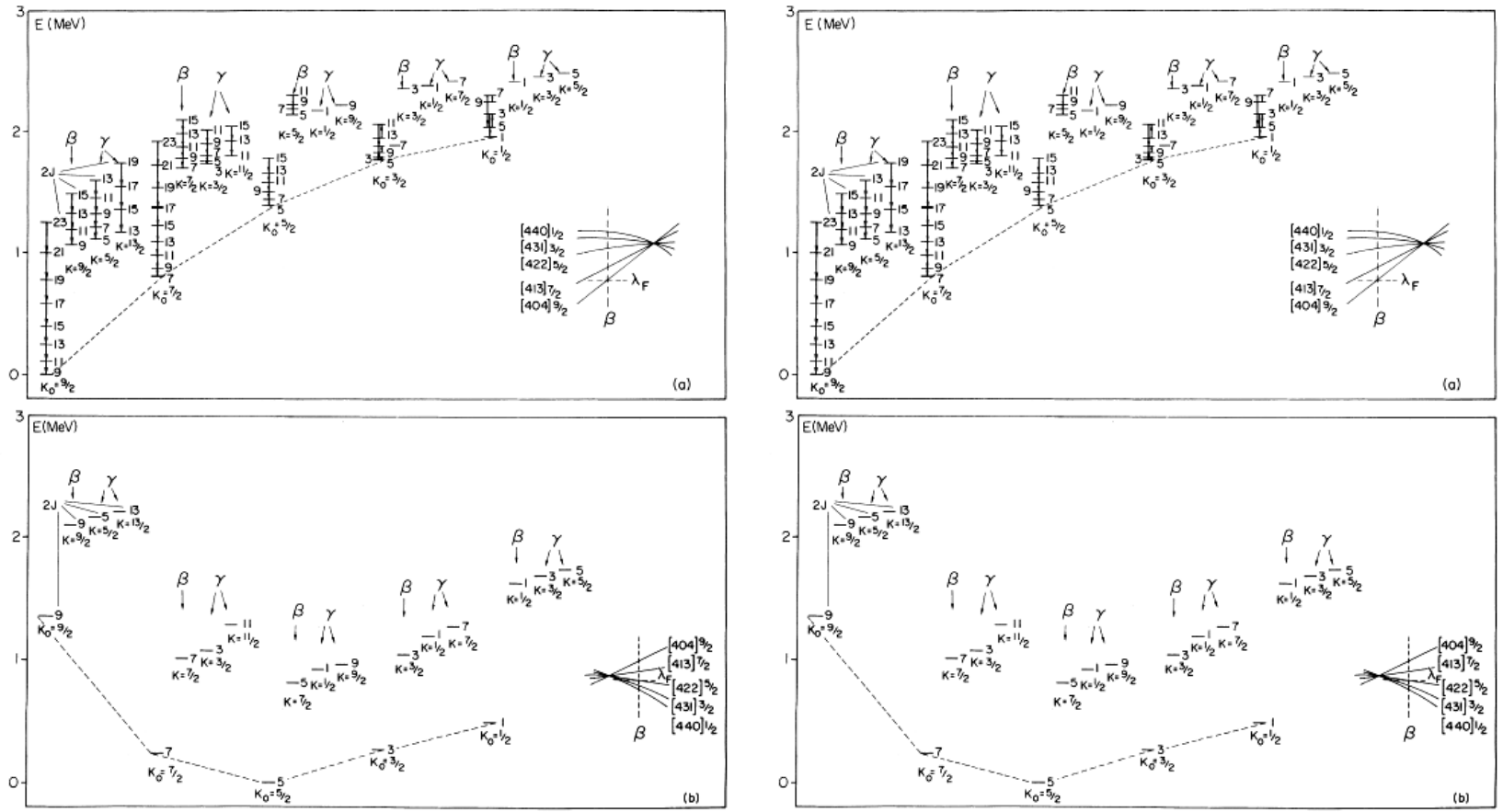

coupling → **bands !!!!!**

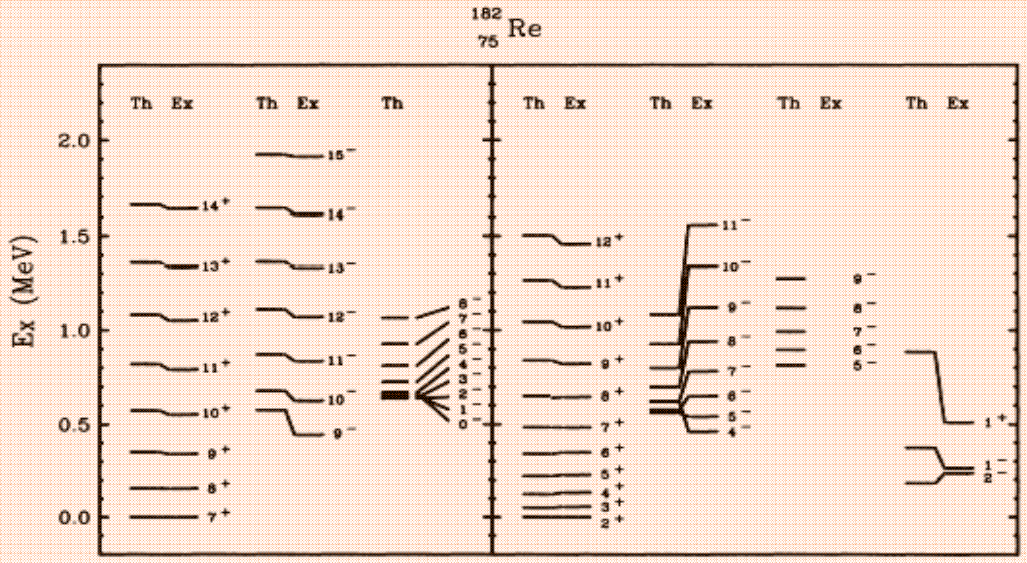

IBFFA-calculated excitation energies for states in odd-odd ^{182}Re compared with experimental data. Because the experimental separation between the 7^+ triplet and 2^+ singlet couplings is not known, the figure is divided into two parts, using each coupling as the reference point. Otherwise, the triplet coupling is shown on the left of a pair of bands, the singlet coupling on the right. For example; 9^- triplet, 0^- singlet.

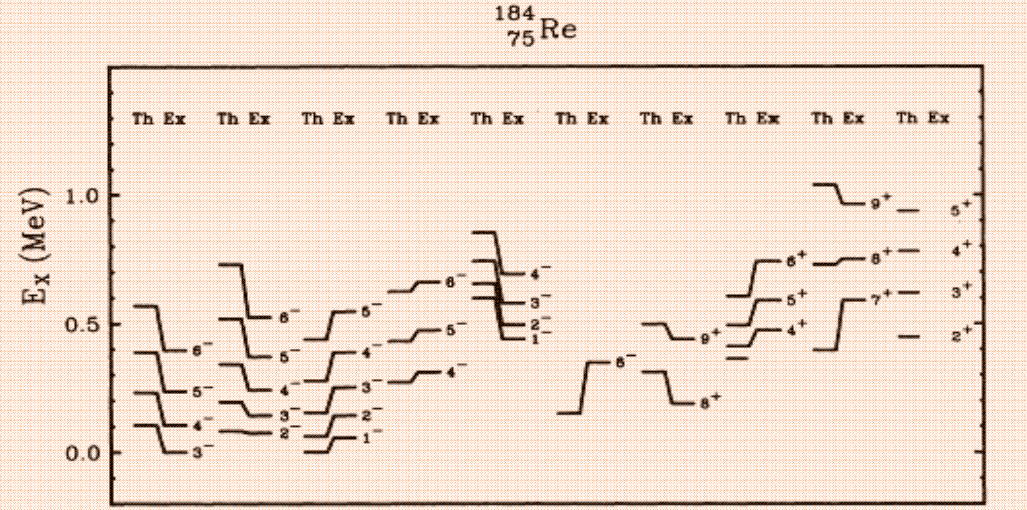

IBFFA-calculated excitation energies for states in odd-odd ^{184}Re compared with experimental data. The bands are plotted in pairs, with the triplet coupling on the left, the singlet coupling on the right of each pair.

Scholten
PRC 37

Quadrupole moments for odd-odd Re isotopes.

Isotope	J^π	Q_{IBA} (e b)	Q_{exp} (e b)
^{180}Re	6^-	6.50	
	1^-	6.45	
^{182}Re	7^+	5.66	<6.4
	2^+	5.40	>6.6
^{184}Re	3^-	5.06	7.9 ± 0.7
	8^+	4.83	

Magnetic moments for odd-odd Re isotopes.

Isotope	J^π	μ_{IBA} (μ_{N})	μ_{exp} (μ_{N})
^{180}Re	6^-	2.41	
	1^-	2.35	
^{182}Re	7^+	2.33	2.76 ± 0.07
	2^+	3.28	3.07 ± 0.24
^{184}Re	3^-	3.19	2.50 ± 0.19
	8^+	2.09	2.89 ± 0.13

The investigations of odd-A nuclei have revealed the following decoupled–strongly coupled rule:

(i) The strongly coupled band pattern arises if the odd fermion is a particle coupled to an oblate core, or a hole coupled to a prolate core.

(ii) The decoupled band pattern arises if the odd particle is coupled to a prolate core or a hole to the oblate core.

This rule was extended to odd-odd nuclei in the case of coupling two quasiparticles to the asymmetric rotor.

Rules (i) and (ii) can be expressed in terms of quadrupole moments of the odd particle and the core Taking into account the signs of quadrupole moments $Q(j)<0$, $Q(j^{-1})>0$, $Q(2_1^{\text{prolate}})<0$, and $Q(2_1^{\text{oblate}})>0$, the rule reads

$$\text{if } Q(\bar{j})\cdot Q(2_1^{\text{core}}) \begin{cases} <0, & \text{the band is strongly coupled} \\ >0, & \text{the band is decoupled} , \end{cases}$$

where $\bar{j}$ denotes the odd quasiparticle coupled to the core.

This rule is of more general character, independent of the particular nature of the core. It applies as well to the IBFM and IBFFM.

We note that the case of two particles or holes coupled to the core, referred to as the "peaceful" case in the particle–plus–asymmetric rotor model, corresponds to the inverted parabola of the parabolic rule for odd-odd nuclei;[2] this yields the bandheads with angular momenta $J=j_p+j_n$ and $J=|j_p-j_n|$ as the lowest states on two branches of the parabola.

By coupling the proton particle j_1 and the neutron particle j_2 to the SU(3) boson core, there arise $2(j_1+\frac{1}{2})(j_2+\frac{1}{2})$ bands, based on the states of angular momenta $J=J_1\pm J_2$, with $J_1=j_1, j_1-1, \ldots, \frac{1}{2}$ and $J_2=j_2, j_2-1, \ldots, \frac{1}{2}$. For the particular interaction strengths Γ_1^{SUSY} and Γ_2^{SUSY} the band based on the lowest $J=j_1+j_2$ state exhibits an exact $J(J+1)$ energy rule, with the same moment of inertia as for the ground-state band of the boson core. Furthermore, the states of this band are characterized by the exact quantum numbers $(K_1=j_1, K_2=j_2)K=j_1+j_2$, defined according to the IBFFM relation The other IBFFM bands in the odd-odd system deviate from the $J(J+1)$ energy rule; in general, more so with increasing energy (decrease of K_1, K_2). Simultaneously, the IBFFM wave functions expressed in the KR basis are a mixture of different K values. However, in each state a particular KR basis state dominates. In this way we can attribute approximate quantum numbers $(K_1, K_2)K$ to each state.

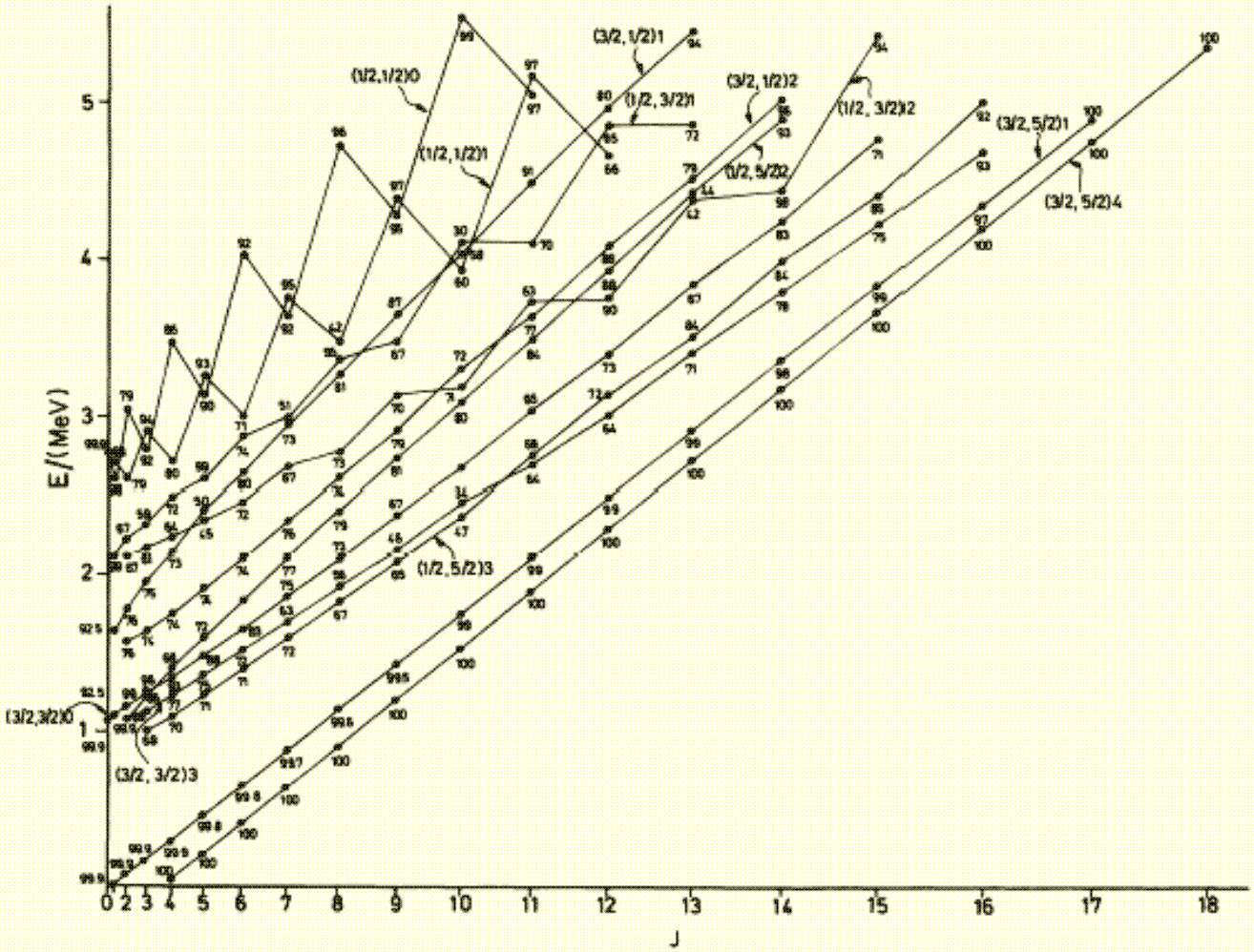

Twelve ground-state bands calculated in the IBFFM for the odd-odd system with $j_1 = \frac{3}{2}$ proton hole and $j_2 = \frac{5}{2}$ neutron hole coupled to the SU(3) prolate boson core. The $J(J+1)$ scale is employed for the angular momentum axis.

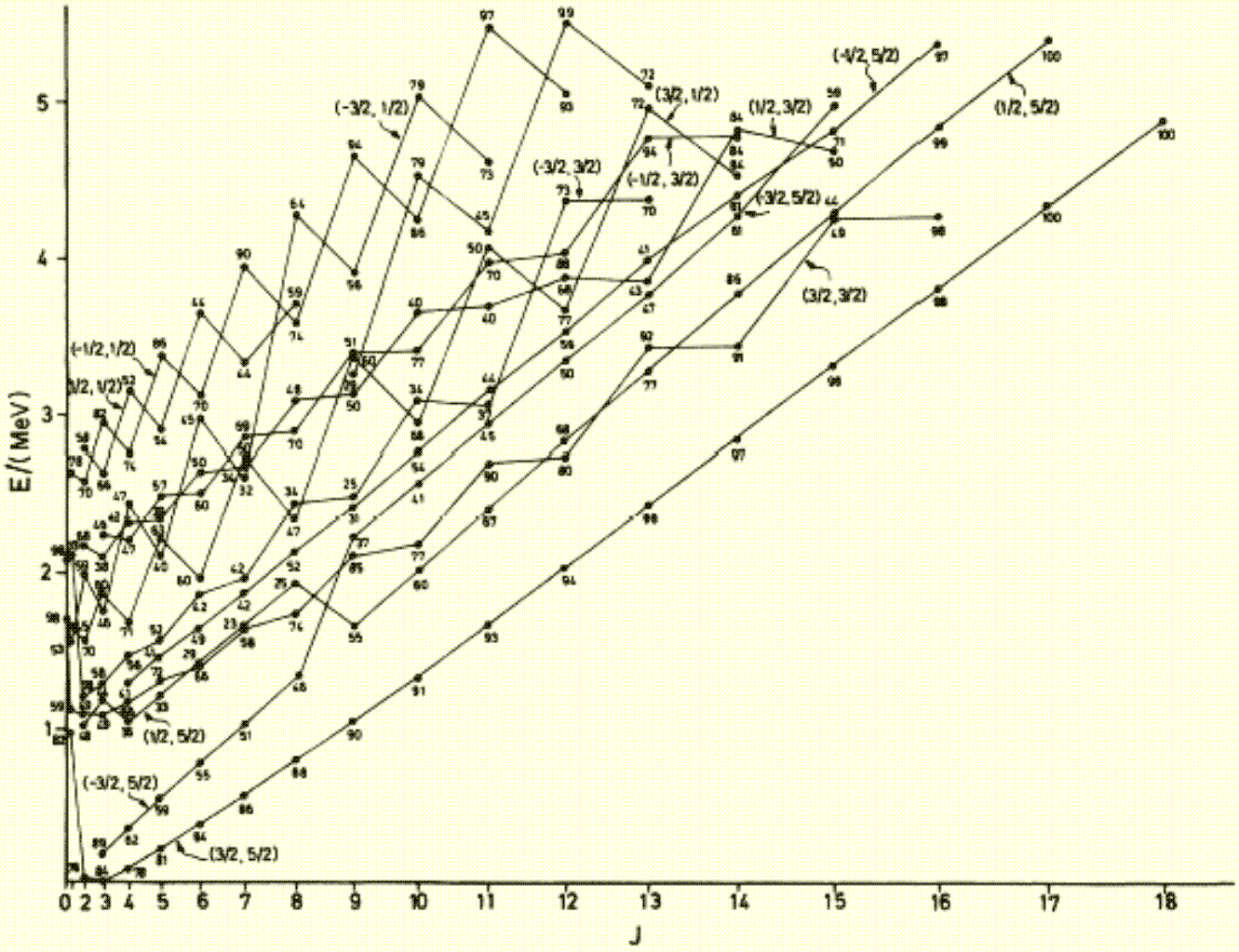

The IBFFM ground-state bands for the odd-odd system with $j_1 = \frac{3}{2}$ proton particle and $j_2 = \frac{5}{2}$ neutron hole coupled to the SU(3) prolate boson core.

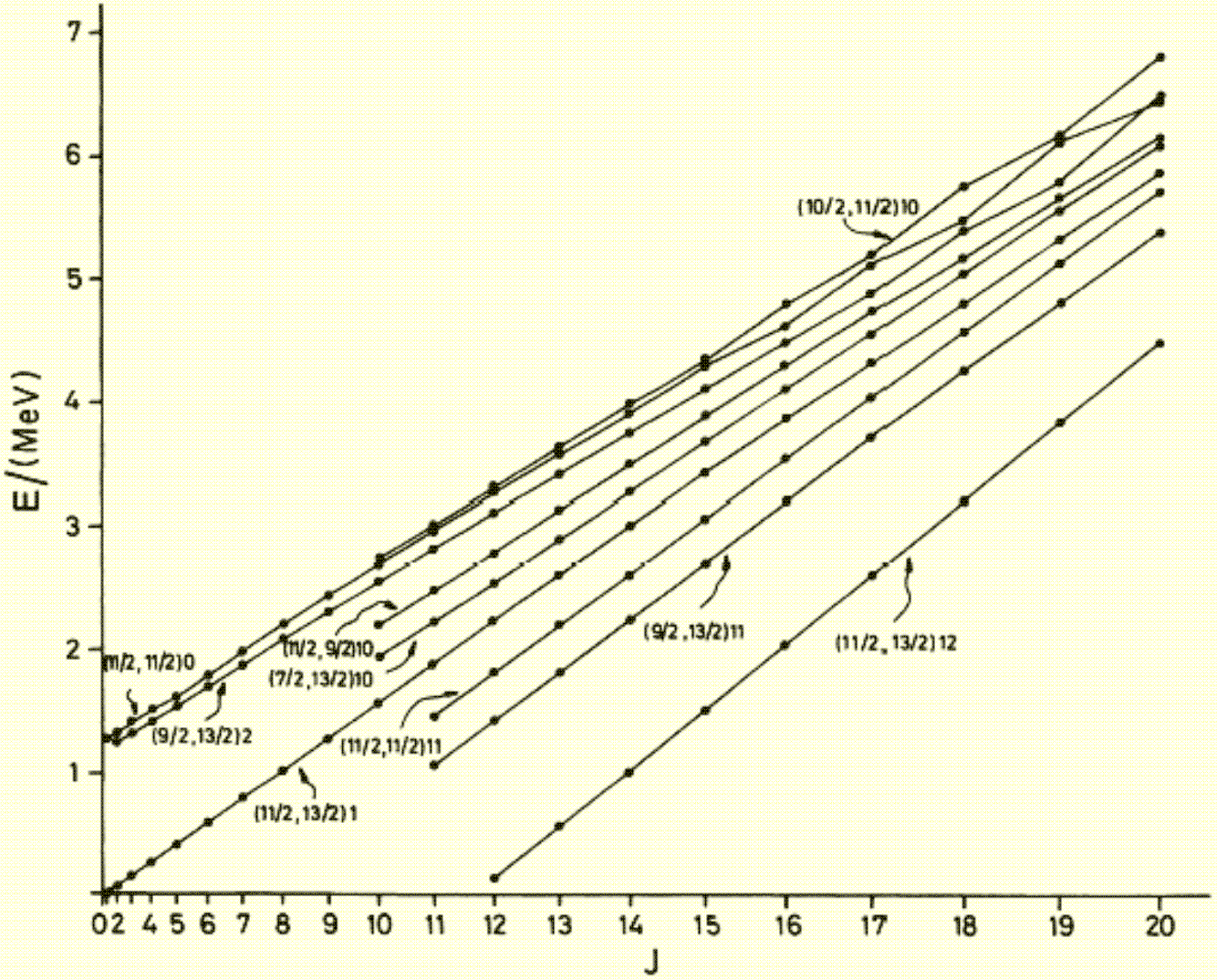

Lowest bands in the odd-odd system with $j_1 = \frac{11}{2}$ proton hole and $j_2 = \frac{13}{2}$ neutron hole coupled to the SU(3) prolate boson core.

Realistic case: Dynamical and exchange interactions different from zero and not limited by supersymmetry constraints

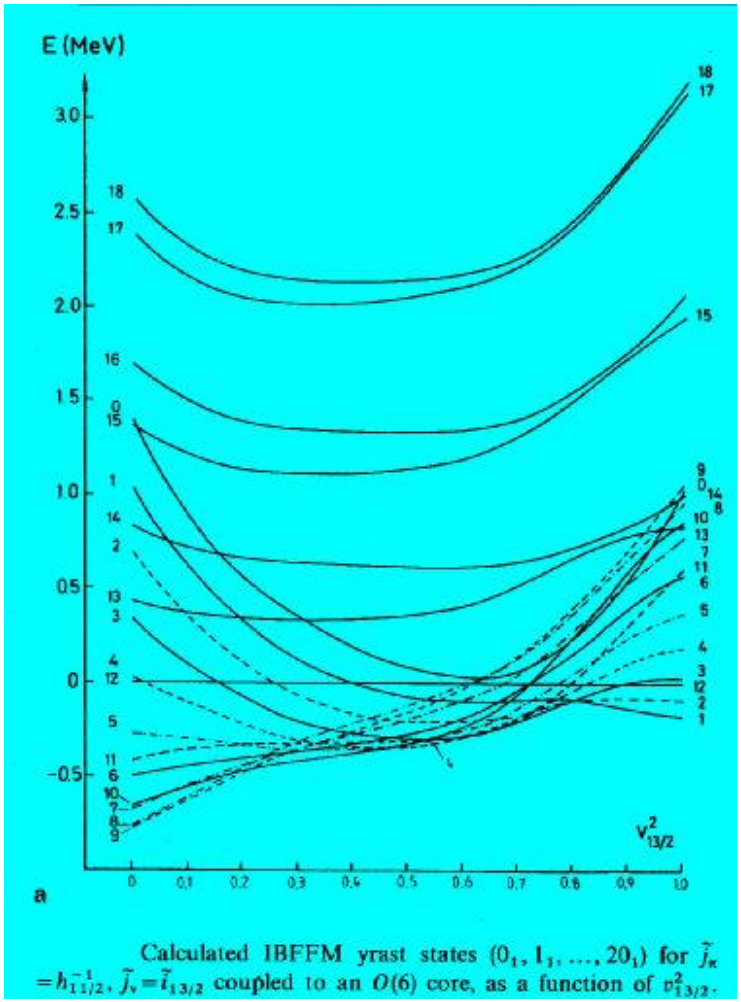

Calculated IBFFM yrast states $(0_1, 1_1, \ldots, 20_1)$ for $\tilde{j}_\pi = h^{-1}_{11/2}$, $\tilde{j}_\nu = \tilde{l}_{13/2}$ coupled to an $O(6)$ core, as a function of $v^2_{13/2}$.

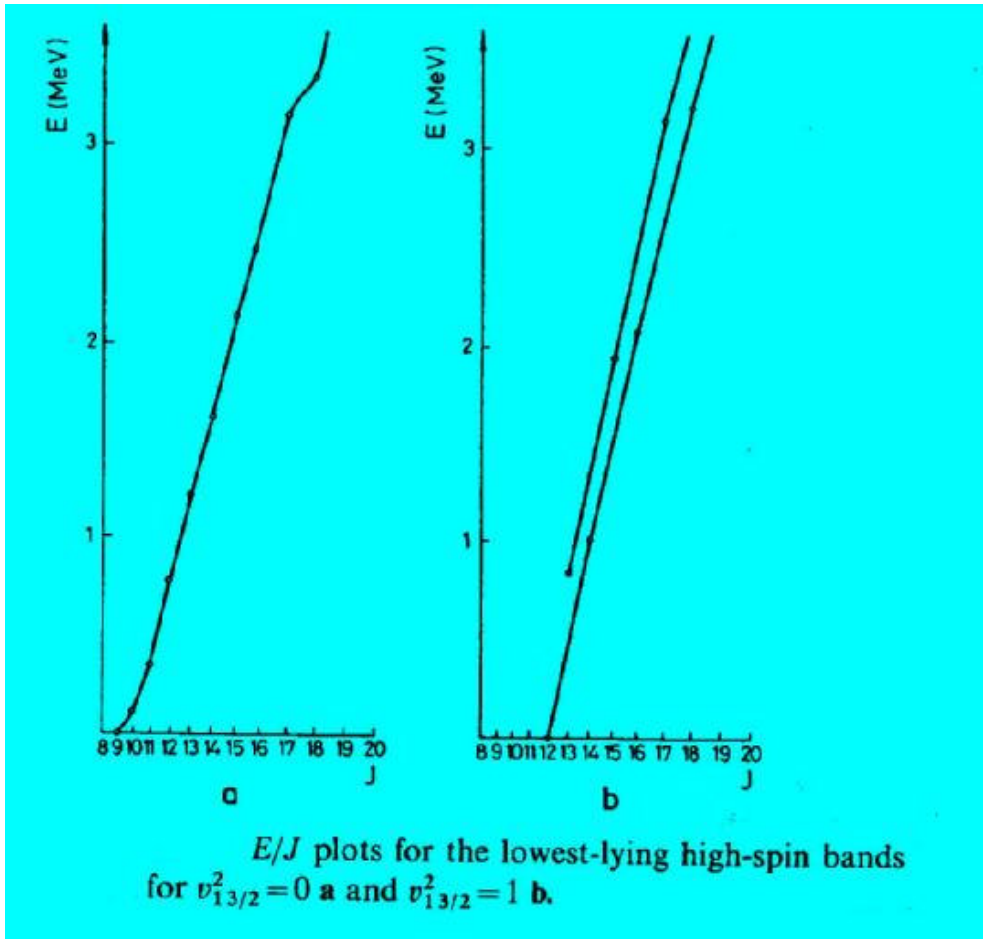

E/J plots for the lowest-lying high-spin bands for $v^2_{13/2}=0$ **a** and $v^2_{13/2}=1$ **b**.

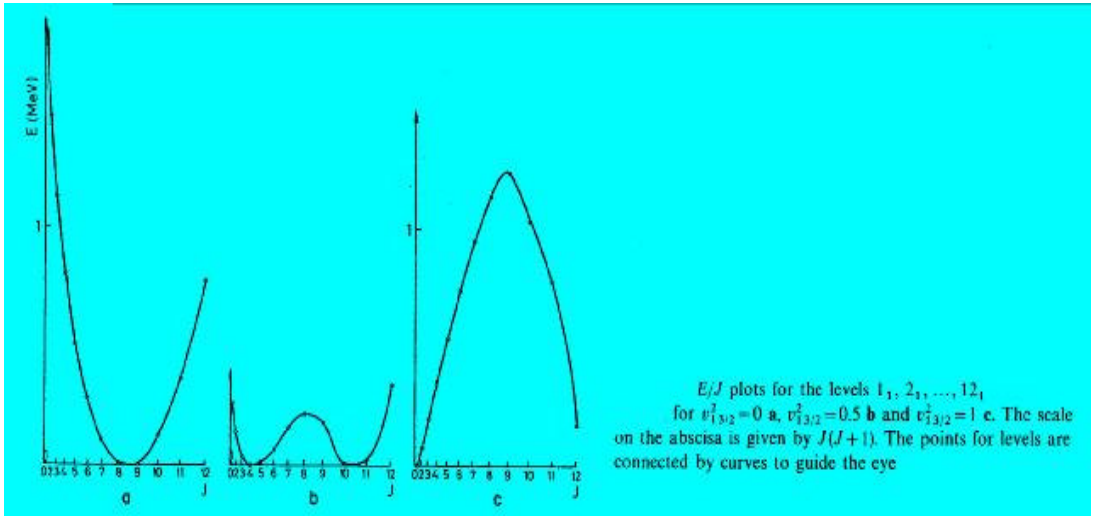

E/J plots for the levels $1_1, 2_1, \ldots, 12_1$ for $v^2_{13/2}=0$ **a**, $v^2_{13/2}=0.5$ **b** and $v^2_{13/2}=1$ **c**. The scale on the abscisa is given by $J(J+1)$. The points for levels are connected by curves to guide the eye

The head of the lowest high-spin band is

$$J=j_\pi+j_\nu-3=9 \quad \text{for } v^2_{13/2}\lesssim 0.2,$$
$$J=j_\pi+j_\nu-2=10 \quad \text{for } 0.2\lesssim v^2_{13/2}\lesssim 0.5,$$
$$J=j_\pi+j_\nu-1=11 \quad \text{for } 0.5\lesssim v^2_{13/2}\lesssim 0.8$$

and

$$J=j_\pi+j_\nu=12 \quad \text{for } 0.8\lesssim v^2_{13/2}.$$

A pronounced feature is rather broad region with $J=j_\pi+j_\nu-1=11$ level as the lowest high-spin state. This resembles the $J=j-1$ anomaly for rather broad region around $v^2=0.5$ in odd-even nuclei

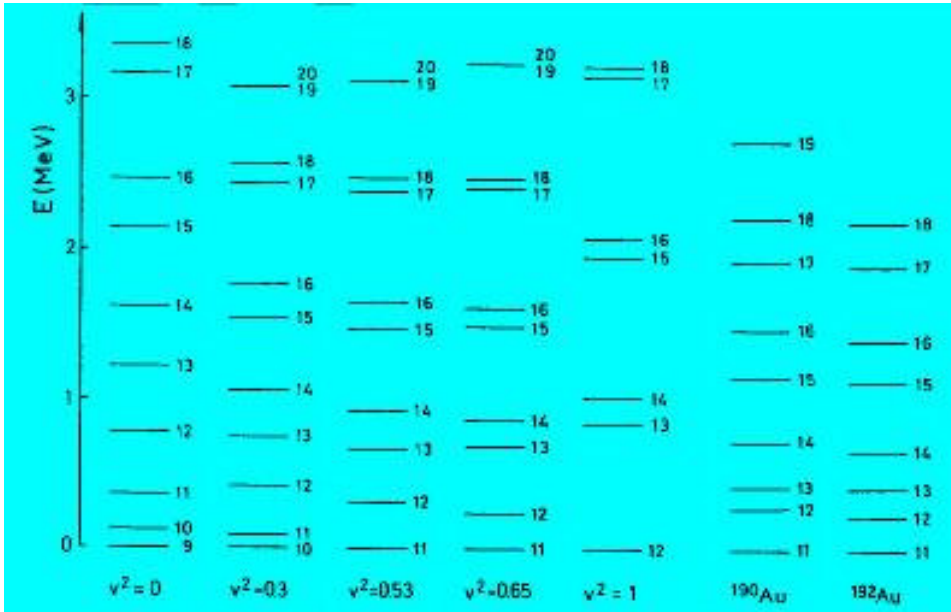

Characteristic lowest high-spin band patterns associated with $O(6)$ limit for several values of $v^2_{13/2}$ in the illustrative IBFFM calculation. Examples with all possible high-spin band heads are presented. For comparison, the experimental bands in ^{190,192}Au are presented to the right. We note that the Au-region is approximately associated with an $O(6)$ symmetry, but the present calculation is not fitted to Au isotopes

Calculated IBFFM yrast states (0_1, 1_1, ..., 20_1) for $\vec{j}_\pi = h^{-1}_{11/2}$, $\vec{j}_\nu = \vec{i}_{13/2}$ coupled to an $SU(3)$ core, as a function of $v^2_{13/2}$.

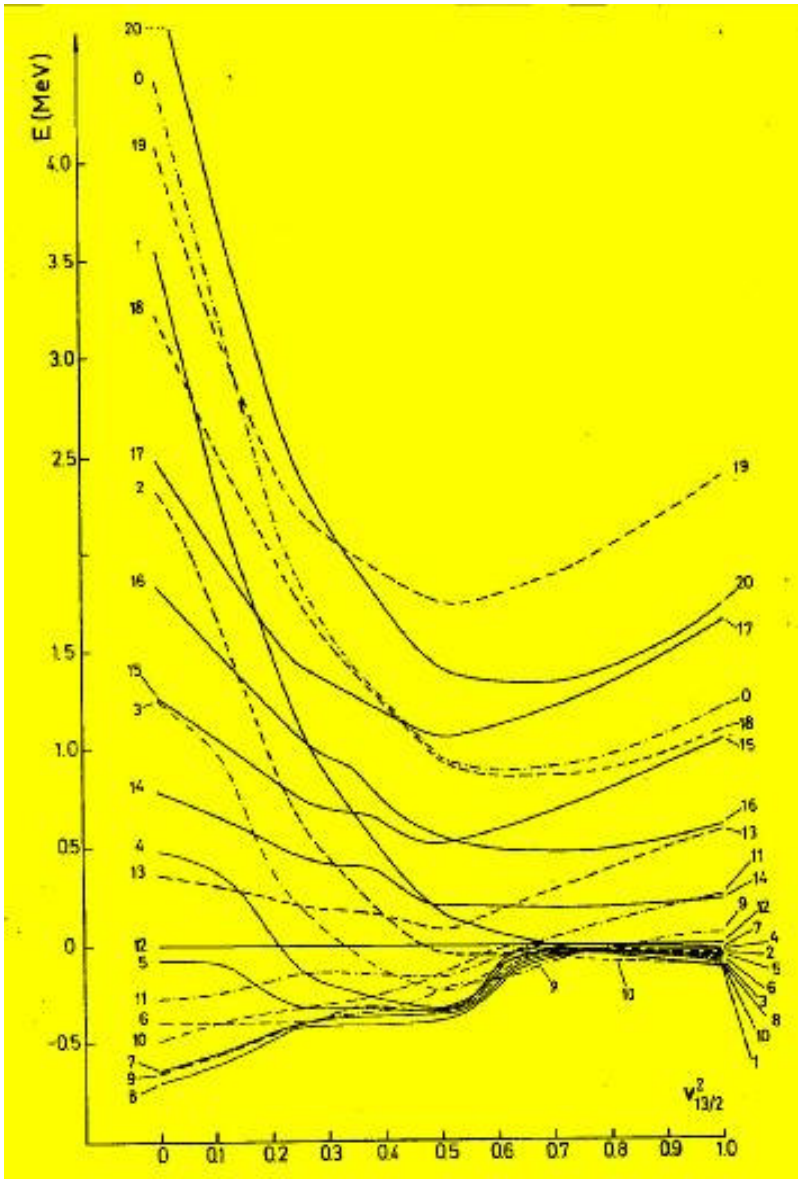

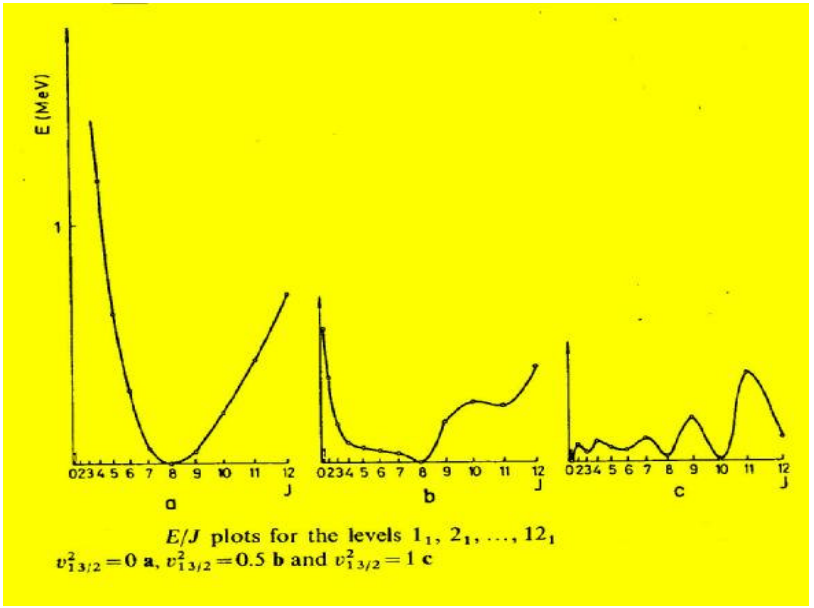

E/J plots for the levels 1_1, 2_1, ..., 12_1 $v^2_{13/2}=0$ **a**, $v^2_{13/2}=0.5$ **b** and $v^2_{13/2}=1$ **c**

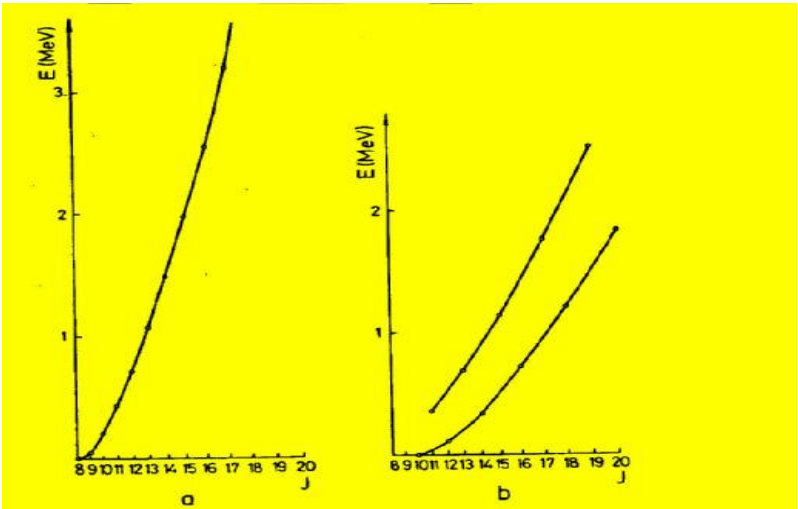

E/J plots for the lowest-lying high-spin bands for $v^2_{13/2}=0$ **a** and $v^2_{13/2}=1$ **b**

Transitional nuclei

^{68}As

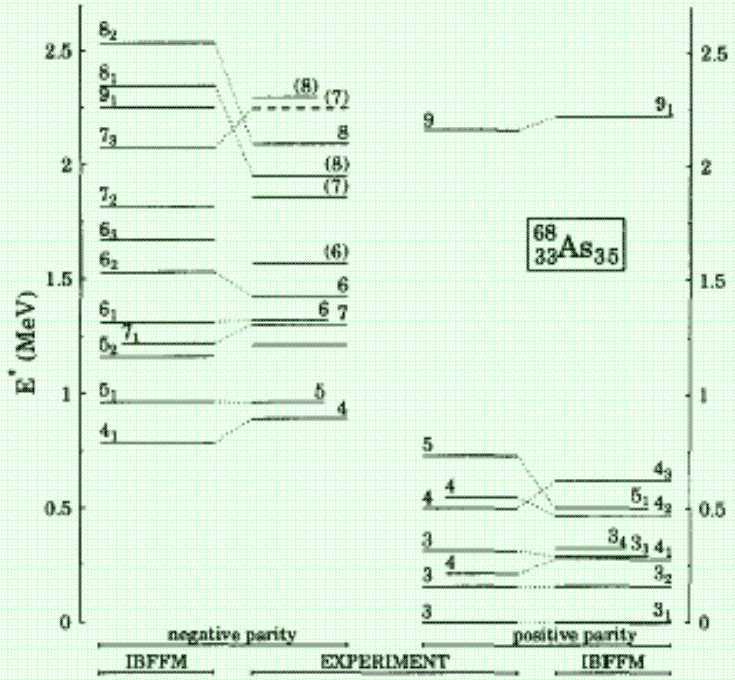

Experimental and theoretical IBFFM energy spectra of the low-lying states in ^{68}As. Up to 0.6 MeV the positive parity levels 3^+, 4^+, 5^+ are shown. In addition, the high spin isomer 9_1^+ is shown. For negative parity the calculated states with $J^\pi = 4_1^-, 5_1^-, 5_2^-, 6_1^-, 6_2^-, 6_3^-, 7_1^-, 7_2^-, 7_3^-, 8_1^-, 8_2^-, 9_1^-$ are shown.

Calculated in IBFFM branching ratios for ^{68}As compared with the experimental data

E^*_{exp} (MeV)	J^π_{exp} ($\hbar$)	$J^\pi_i \to J^\pi_f$ (theor.)	I_γ Exp.	I_γ Theor.
0.158	3^+	$3^+_2 \to 3^+_1$	100(6)	100
0.214	4^+	$4^+_1 \to 3^+_2$	6(2)	5
		$\to 3^+_1$	100(14)	100
0.313	3^+	$3^+_3 \to 4^+_1$	<2	4
		$\to 3^+_2$	16(2)	86
		$\to 3^+_1$	100(2)	100
0.500	4^+	$4^+_3 \to 3^+_3$	5(1)	12
		$\to 4^+_1$	5(1)	5
		$\to 3^+_1$	100(2)	100
0.550	4^+	$4^+_2 \to 3^+_3$	9(1)	100
		$\to 4^+_1$	36(2)	16
		$\to 3^+_2$	100(4)	9
		$\to 3^+_1$	48(2)	10
0.733	5^+	$5^+_1 \to 4^+_2$	17(2)	3
		$\to 4^+_3$	<6	26
		$\to 4^+_1$	100(5)	100
3.183	$11^{(+)}$	$11^+_1 \to 9^+_1$	100(3)	100
0.965	$5^{(-)}$	$5^-_1 \to 4^-_1$	100(3)	100
1.304	$7^{(-)}$	$7^-_1 \to 5^-_1$	100(3)	100
1.323	$6^{(-)}$	$6^-_1 \to 5^-_1$	100(4)	100
		$\to 4^-_1$	<3	4
1.427	$6^{(-)}$	$6^-_2 \to 5^-_2$	8(2)	2
		$\to 5^-_1$	100(5)	100
1.956	(8^-)	$8^-_1 \to 6^-_1$	100(8)	100
		$\to 7^-_1$	23(6)	16
2.094	$8^{(-)}$	$8^-_2 \to 7^-_1$	100(3)	100
2.251	(7^-)	$7^-_3 \to 6^-_2$	<55	75
		$\to 6^-_1$	100(15)	100
		$\to 5^-_2$	<40	45

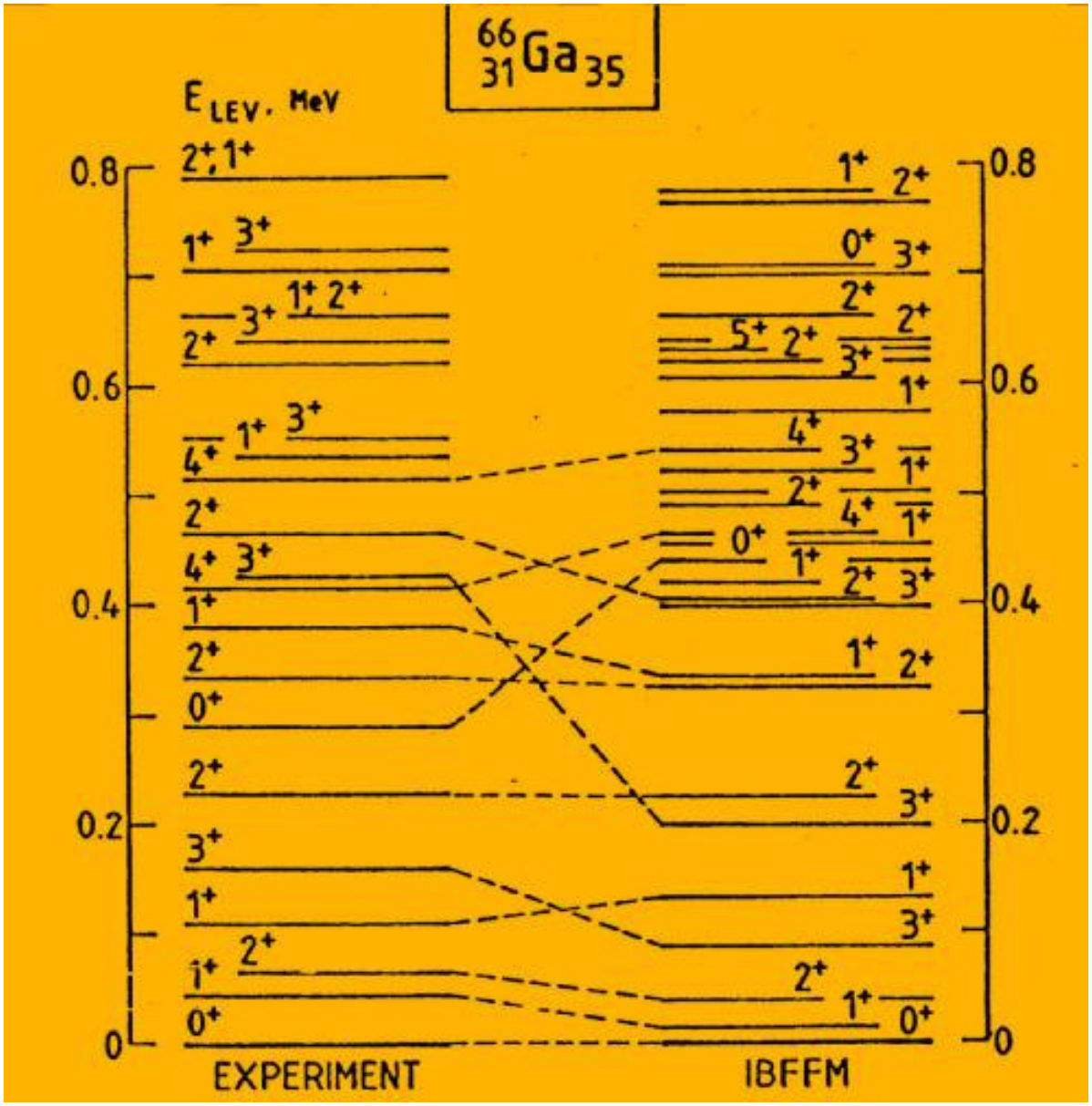
$^{66}_{31}Ga_{35}$
$E_{LEV.}$ MeV
0.8
0.6
0.4
0.2
0
EXPERIMENT
IBFFM

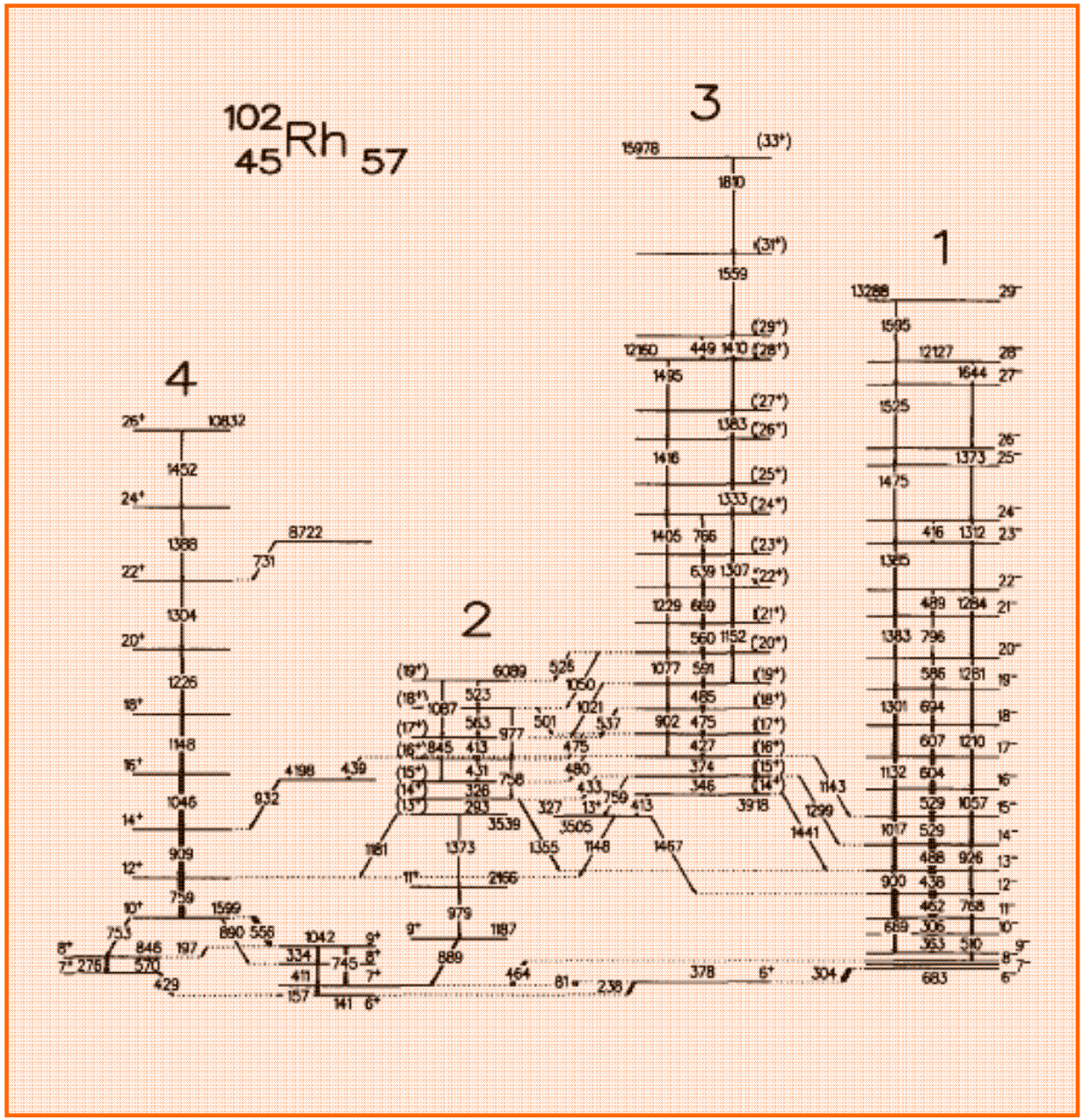
102 45 Rh 57
4
3
2
1
10832
8722
731
4198
439
932
1452
1388
1304
1226
1148
1046
909
759
1599
890
556
753
846
197
276
570
429
1042
334
745
411
157
141
979
889
187
464
81
2166
1181
1373
1355
1148
1467
6089
525
1050
1021
517
1087
523
563
977
501
845
413
475
480
431
758
433
326
759
327
293
413
3539
3505
3918
1143
1299
1441
15978
1810
1559
12150
449
1410
1495
1416
1383
1333
1405
766
639
1307
1229
689
560
1152
1077
591
485
902
475
427
374
346
304
238
378
6*
683
13288
1595
12127
1644
1525
1373
1475
416
1312
1385
489
1284
1383
796
586
1261
1301
694
607
1210
1132
604
529
1057
1017
529
488
926
900
438
462
768
689
306
353
510

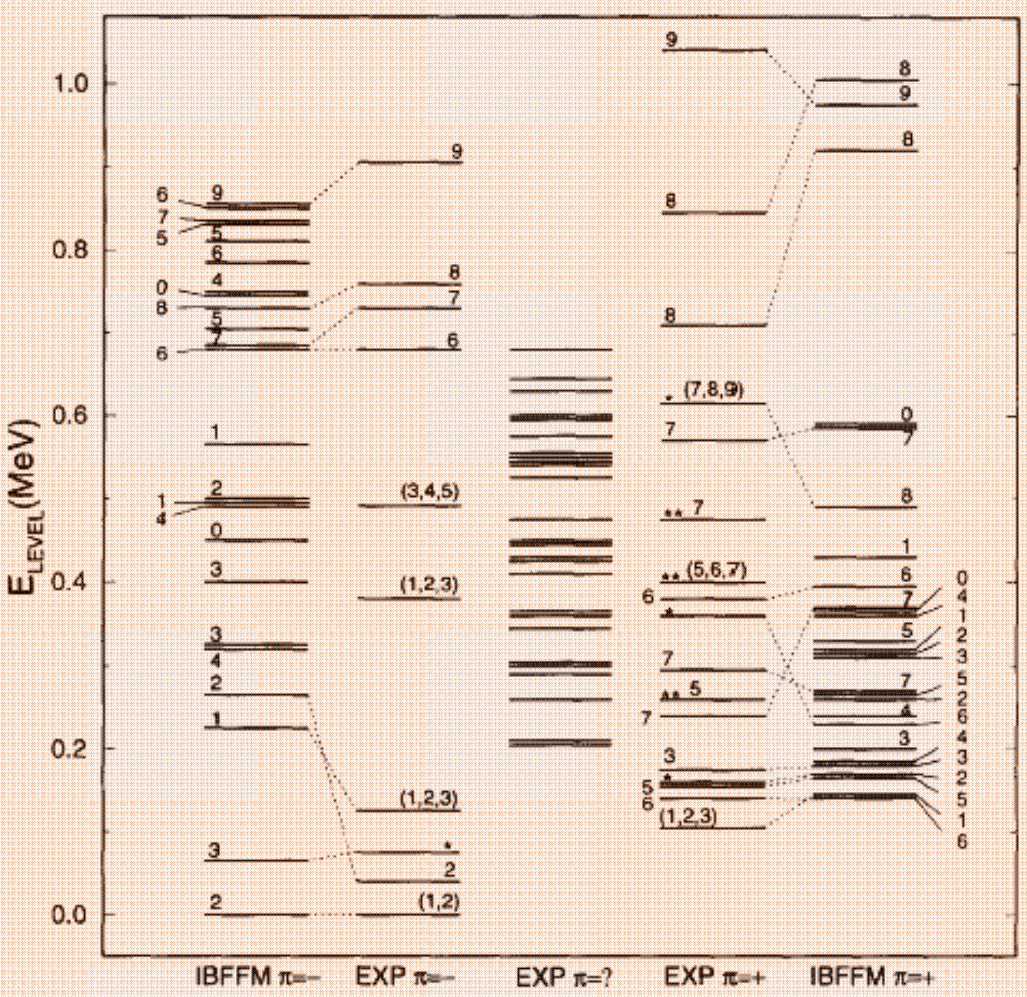

Fig. 4. Low-lying levels in ^{102}Rh calculated with the IBFFM model and compared to experimental ones. For the clarity of the figure, only the three lowest calculated levels for a given spin are shown. The left-hand and right-hand sides of the figure are for the negative- and positive-parity states, respectively. Levels with unidentified parity are shown in the central column. Experimental states of uncertain parity are denoted by $*$. States interpreted as intruders are denoted by $**$.

^{102}Rh

Transition		$B(E2)(e^2b^2)$		$B(M1)(\mu_N^2)$		I_γ	
$I_i^\pi \rightarrow I_f^\pi$	$E_i \rightarrow E_f$	Exp.	IBFFM	Exp.	IBFFM	Exp.	IBFFM
$2_2^- \rightarrow 2_1^-$	42 → 0		0.0089	0.0054(18)	0.0033	100	100
$3_1^- \rightarrow 2_2^-$	76 → 42		0.0206		0.0731		68
$\rightarrow 2_1^-$	→ 0		0.0065		0.0097		100
$1_1^- \rightarrow 3_1^-$	124 → 76		0.0092				0.0
$\rightarrow 2_2^-$	→ 42		0.0068	0.0072(54)	0.0169	12.9	3.4
$\rightarrow 2_1^-$	→ 0		0.0307	0.034(18)	0.1436	100	100
$5_1^+ \rightarrow 6_1^+$	155 → 141		0.0003		0.0515	100	100
$2_1^+ \rightarrow 1_1^+$	157 → 105		0.0246		1.1948	100	100
$3_1^+ \rightarrow 2_1^+$	179 → 157		0.0109		1.2919	82[a]	43[a]
$\rightarrow 1_1^+$	→ 105		0.0232				0.1[a]
$7_2^+ \rightarrow 5_1^+$	242 → 155		0.0033				0.0
$\rightarrow 6_1^+$	→ 141		0.0342		0.1286	100	100
$7_1^+ \rightarrow 7_2^+$	297 → 242		0.0057		0.0019		8
$\rightarrow 5_1^+$	→ 155		0.0178				20
$\rightarrow 6_1^+$	→ 141	$\geq$0.039[b]	0.0164	$\geq$ 0.093[b]	0.0007	100	100
$6_2^+ \rightarrow 7_1^+$	360 → 297		0.0322		0.2138		100
$\rightarrow 7_2^+$	→ 242		0.0181		0.0287		90
$6_3^+ \rightarrow 6_2^+$	378 → 360		0.0099		0.0002		0.0
$\rightarrow 7_1^+$	→ 297		0.0009	0.045[b]	0.5392	92	69
$\rightarrow 7_2^+$	→ 242		0.0023	0.016[b]	0.0046	58	3
$\rightarrow 5_1^+$	→ 155	0.0063[b]	0.0006		0.0375	83	100
$\rightarrow 6_1^+$	→ 141	0.0044[b]	0.0038	0.0018[b]	0.0309	100	100
$7_3^+ \rightarrow 6_3^+$	570 → 378		0.0343		0.1572		19
$\rightarrow 6_2^+$	→ 360		0.0000		0.0088		1.4
$\rightarrow 7_1^+$	→ 297		0.0018		0.0000	5	0.1
$\rightarrow 7_2^+$	→ 242		0.0000		0.0035		2.1
$\rightarrow 5_1^+$	→ 155		0.0076		0.0000		1.1
$\rightarrow 6_1^+$	→ 141		0.0016		0.0728	100	100
$8_1^+ \rightarrow 7_3^+$	616 → 570		0.0080		0.2705		0.3
$\rightarrow 6_3^+$	→ 378		0.0009				0.0
$\rightarrow 6_2^+$	→ 360		0.0228				0.2
$\rightarrow 7_1^+$	→ 297		0.0374		0.2572	100	100
$\rightarrow 7_2^+$	→ 242		0.0022		0.0006		0.5
$\rightarrow 6_1^+$	→ 141		0.0020				0.4

^{102}Rh

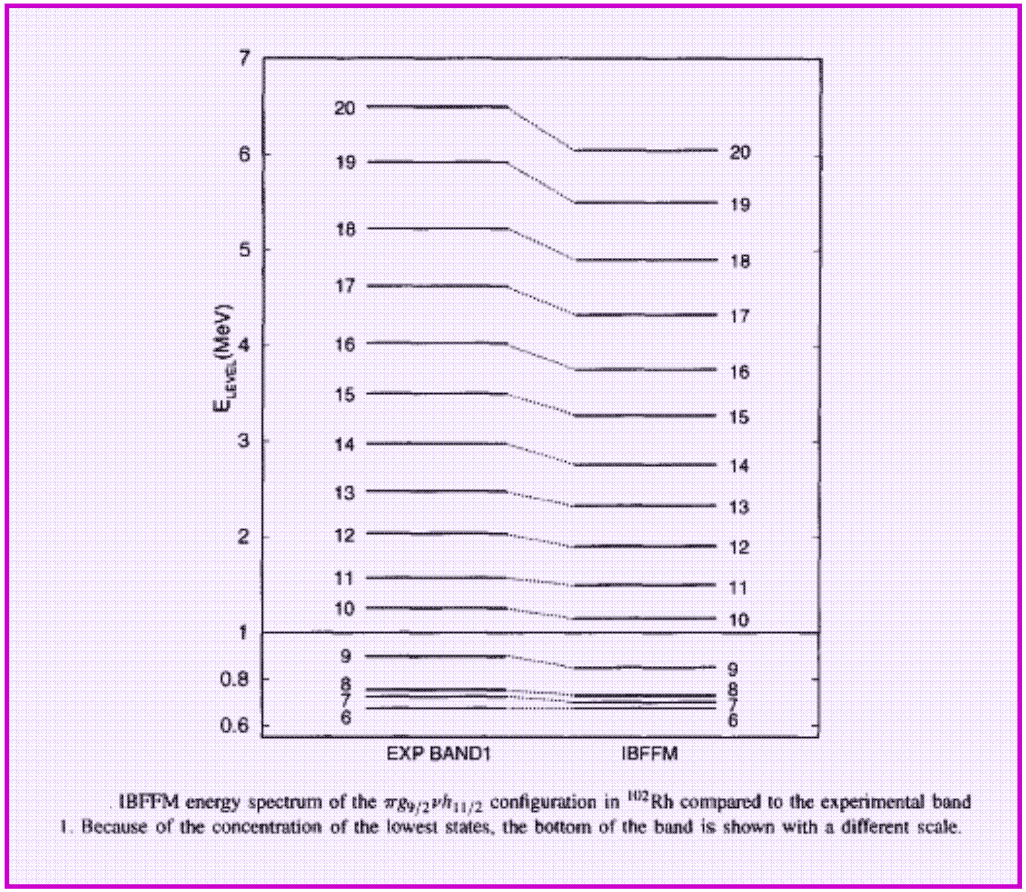

IBFFM energy spectrum of the $\pi g_{9/2}\nu h_{11/2}$ configuration in ^{102}Rh compared to the experimental band 1. Because of the concentration of the lowest states, the bottom of the band is shown with a different scale.

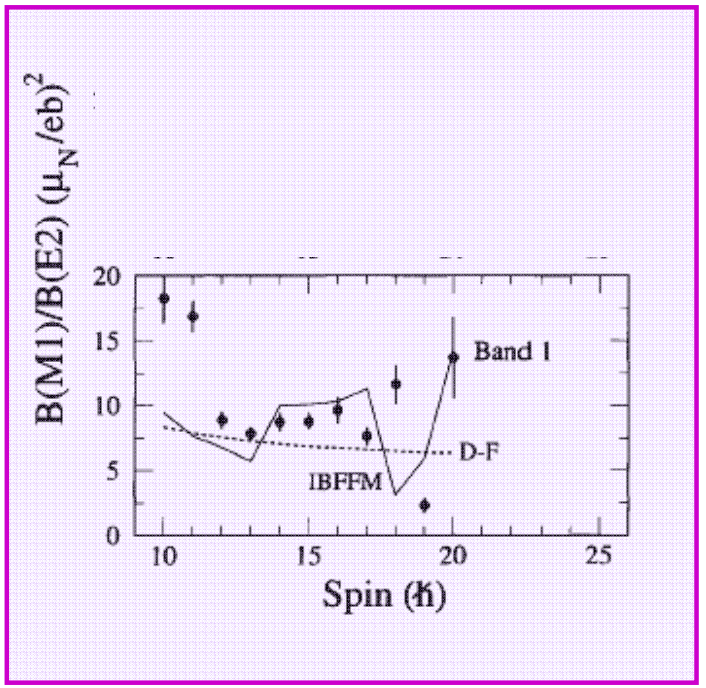

π g9/2 ν h11/2

Full line IBFFM

Dashed line Donau-Frauendorf model

The ΔI=2 positive-parity band 4

In the present IBFFM calculation we obtain two positive-parity high-spin bands, based on $\pi p_{1/2}\nu h_{11/2}$ and $\pi g_{9/2}\nu g_{7/2}$ two-quasiparticle configurations, respectively These bands are clearly formed above the 10^+ state, while for lower spins there is a stronger configuration mixing. The two lowest 10^+ states are based on the $(\pi p_{1/2}\nu h_{11/2})6, 2\ 4; 10$ (50%) and $(\pi g_{9/2}\nu g_{7/2})8, 1\ 2; 10$ (59%) configurations These two calculated bands appear close lying and they cross at angular momentum $I \approx 15\hbar$. Contrary to the experimental band 4 which is of $\Delta I = 2$ type with signature $\alpha = 0$, the calculated bands show doublet-type structures. The $\pi p_{1/2}\nu h_{11/2}$ configuration is associated with a much larger signature splitting than the $\pi g_{9/2}\nu g_{7/2}$ configuration and exhibit a pronounced tendency towards decoupled band (On this basis we attribute the $\pi p_{1/2}\nu h_{11/2}$ configuration to band 4.

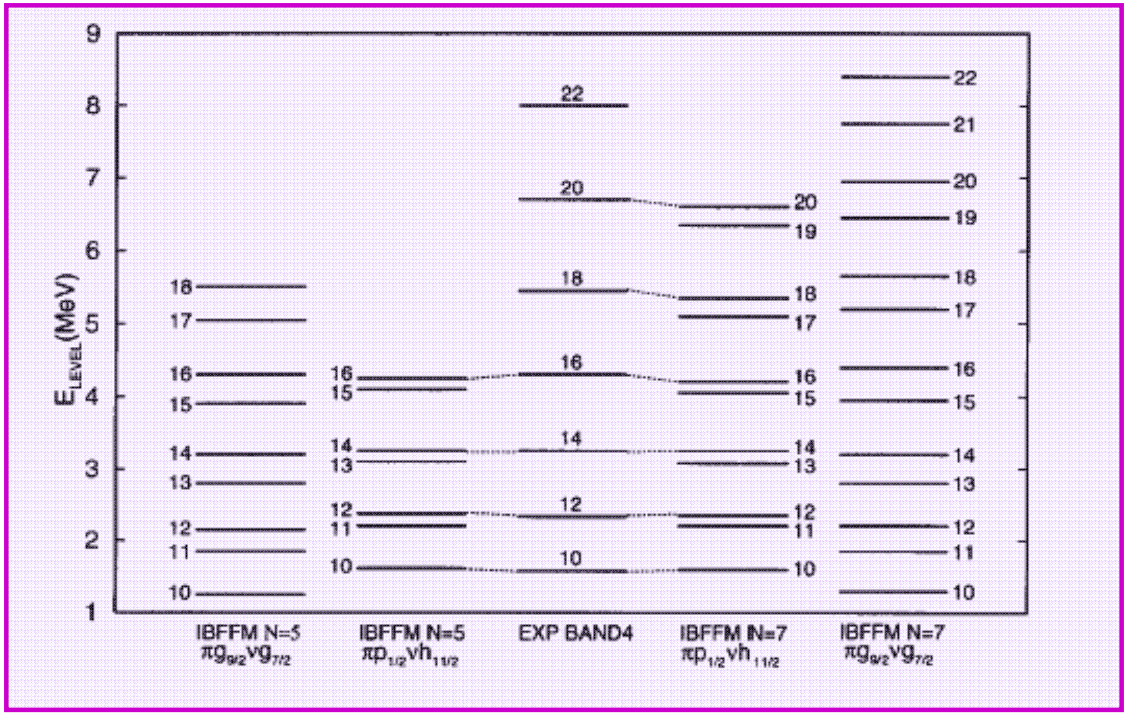

B(E2) and B(M1) reduced transition probabilities calculated between states of the $\pi p_{1/2}\nu h_{11/2}$ configuration with $N = 7$ in ^{102}Rh and comparison of the intensities of γ-rays observed in band 4 with those calculated for the above configuration

Transition	$B(\mathrm{E2})(e^2b^2)$	$B(\mathrm{M1})(\mu_N^2)$	I_γ	
	IBFFM	IBFFM	Exp.	IBFFM
$12^+ \rightarrow 11^+$	0.0016	0.0073		0.0
$12^+ \rightarrow 10^+$	0.4295		100	100
$14^+ \rightarrow 13^+$	0.0021	0.0001		0.0
$14^+ \rightarrow 12^+$	0.1003		100	100
$16^+ \rightarrow 15^+$	0.0005	0.0049		0.1
$16^+ \rightarrow 14^+$	0.0418		100	100
$18^+ \rightarrow 17^+$	0.0010	0.0019		0.0
$18^+ \rightarrow 16^+$	0.1076		100	100
$20^+ \rightarrow 19^+$	0.0011	0.0061		0.1
$20^+ \rightarrow 18^+$	0.0634		100	100

The two remaining experimental bands, bands 2 and 3, are expected to be based on four-quasiparticle states involving broken neutron pairs, in particular the $\nu h_{11/2}^2$ broken pair, so that four-quasiparticle states should be coupled to the boson core. The model including broken pairs of fermions has not been applied yet to odd–odd nuclei and therefore the corresponding theoretical states are missing in the present IBFFM calculations.

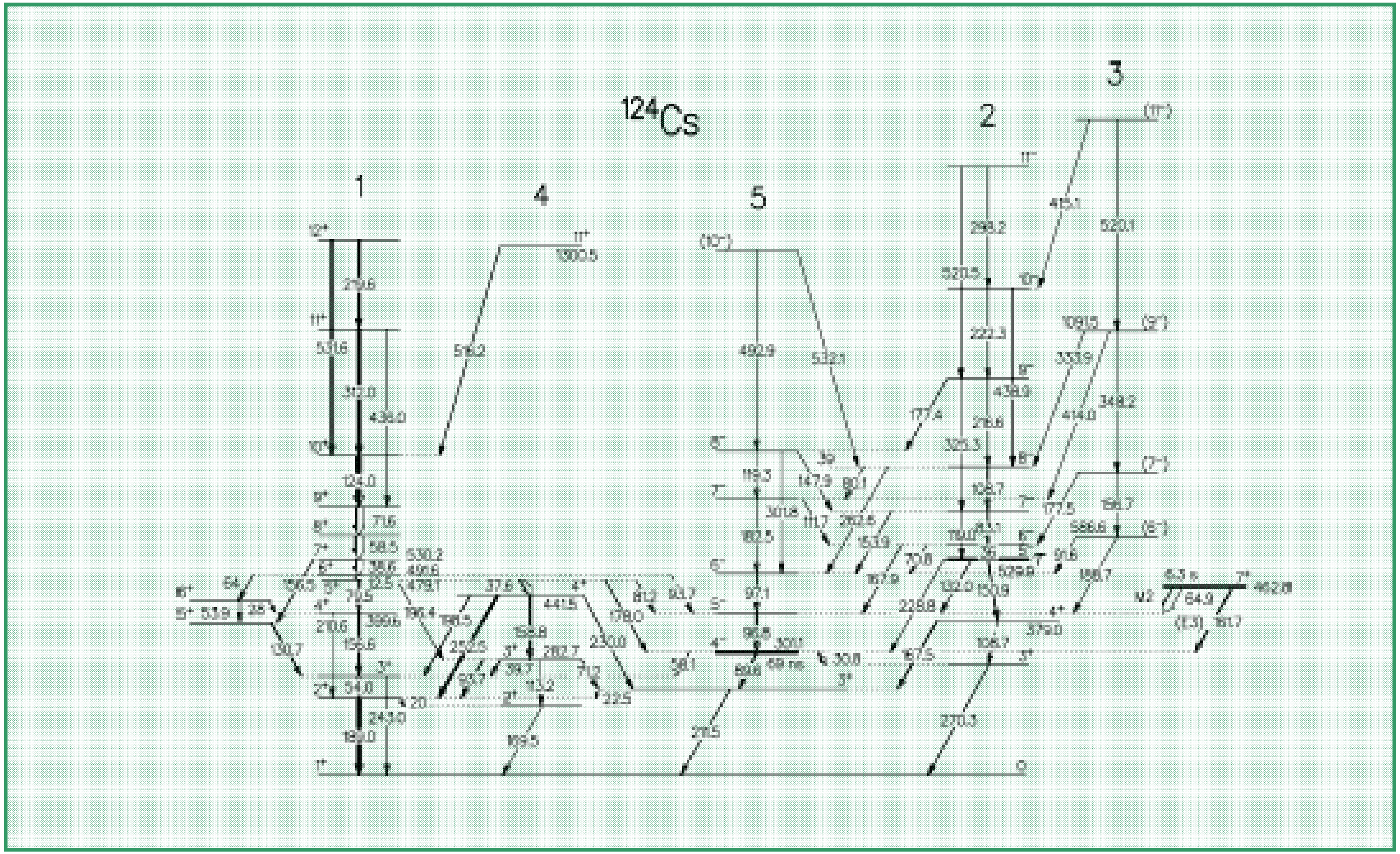

^{124}Cs
1
2
3
4
5
12+
11+
10+
9+
8+
7+
6+
5+
4+
3+
2+
1+
0
(10−)
11−
(11−)
10−
(9−)
9−
8−
(7−)
7−
(6−)
6−
5−
4−
3+
219.6
531.6
312.0
436.0
516.2
1300.5
124.0
71.6
58.5
38.6
32.5
530.2
490.6
479.1
492.9
532.1
298.2
520.5
415.1
520.1
222.3
438.9
333.9
348.2
414.0
177.4
325.3
218.8
108.7
177.5
156.7
586.6
91.6
188.7
529.9
132.0
150.9
379.0
167.5
270.3
211.5
189.5
189.0
243.0
54.0
53.9
130.7
156.6
210.6
356.6
196.4
198.5
252.5
158.8
282.7
39.7
93.7
113.2
22.5
230.0
178.0
81.2
441.5
37.6
97.1
96.8
301.1
69 ns
89.6
30.8
58.1
182.5
301.8
111.7
119.3
147.9
80.1
262.6
153.9
167.9
228.8
6.3 s
462.8
M2
64.9
(E3)
161.7

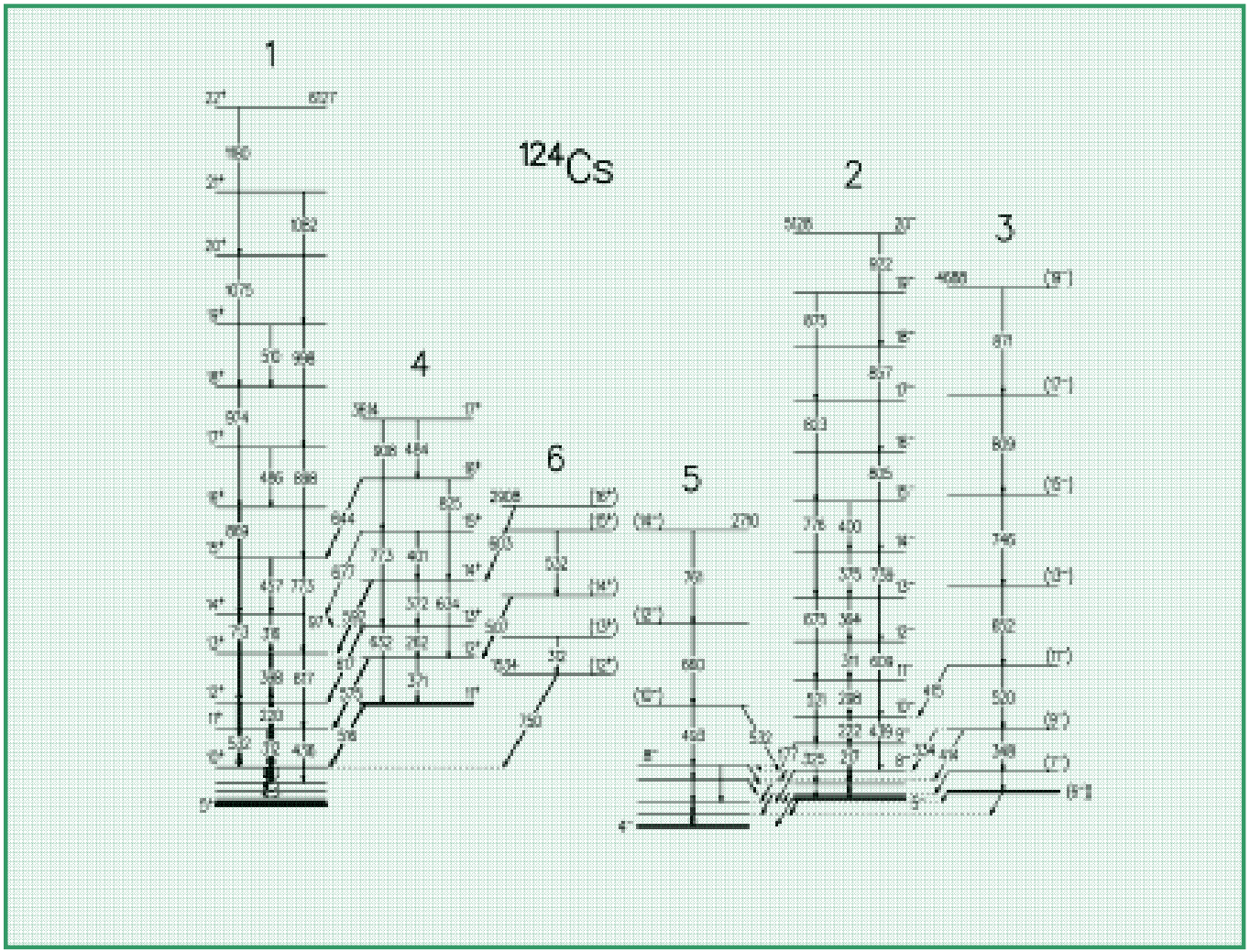
124Cs
1
2
3
4
5
6

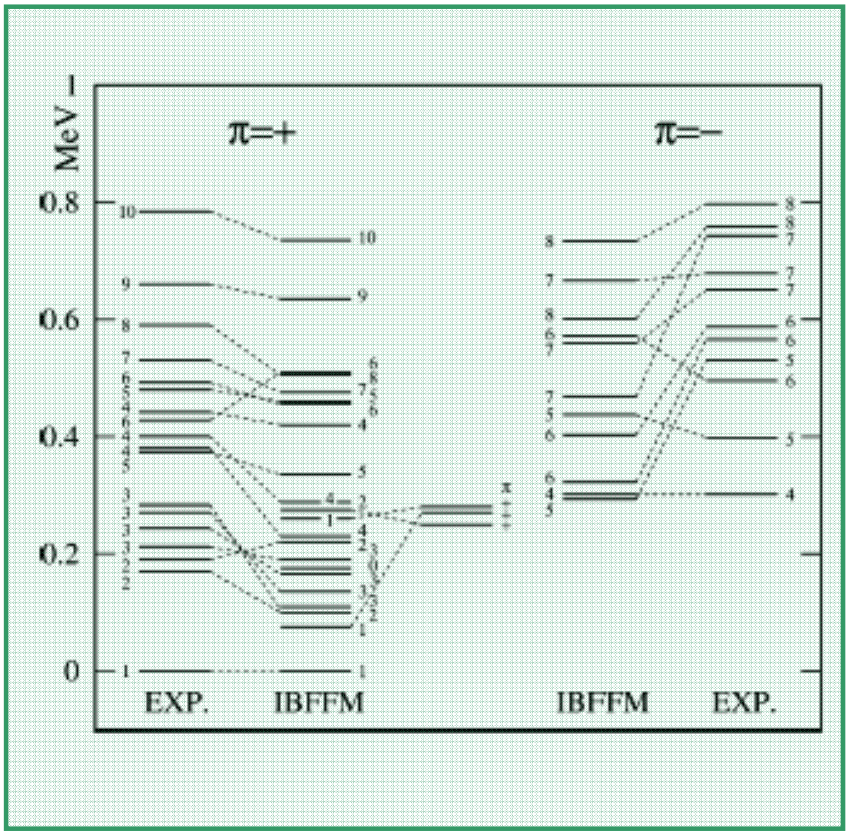

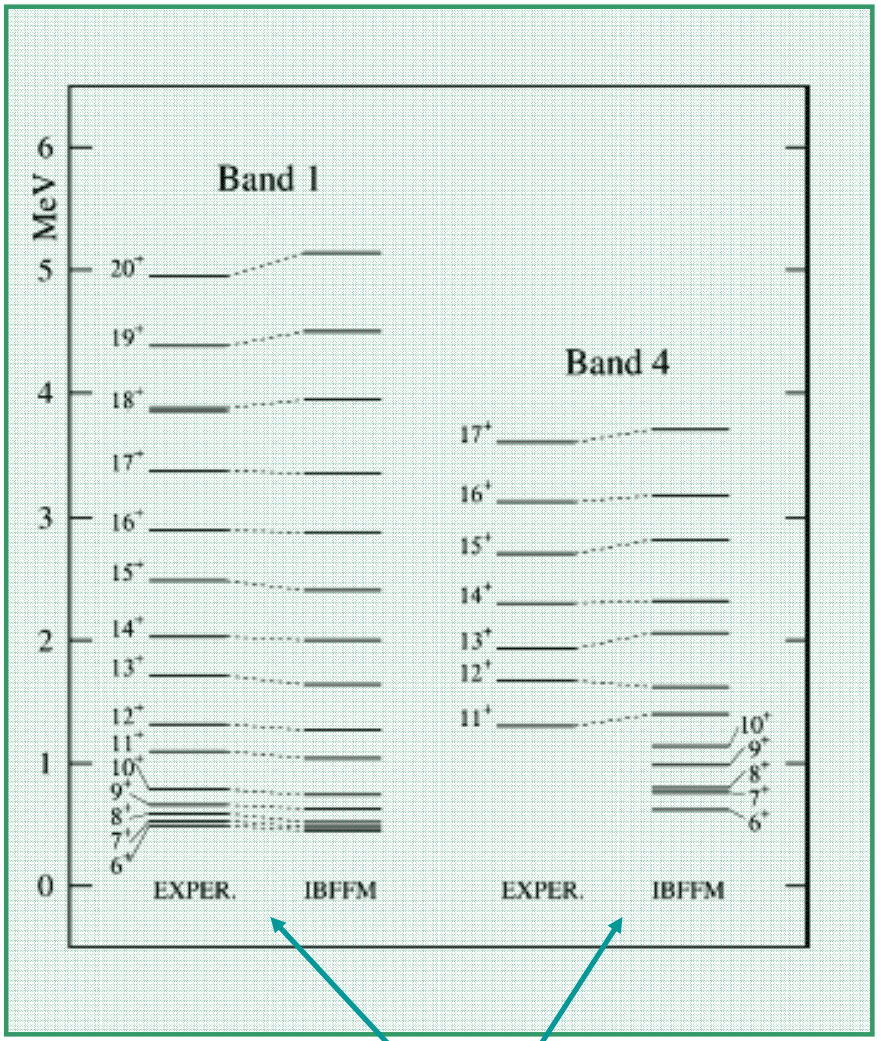

^{124}Cs

π h11/2 ν h11/2

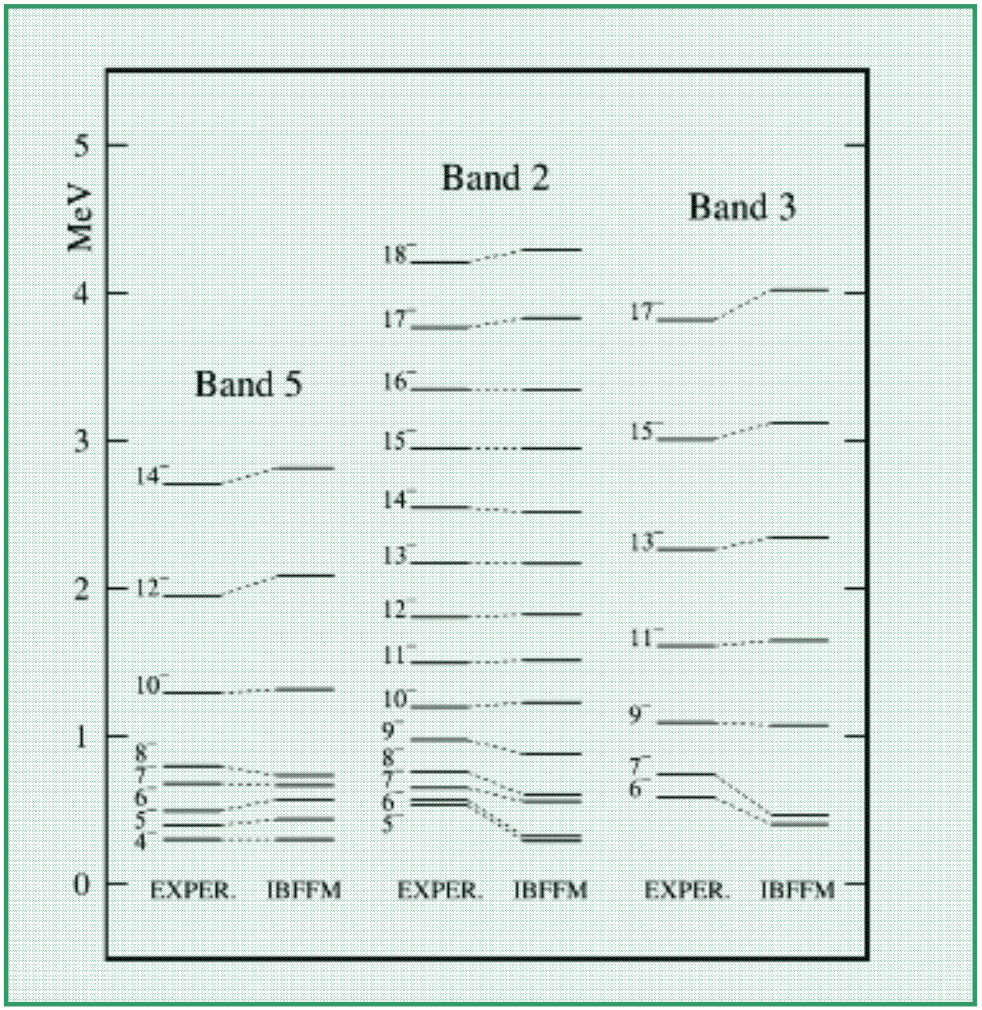

^{124}Cs

Wave functions are very complex !!!!

There is a strong configuration mixing

IBFFM is able to properly predict the structure of high spin states in a multy-j case

on the basis of the IBFFM analysis we propose that the negative-parity bands presented have a $\pi(d_{5/2}g_{7/2})\nu h_{11/2}$ configuration in their low-spin part and, starting from $I \approx 12$, are almost pure $\pi h_{11/2}\nu g_{7/2}$, with band 2 being the yrast structure and bands 3 and 5 the yrare structures. Thus the collective band structures start at spin $I \approx 12$.

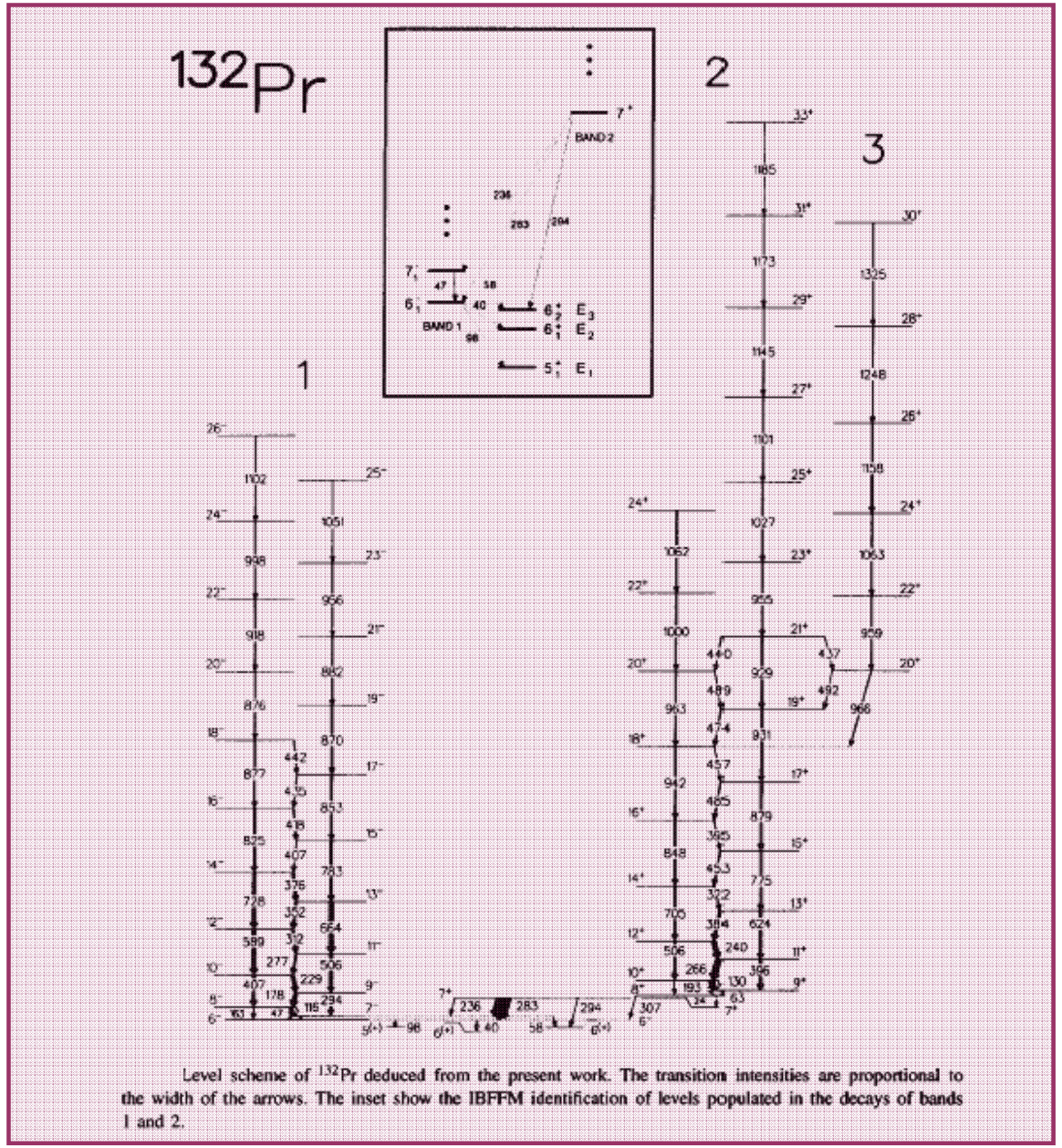

Level scheme of ^{132}Pr deduced from the present work. The transition intensities are proportional to the width of the arrows. The inset show the IBFFM identification of levels populated in the decays of bands 1 and 2.

Mixing of configurations with different parity both for protons and for neutrons (high with low spin states)

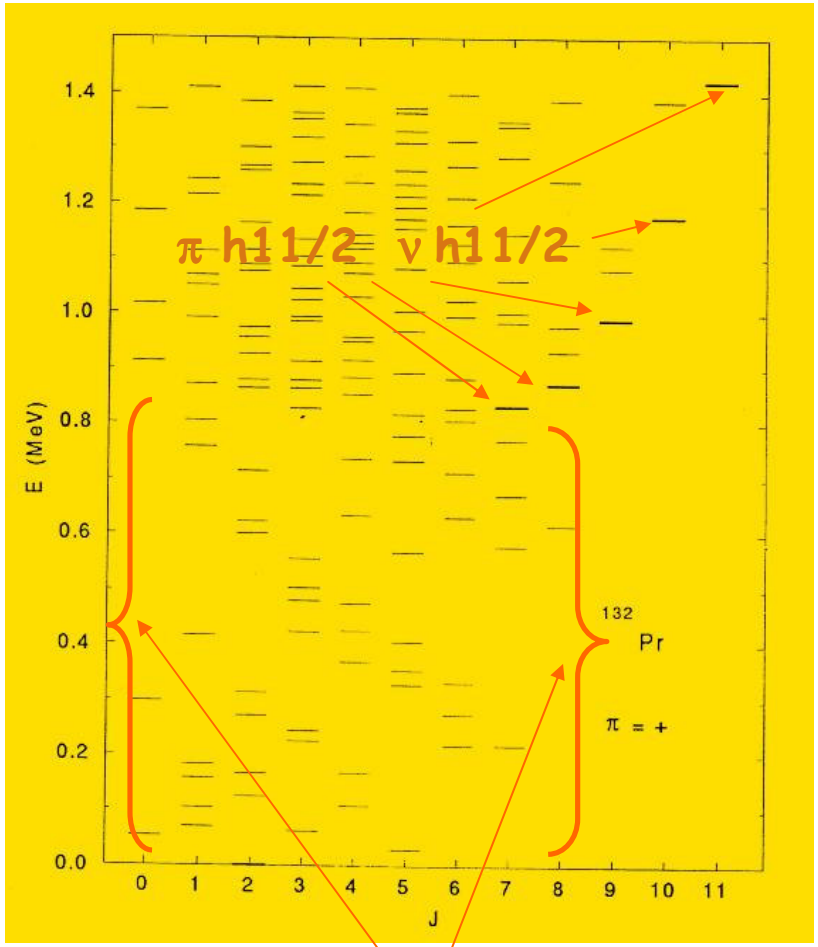

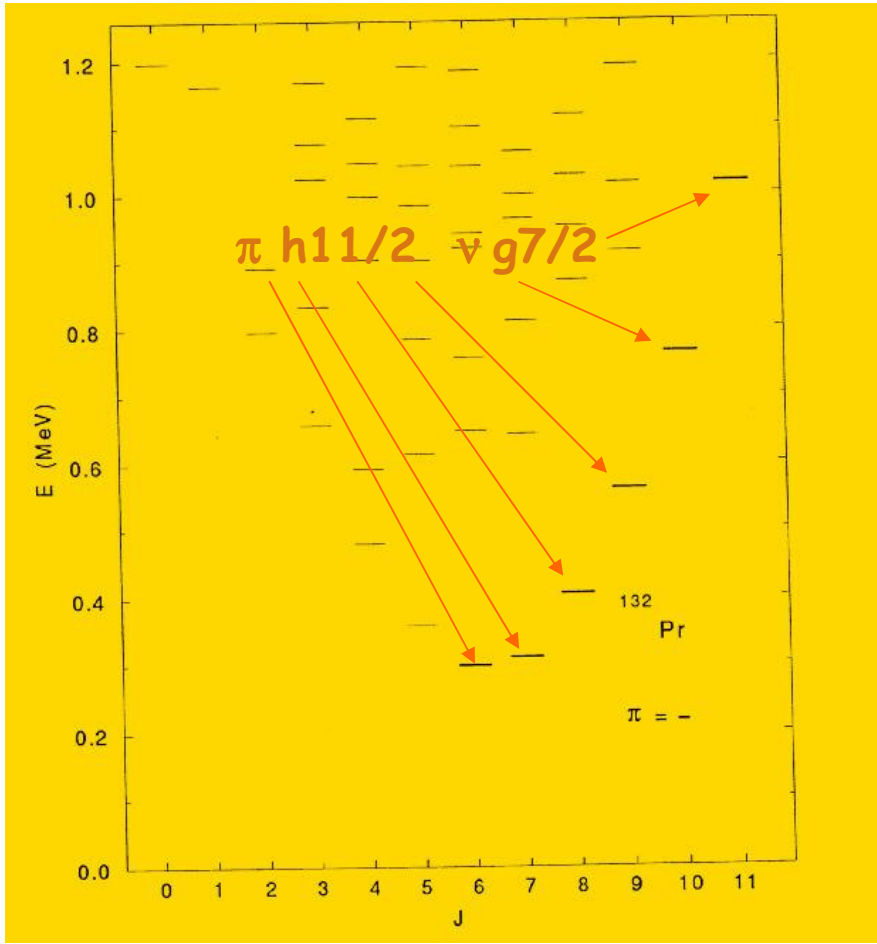

Positive parity proton and positive parity neutron configurations

Transitional SU(3) – O(6) ^{126}Pr nucleus

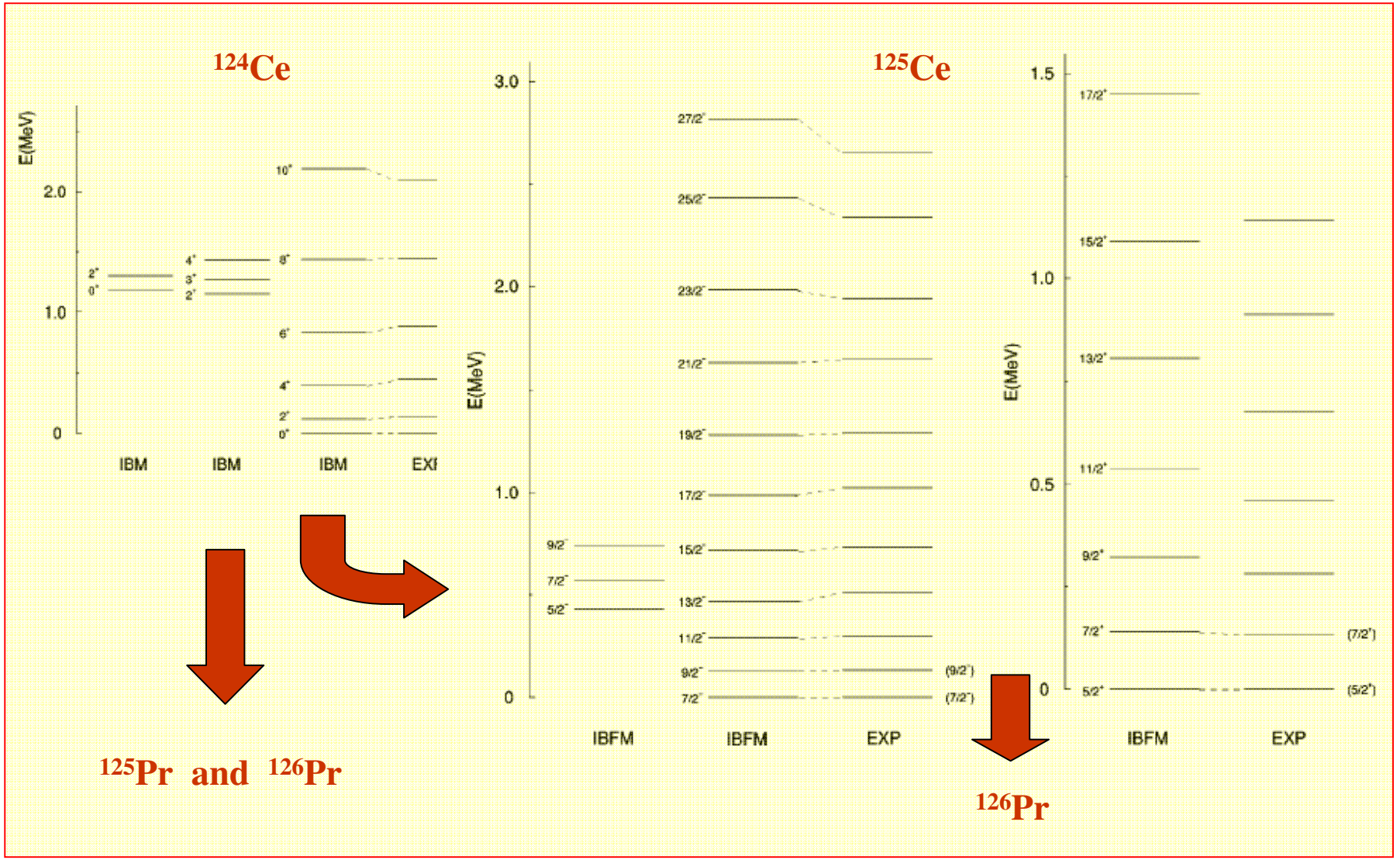

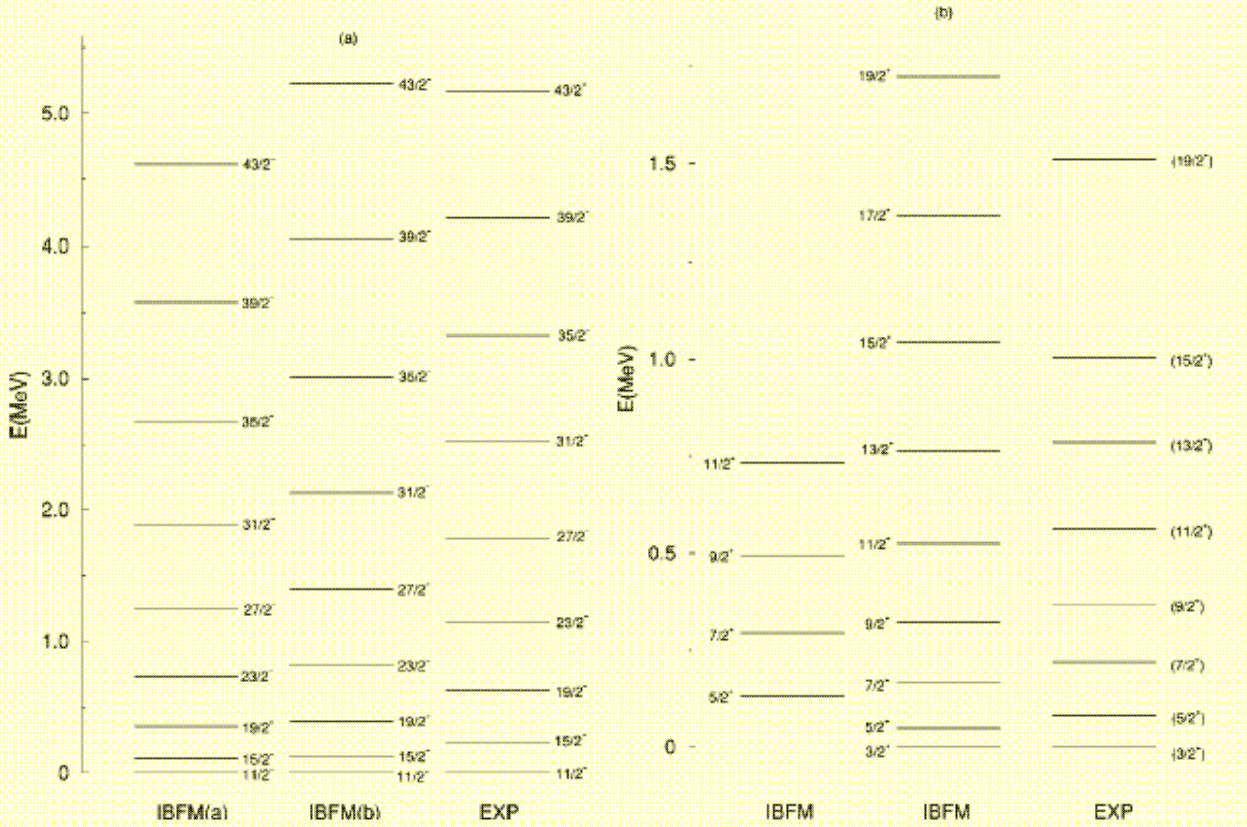

FIG. 12. The negative parity (a) and positive parity (b) yrast states in the odd-Z nucleus ^{125}Pr are compared with the experimental states of ^{127}Pr.

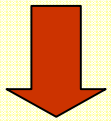

^{126}Pr

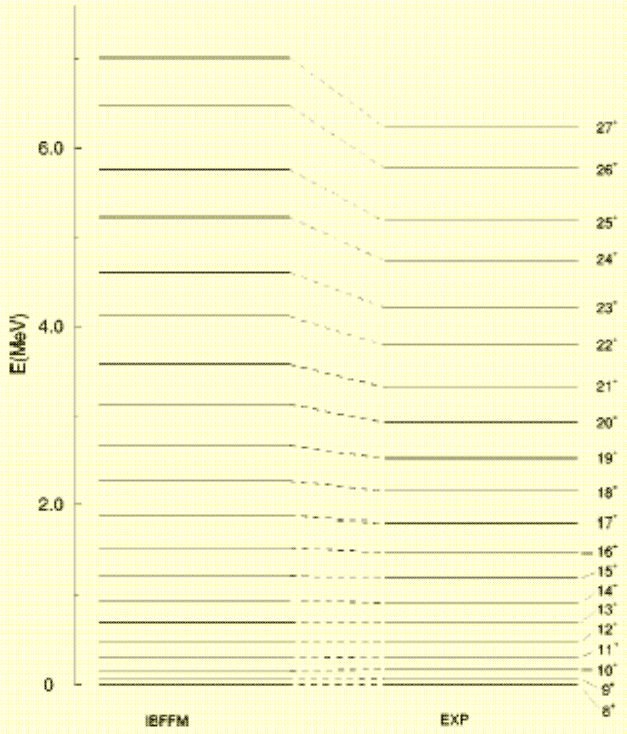

FIG. 13. The yrast sequence of high angular momentum positive parity states based on the $\pi h_{11/2} \otimes \nu h_{11/2}$ configuration is compared with its experimental counterpart in ^{126}Pr. The assignment for the band head, i.e., the lowest observed state is 8^+.

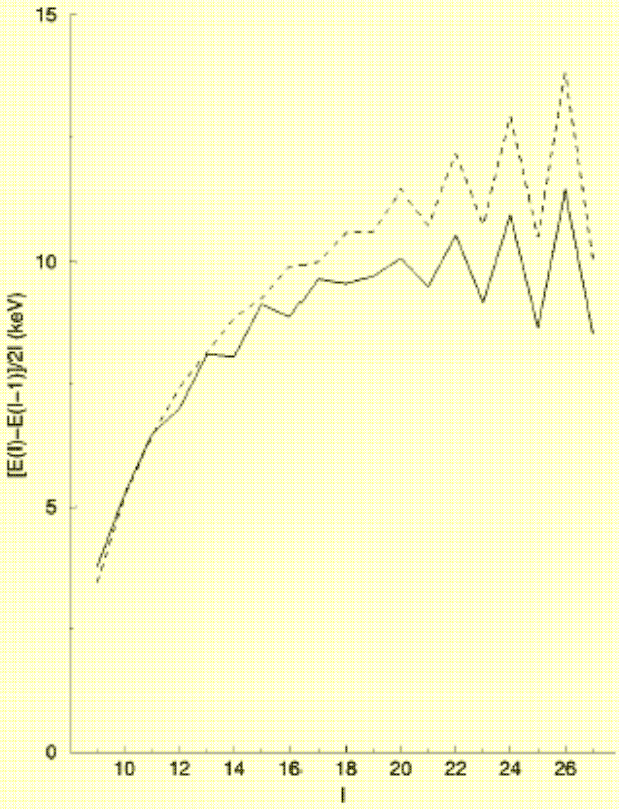

FIG. 14. The IBFFM (dashed line) and the experimental (solid line) $[E(I)-E(I-1)]/2I$ vs I plots for the $\pi h_{11/2} \otimes \nu h_{11/2}$ yrast band in ^{126}Pr. The state 8^+ is assigned to the band head.

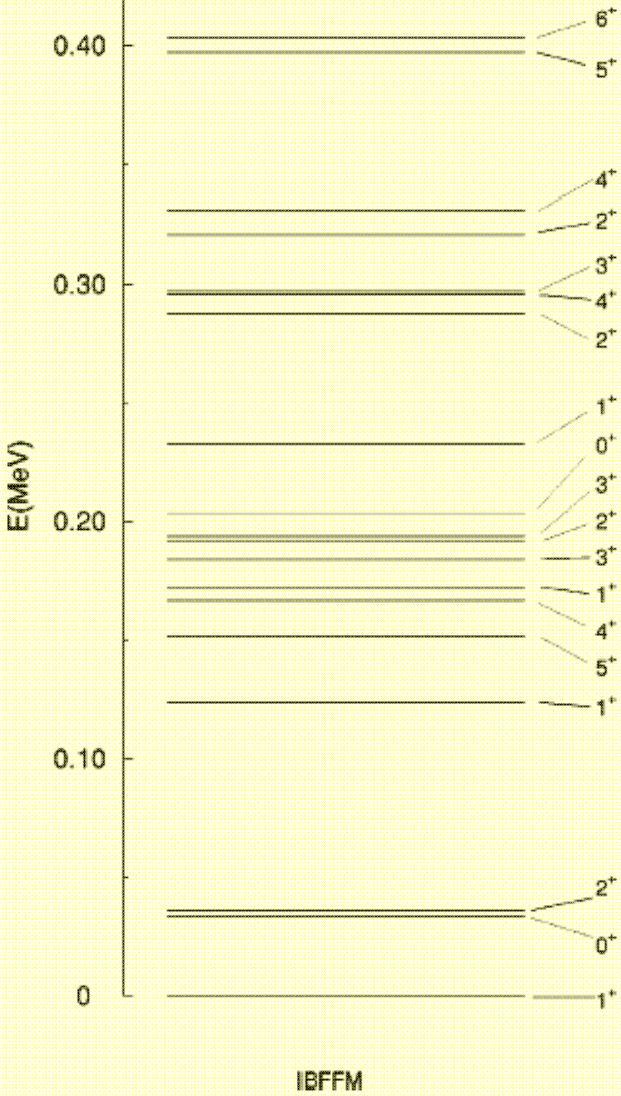

The IBFFM prediction for low angular momentum states in ^{126}Pr. These states are based on positive parity proton and neutron configurations.

The IBFFM analysis predicts the existence of another isomer in ^{126}Pr: 5^+ at $\approx$150 keV excitation energy. Its isomeric character depends strongly on the choice of the proton-neutron interaction. In the present calculation, 5_1^+ is below 4_1^+ and therefore it is an isomer with a possible γ decay to 2_1^+. This transition is slow enough to allow for a β decay that has been reported

^{198}Au

The first odd-odd nucleus calculated in IBFFM

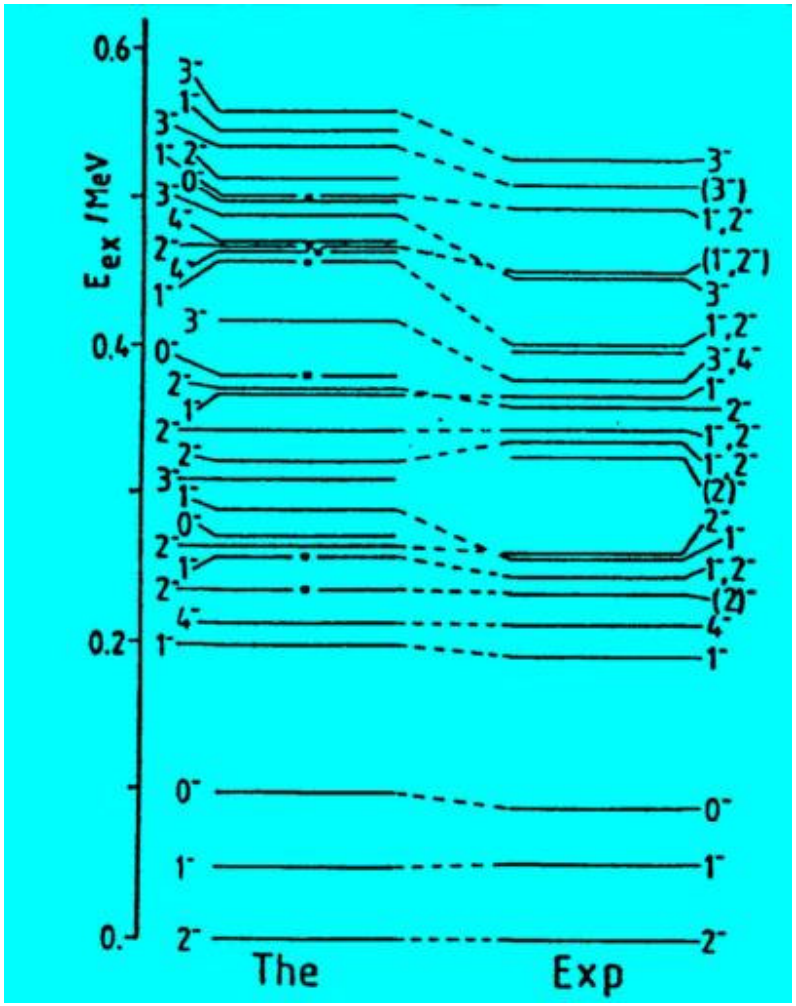

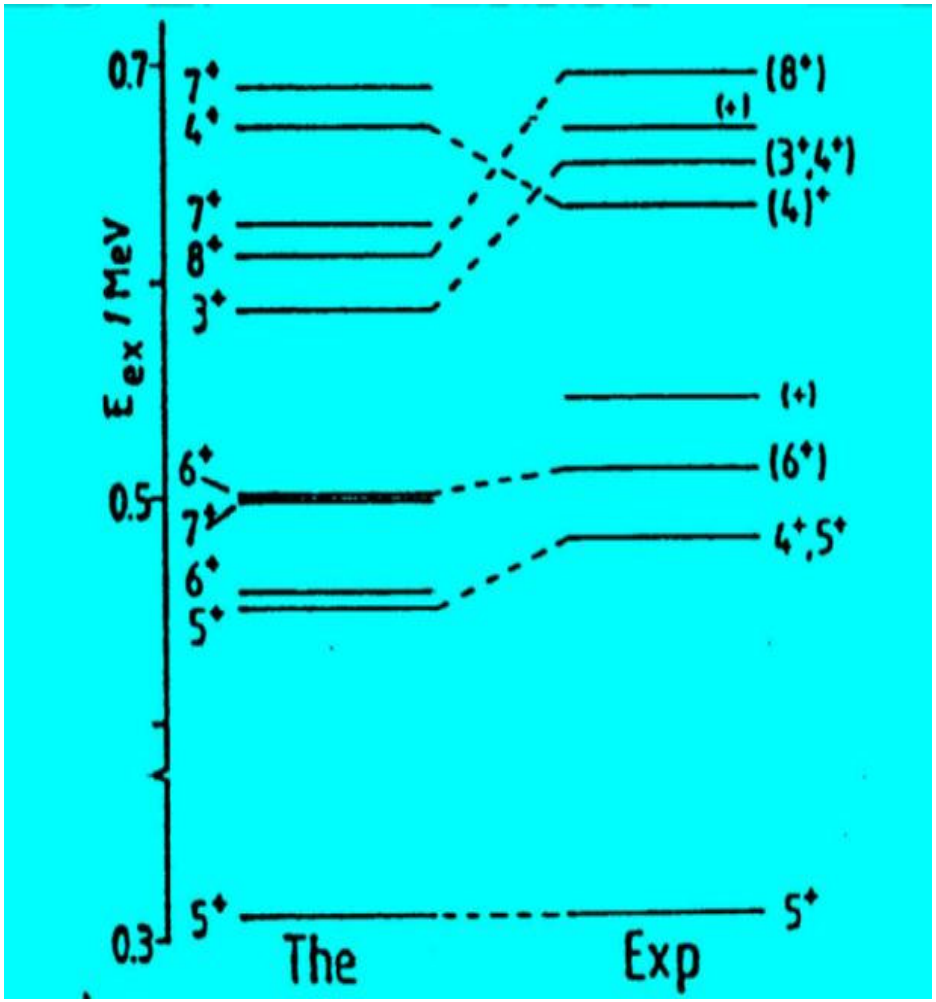

Chirality in nuclei

I call any geometrical figure, or group of points, chiral,
and say it has chirality, if its image in a plane mirror,
ideally realized, cannot be brought to coincide with itself.

Lord Kelvin, 1904.

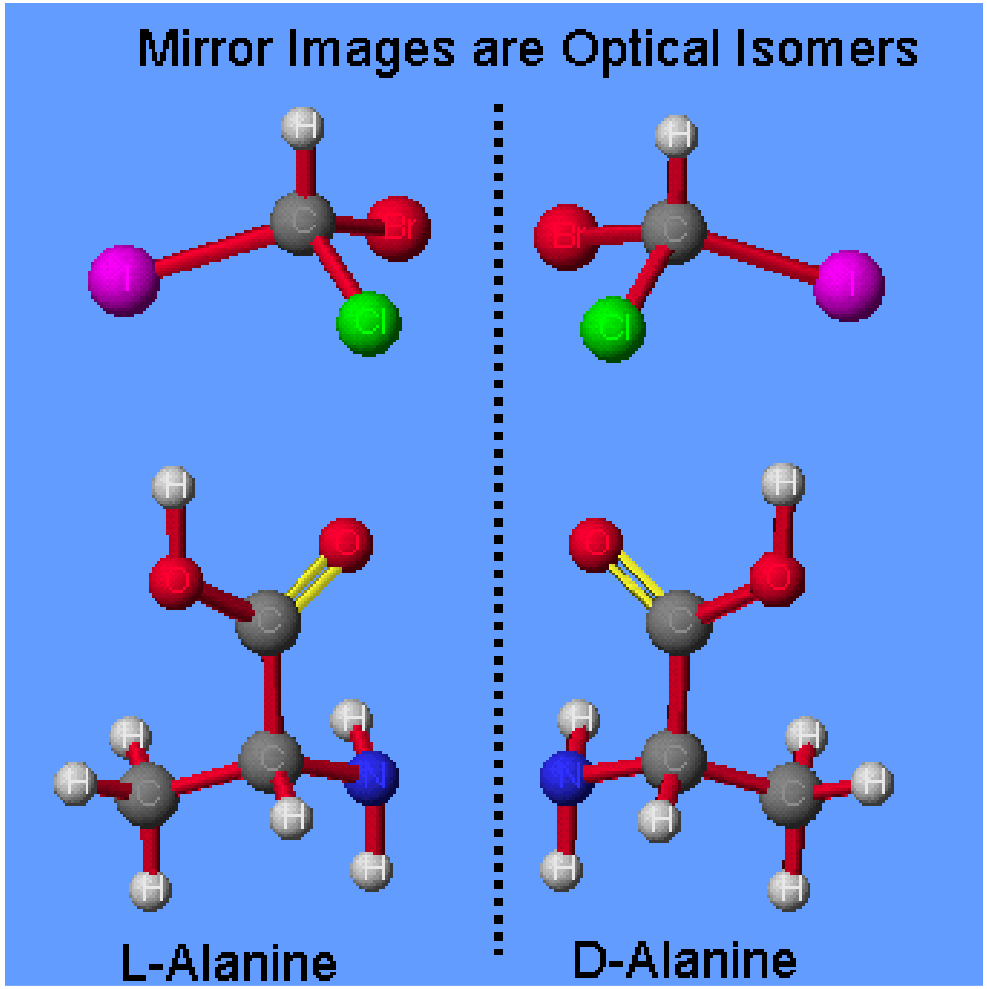

Numerous examples :

- Chemistry
- Biology
- Pharmacy
- Particle physics

Atomic nuclei ?

- Chirality in molecules is static
- Chirality in nuclei has (?) dynamical origin

It relates to the orientation of angular momenta in respect to some well defined axes

! The three angular momenta can be arranged to form a left-handed and a right-handed system

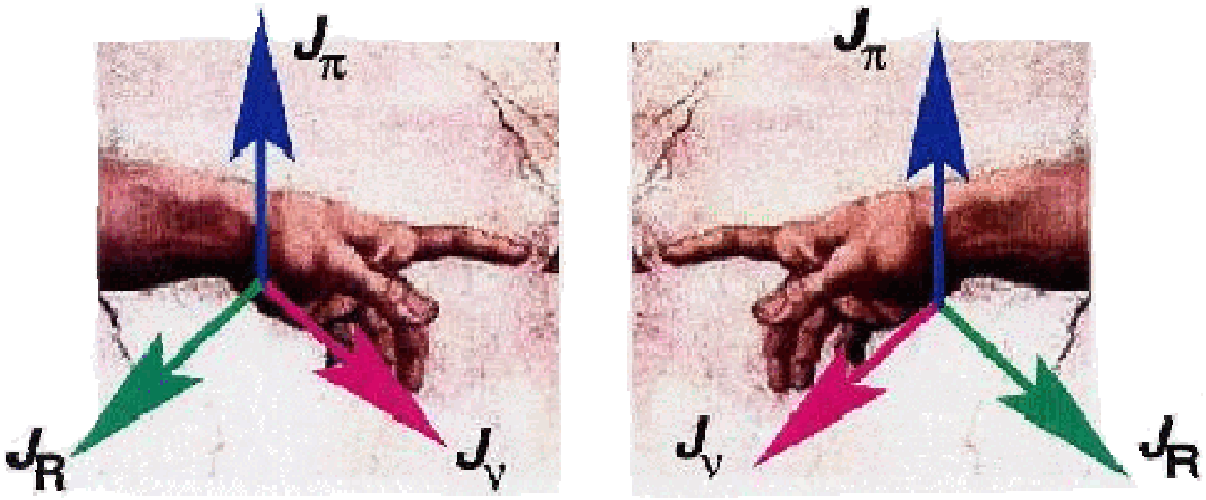

Candidates ?

Three angular momenta → odd-odd nuclei
(rotational core + proton + neutron)

Three axes → rotational core has to be triaxial
(angular momentum aligned along the intermediate axis)

Angular momentum of one fermion aligned along the short axis
The fermion has to be of particle type (BCS occupation < 0.5)

Angular momentum of the other fermion aligned along the long axis
The fermion has to be of hole type (BCS occupation > 0.5)

The angular momenta of both fermions have to be big enough

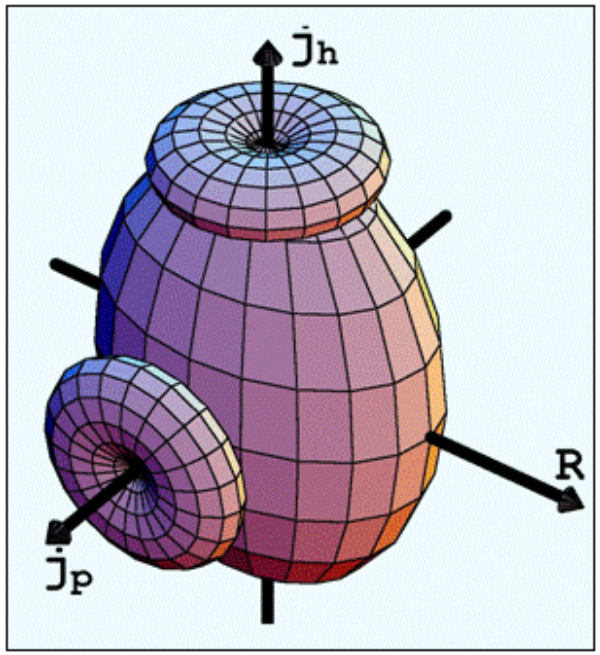
jh
R
jp

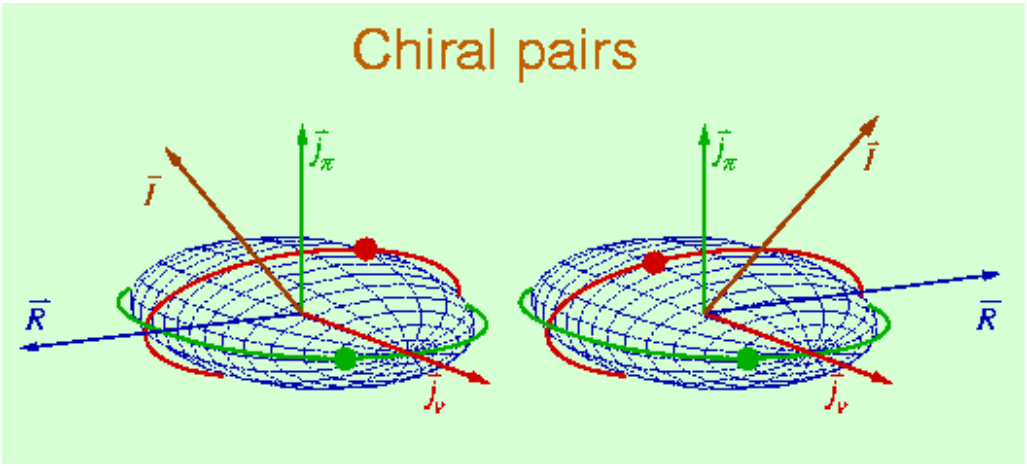
Chiral pairs
$\vec{I}$
$\vec{j}_\pi$
$\vec{R}$
j_ν
$\vec{I}$
$\vec{j}_\pi$
$\vec{R}$
j_ν

The system is chiral if it is not symmetric to mirror-reflection S in any plane. For nuclear rotation, instead of S, the operator R^T (the product of time reversal and rotation through 180^0) has to be used (angular momentum is an axial pseudo-vector).

For a given spin, the two states of the doublet in the laboratory system are $|+\rangle$ and $|-\rangle$, while the left-handed and right-handed states in the body-fixed system are $|L\rangle$ and $|R\rangle$.

$$|+\rangle = \frac{1}{\sqrt{2}}\left(|L\rangle + |R\rangle\right) \qquad |-\rangle = \frac{1}{\sqrt{2}}\left(|L\rangle - |R\rangle\right)$$

$$R^T|L\rangle = |R\rangle \qquad R^T|R\rangle = |L\rangle$$

$$R^T|+\rangle = |+\rangle \qquad R^T|-\rangle = |-\rangle$$

The Hamiltonian H is invariant under R^T

$$\langle L|H|L\rangle = \langle R|H|R\rangle = E$$

$$|\langle L|H|R\rangle| = \Delta \neq 0$$

$$\langle +|H|+\rangle = E + \Delta \qquad \langle -|H|-\rangle = E - \Delta$$

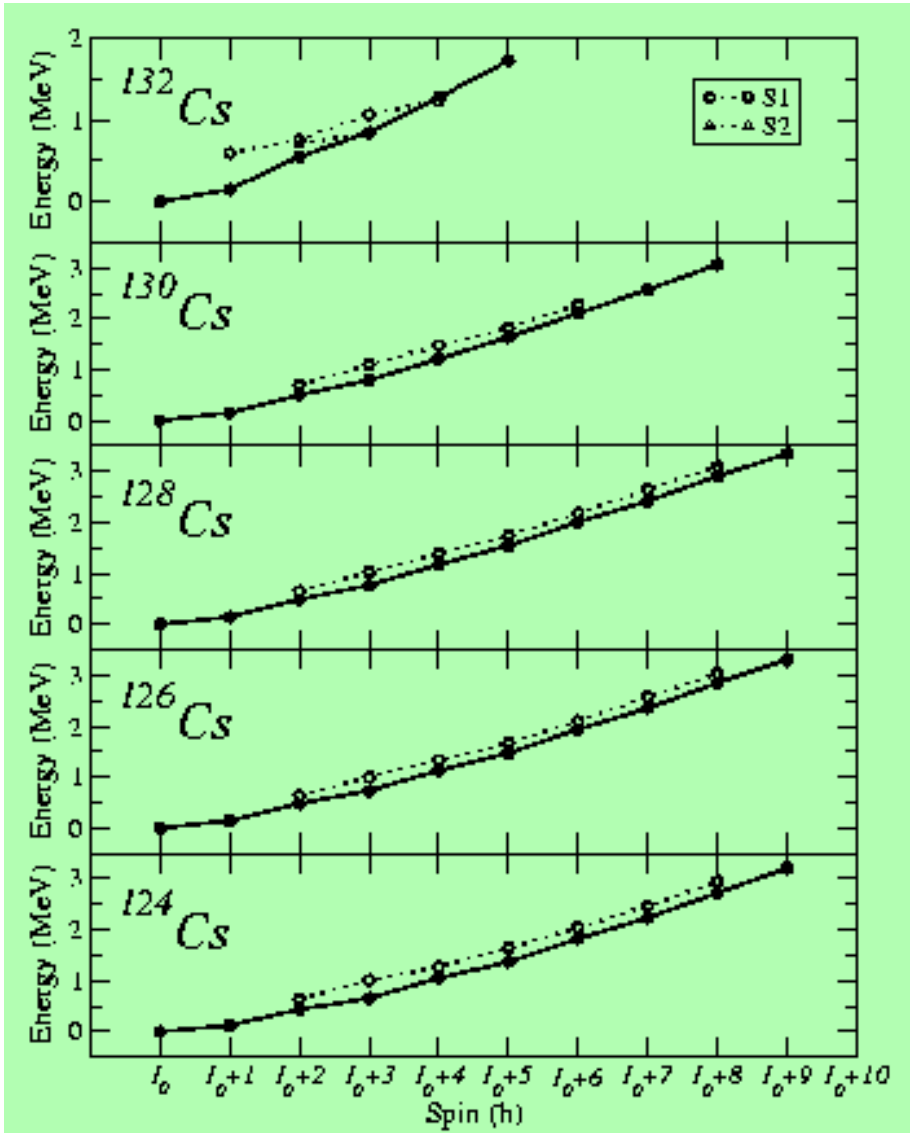
132 Cs
130 Cs
128 Cs
126 Cs
124 Cs
S1
S2
Energy (MeV)
Spin (h)
I0 I0+1 I0+2 I0+3 I0+4 I0+5 I0+6 I0+7 I0+8 I0+9 I0+10

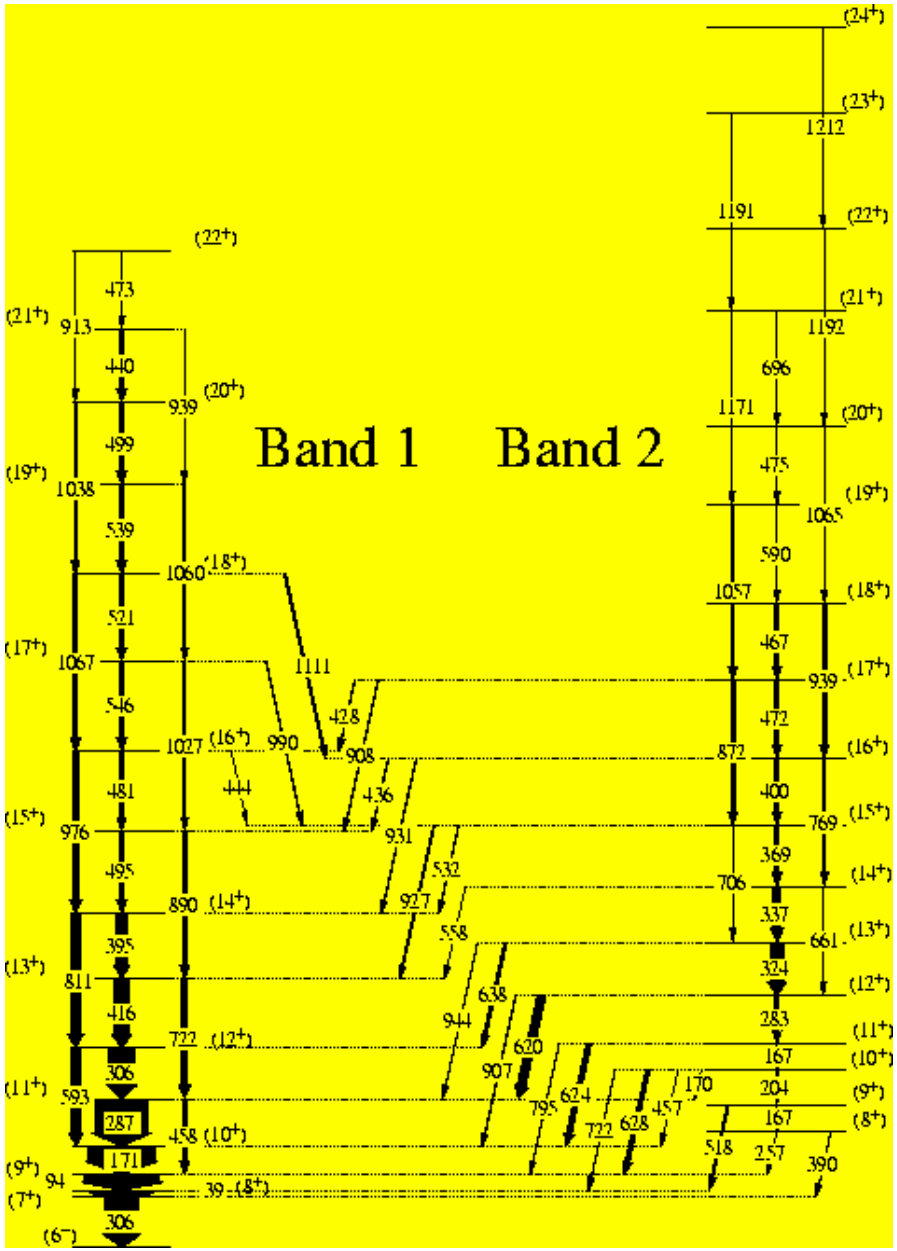
Band 1
Band 2

134 Pr

Models

- Tilted axis cranking model
- Particle-core coupling model
- Two quasiparticle + triaxial rotor model
- Interacting boson fermion fermion model

K. STAROSTA *et al.*

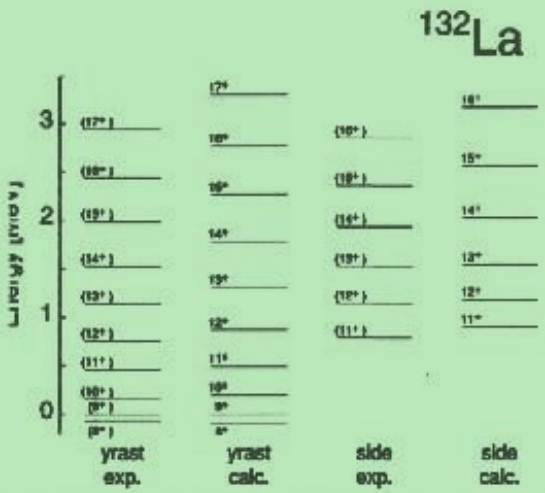

Comparison between energies of excited states in the partner band in ^{132}La with those calculated for $\pi h_{11/2}\nu^{-1}h_{11/2}$ particle-hole coupling with a rigid triaxial rotor

Theoretical states are shown only when the corresponding experimental states are known.

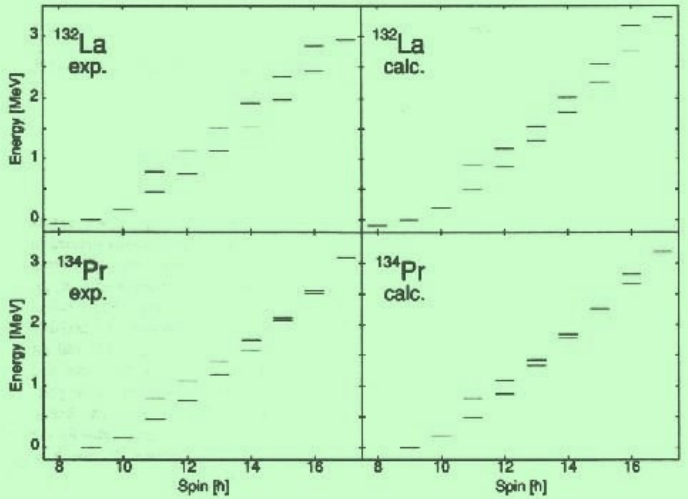

Comparisons between energies of observed $\pi h_{11/2}\nu^{-1}h_{11/2}$ states in ^{132}La (top) and ^{134}Pr (bottom) with those calculated for $\pi h_{11/2}\nu^{-1}h_{11/2}$ particle-hole coupling with a rigid triaxial rotor.

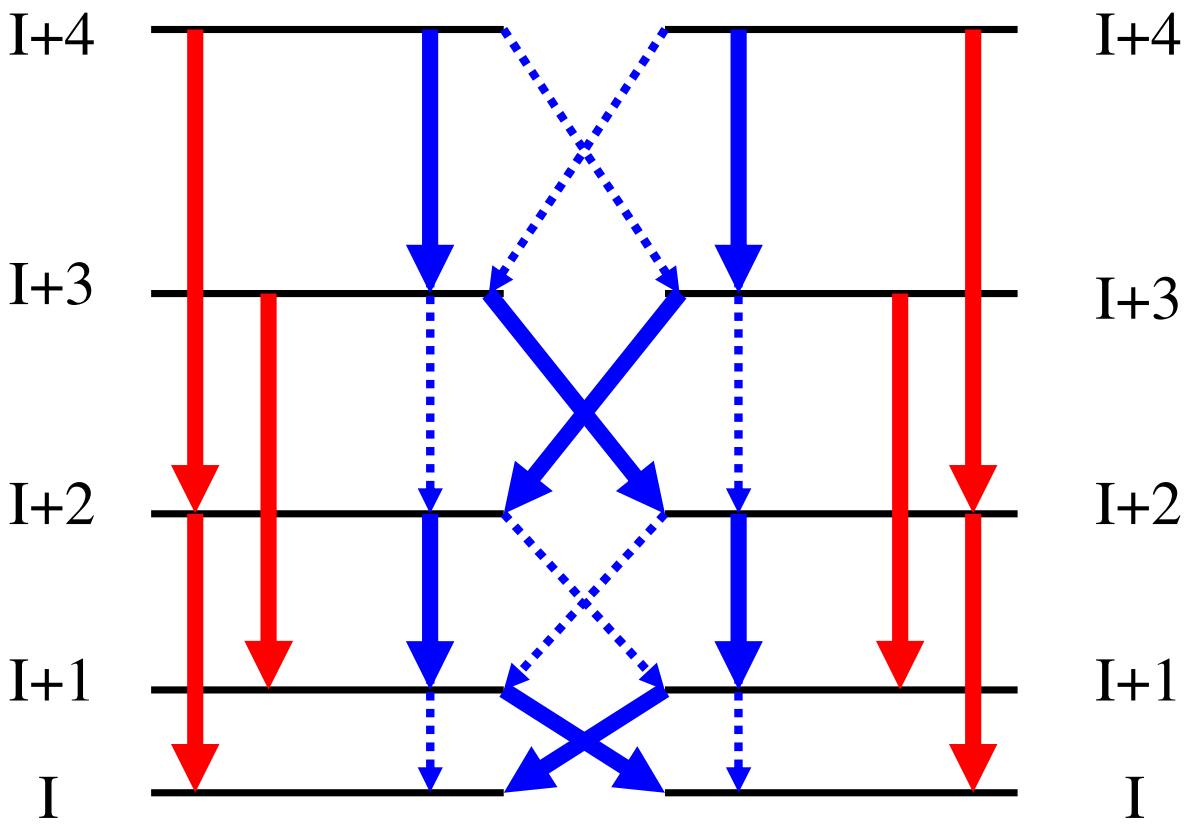

B(E2) de-exciting analogue states in both bands EQUAL

B(M1) de-exciting analogue states in both bands show the odd-even “staggering”

PROBLEM !!!!!!!!!

All odd-nuclei in which chiral (?) bands have been observed are in regions of masses:

A ~ 105
A ~ 130
A ~ 190 (?)

where even-even nuclei are γ–soft and NOT rigid triaxial

The Interacting boson fermion fermion model IBFFM1 (based on one type of boson) cannot describe stable triaxial nuclei, specially not rigid triaxial rotors !!!

BUT !!!!

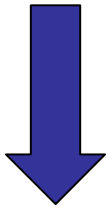

INTERACTING BOSON MODEL

$$
\begin{array}{lcll}
U(6) & \supset & U(5) \supset O(5) \supset O(3) \supset O(2) & vibrational\ limit \\
U(6) & \supset & SU(3) \supset O(3) \supset O(2) & rotational\ limit \\
U(6) & \supset & O(6) \supset O(5) \supset O(3) \supset O(2) & \gamma - soft\ limit
\end{array}
$$

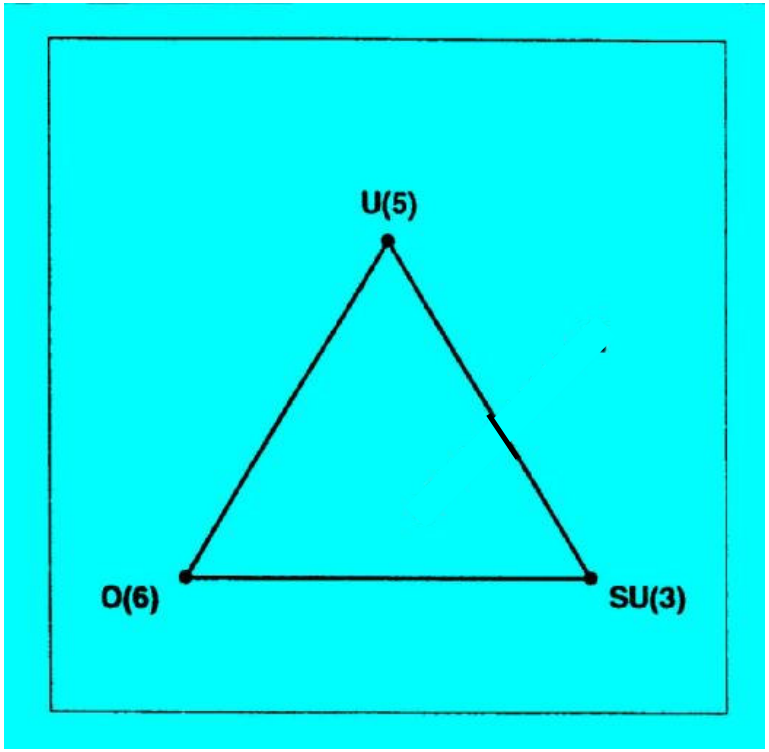

$$H_{IBM} = \epsilon_d \, \hat{n}_d + p \; P \cdot P + k' \; L \cdot L + k \; Q \cdot Q + \boxed{\Theta_3 \left[(d^\dagger \; d^\dagger)_2 \; d^\dagger \right]_3 \cdot \left[(\tilde{d} \; \tilde{d})_2 \; \tilde{d} \right]_3}$$

The first four terms represent the standard Hamiltonian of the Interacting Boson Model (IBM-1). The cubic interaction in the last term, with the strength parameter Θ_3, introduces a degree of triaxiality.

With the inclusion of the three-body term in the boson Hamiltonian, the boson quadrupole operator appearing in the dynamical boson-fermion interaction and in the E2 operator should also be extended to higher order. The standard boson quadrupole operator is modified by including the additional term

$$\eta \left[(d^\dagger \; \tilde{d})_3 \; (d^\dagger \; \tilde{d})_3 \right]_2$$

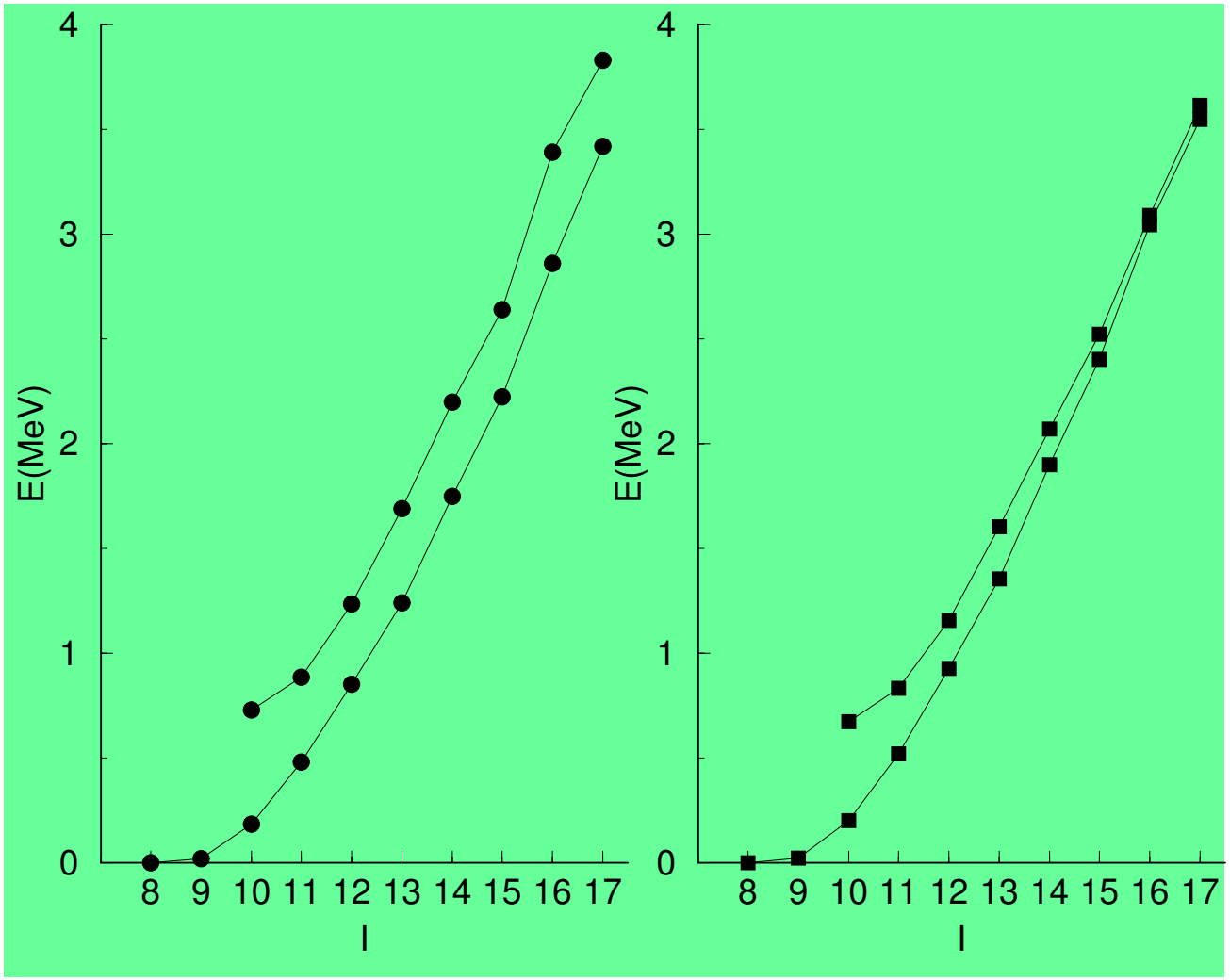

The yrast and yrare $\pi h_{11/2} \otimes \nu h_{11/2}$ bands in ^{134}Pr calculated in the IBFFM for the ^{134}Ce core without triaxiality (left panel, $\Theta_3 = 0$), and with stable triaxial deformation (right panel, $\Theta_3 = 0.03$ MeV).

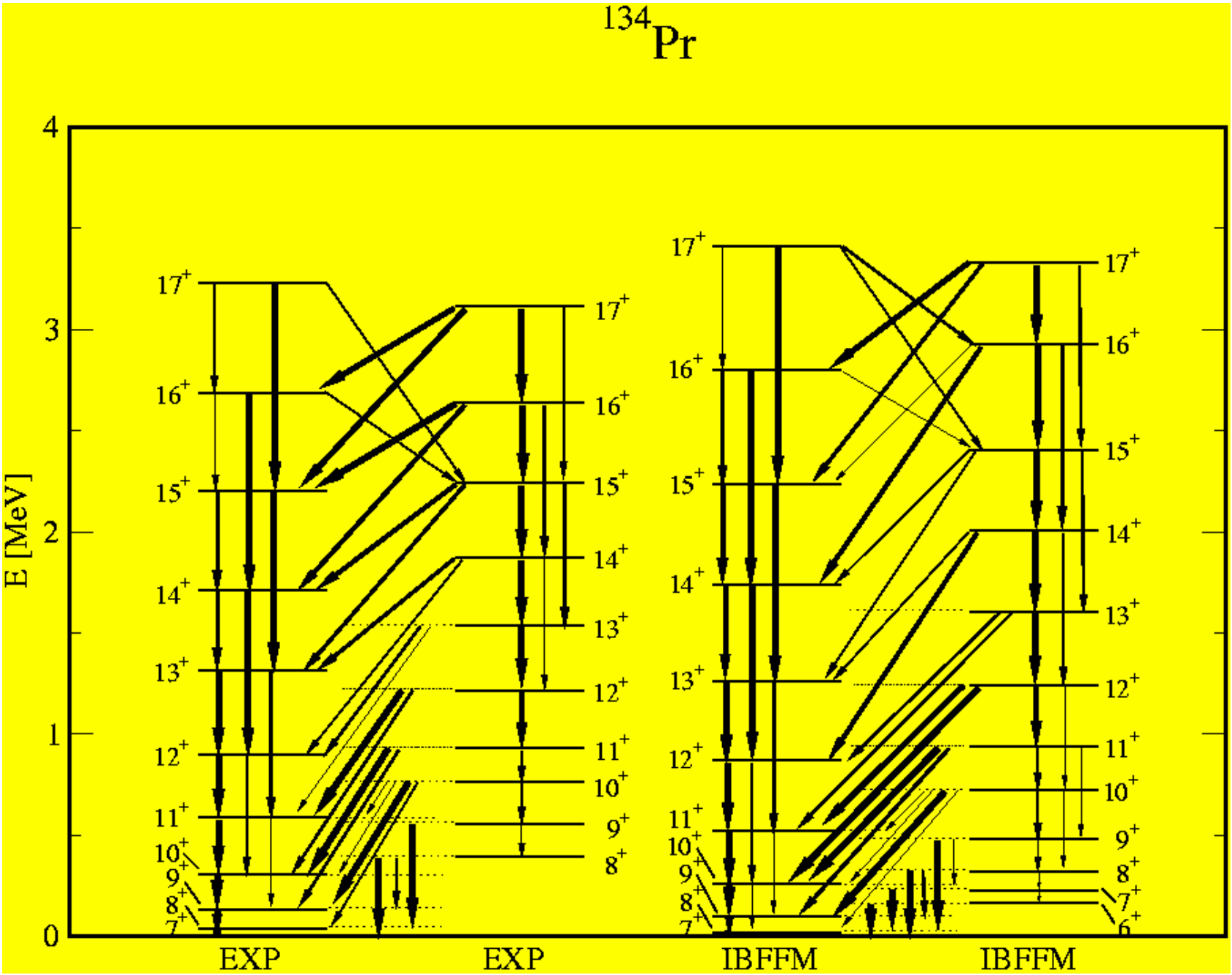
134Pr
E [MeV]
0
1
2
3
4
17+
16+
15+
14+
13+
12+
11+
10+
9+
8+
7+
6+
EXP
EXP
IBFFM
IBFFM

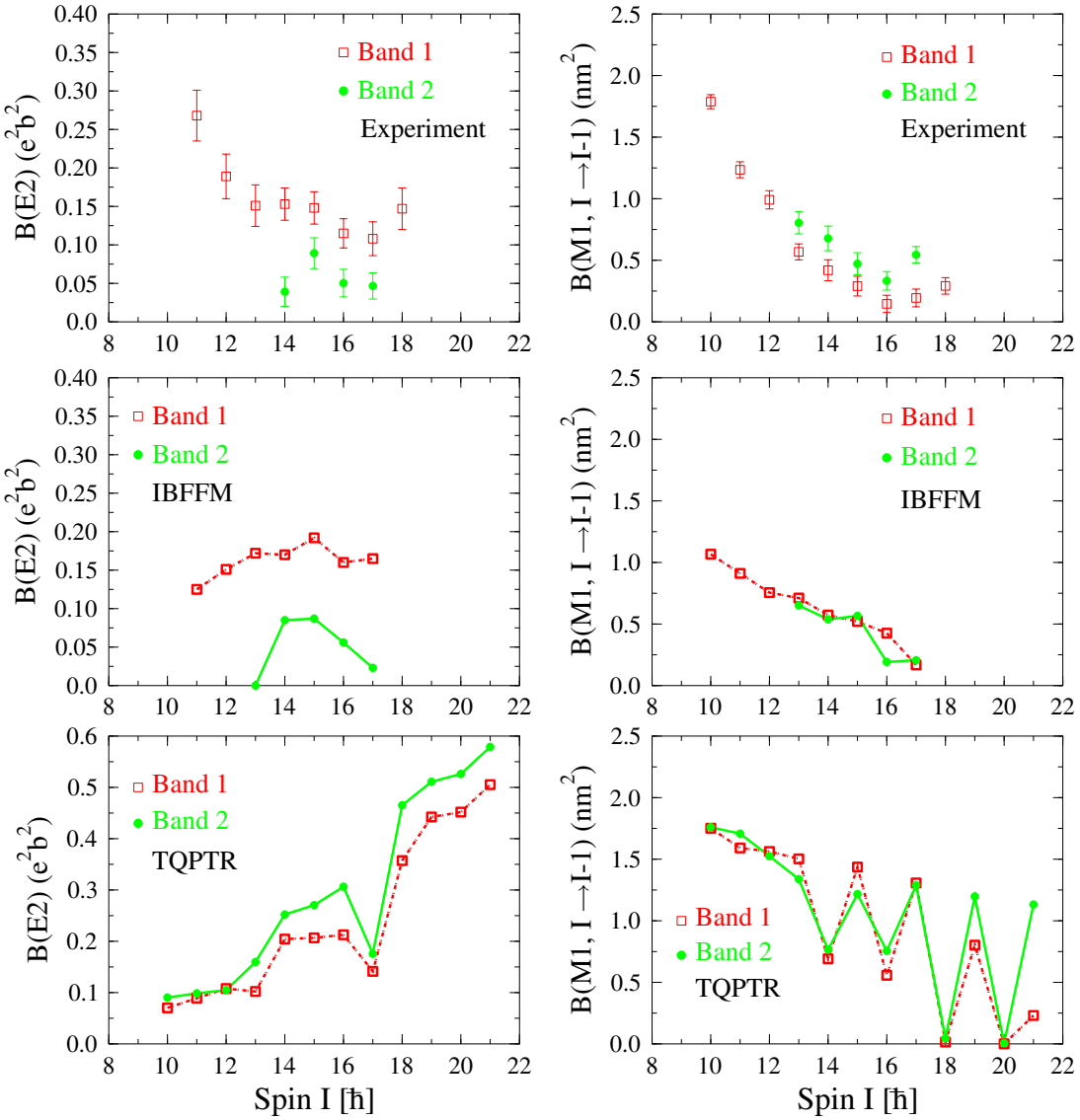
B(E2) (e²b²)
B(M1, I →I-1) (nm²)
Band 1
Band 2
Experiment
IBFFM
TQPTR
Spin I [ħ]

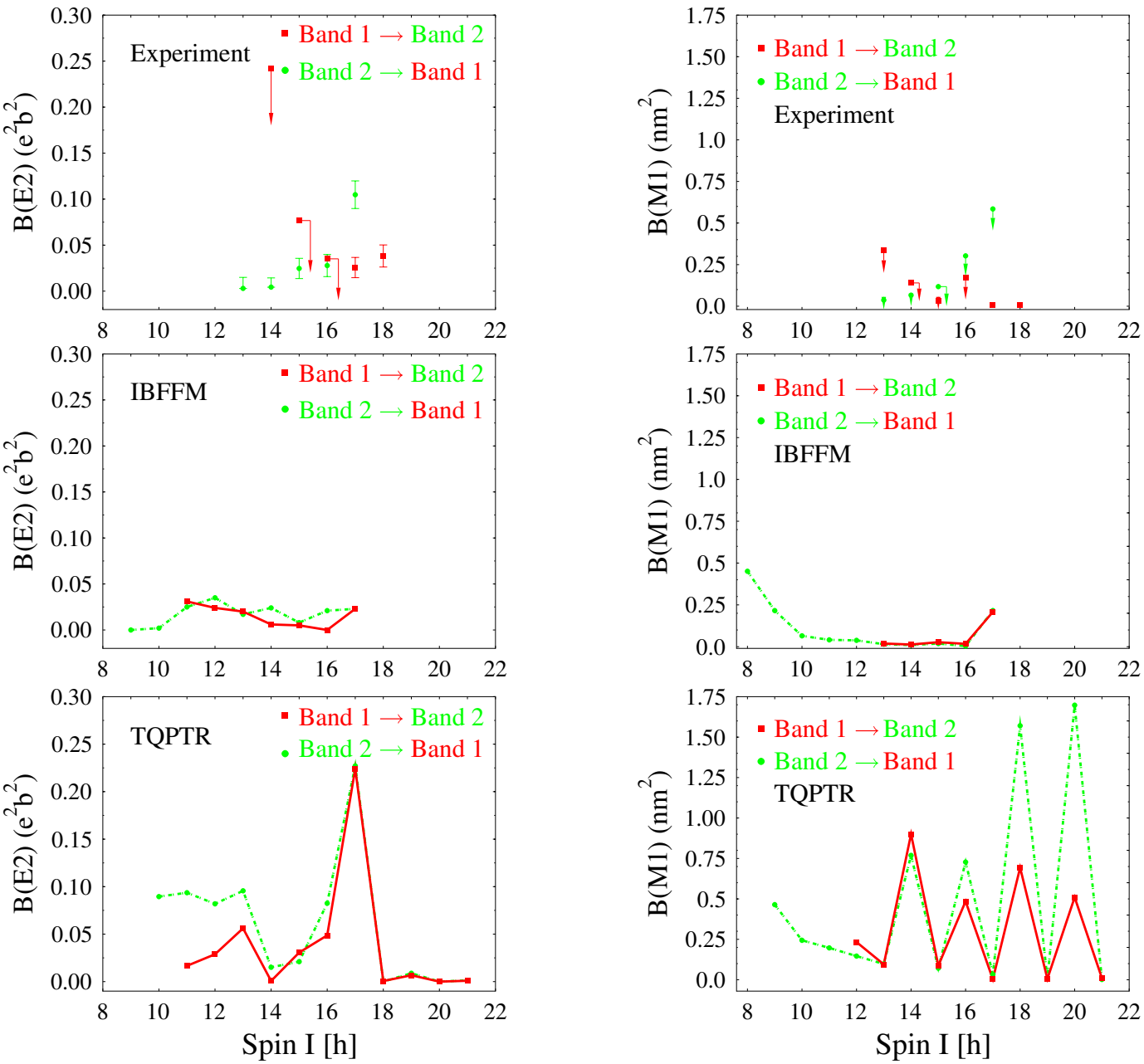
Experiment
IBFFM
TQPTR
Band 1 → Band 2
Band 2 → Band 1
B(E2) (e²b²)
B(M1) (nm²)
Spin I [h]

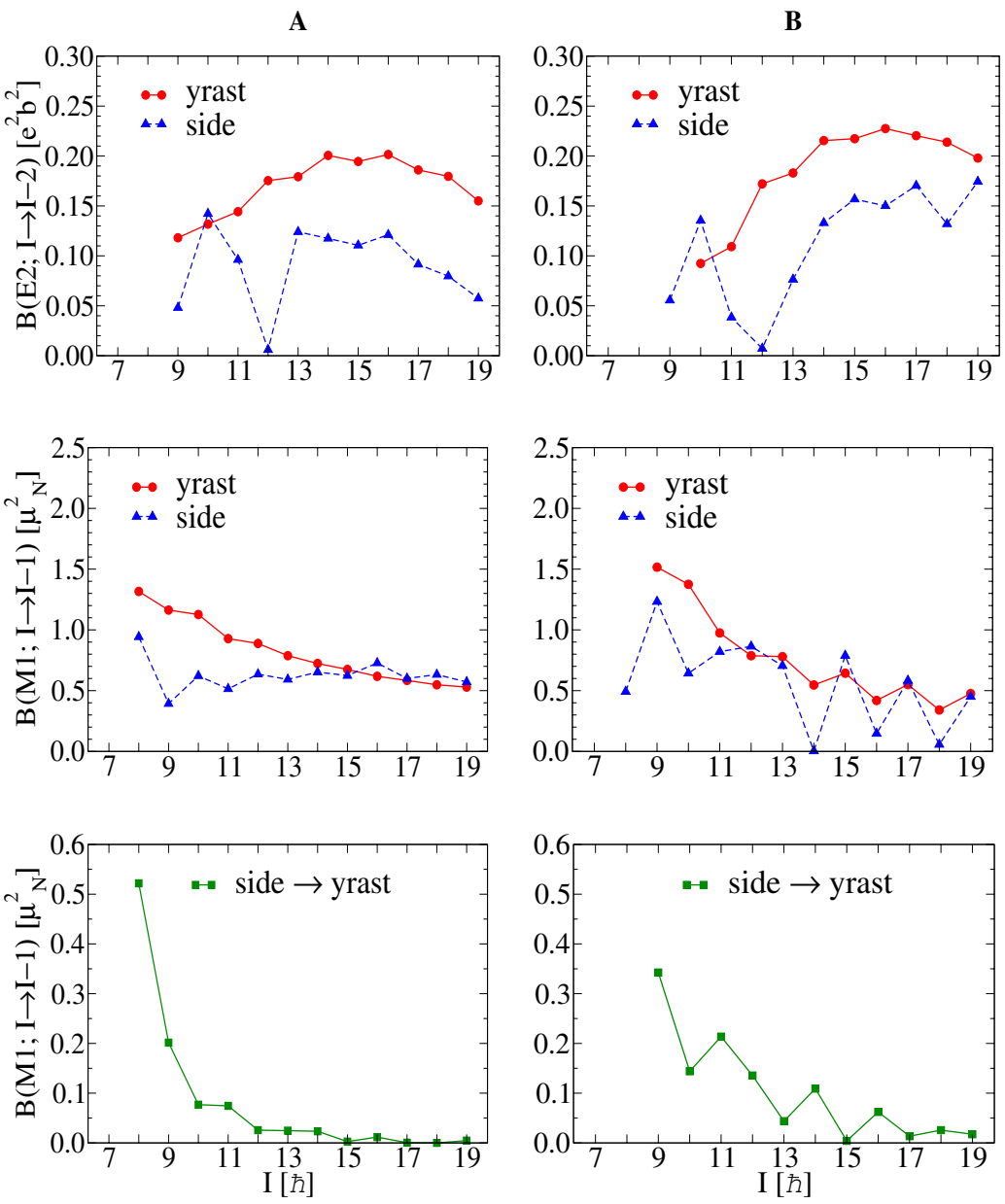

The difference is in shape fluctations

More pronounced in A than in B

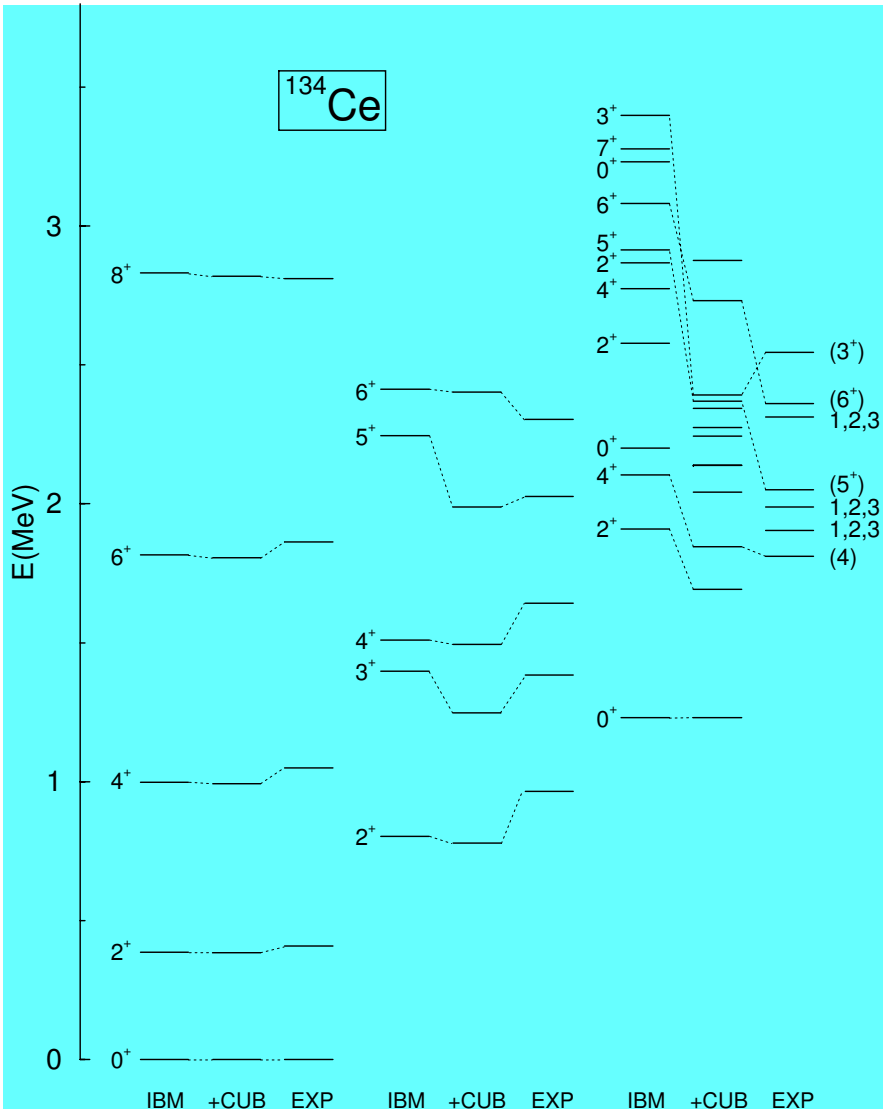

Coupling to:

Rigid ground state band

"Static chirality"

(Realized ???)

Soft ground state and γ band

Full dynamic chirality

Soft ground state and γ band and higher lying core structures

Weak dynamic chirality